2003-33

Final Report

# Effects of Vertical Pre-Release Cracks on Prestressed Bridge Girders


Research

## Technical Report Documentation Page

| 1. Report No. | 2. | 3. Recipients Accession No. | |
|---|---|---|---|
| MN/RC 2003-33 | | | |
| 4. Title and Subtitle<br>EFFECTS OF VERTICAL PRE-RELEASE CRACKS ON PRESTRESSED BRIDGE GIRDERS | | 5. Report Date<br>October 2003<br>6. | |
| 7. Author(s)<br>Eray Baran, Catherine French, Carol Shield | | 8. Performing Organization Report No. | |
| 9. Performing Organization Name and Address<br>University of Minnesota<br>Department of Civil Engineering<br>500 Pillsbury Drive SE<br>Minneapolis, MN 55455-0220 | | 10. Project/Task/Work Unit No.<br>11. Contract (C) or Grant (G) No.<br>(c) 74708 (wo) 152 | |
| 12. Sponsoring Organization Name and Address<br>Minnesota Department of Transportation<br>395 John Ireland Boulevard Mail Stop 330<br>St. Paul, Minnesota 55155 | | 13. Type of Report and Period Covered<br>Final Report, 1999-2003<br>14. Sponsoring Agency Code | |

15. Supplementary Notes

www.lrrb.gen.mn.us/pdf/200333.pdf

Tables and Figures; Appendix A, Pilot Study; Appendix B, Prestressing Strand Tension Tests; Appendix C, Vibrating Wire Gage Data; Appendix D, Load-Displacement Plots for Near-Crack LVDTs; and appendix F, Ultimate Flexural Capacity Calculations, are available by contacting Mn/DOT Research Services Section.

16. Abstract (Limit: 200 words)

Vertical cracks near the midspan of large-sized prestressed concrete bridge girders may develop during the curing process and can extend through the depth of the girder. The cracking is attributed to restrained shrinkage and thermal effects prior to release of the prestressing strands.

Eighteen full-scale Mn/DOT Type 28M prestressed concrete beams were tested to investigate the effects of the cracks on the performance of the beams. Thirteen beams tested in this study incorporated manmade pre-release cracks. All of the beams were tested under static loading to investigate the effects of pre-release cracks on concrete strains, flexural crack initiation and re-opening loads, overall beam stiffness, and ultimate flexural capacity. Three of the beams were subjected to cyclic testing to evaluate possible effects of the pre-release cracks on the strand stress ranges and fatigue life of the beams. Unlike the field observations, the pre-release cracks in the test beams did not close completely under the beam's weight and pre-stressing force. The pre-release cracks were found to cause changes in beam strains around the crack locations.

The overall stiffnesses of the beams were also affected by the reduction in the moment of inertia of the pre-release crack section. Following pre-release crack closure, the beams recover the stiffness comparable to that of the uncracked beams. No significant effect of pre-release cracks was observed on the behavior of the beams near the ultimate capacity.

Results from the cyclic testing of three beams indicated that a beam that develops pre-release cracks is more likely to experience fatigue problems and tend to cause a reduction in the beam's fatigue life. Guidelines are proposed for the assessment of girders that develop pre-release cracks during production.

| 17. Document Analysis/Descriptors | | 18. Availability Statement |
|---|---|---|
| Pre-release cracks<br>Prestressed concrete girders<br>Girder testing | Fatigue<br>Flexural cracking | No restrictions. Document available from:<br>National Technical Information Services,<br>Springfield, Virginia 22161 |

| 19. Security Class (this report) | 20. Security Class (this page) | 21. No. of Pages | 22. Price |
|---|---|---|---|
| Unclassified | Unclassified | 158 | |

# Effects of Vertical Pre-Release Cracks on Prestressed Bridge Girders

## Final Report

Prepared by

Eray Baran
Catherine E. French
Carol K. Shield

Department of Civil Engineering
University of Minnesota

## October 2003

Published by

Minnesota Deparment of Transportation
Office of Research Services
Mail Stop 330
395 John Ireland Boulevard
St. Paul, Minnesota 55155-1899

## ACKNOWLEDGEMENTS

The work on this project was conducted under the sponsorship of the Minnesota Dpeartment of Transportation (Mn/DOT). Appreciation is expressed to the members who served on the Mn/DOT Technical Advisory Panel for their input and assitance. Appreciation is also acknowledged to the Minnesota Supercomputer Institute for the use of the computer software ABAQUS, and Elk River Concrete Products, a division of Cretex Companies Inc., for their cooperation and assistance in fabrication and transportation of the test beams.

The following people are gratefully acknowledged for their help with the fabrication and testing of the beams: Paul Bergson, Altan Altay, Diego Arabbo, Eric Corwin, Cenk Tort, Katsuyoshi Nozaka, Matthew Spink, John Wacker, Nels Ojard, Justin Ocel, Bulent Erkmen, Cheng Xu Yang, Danny Johnson, and Jessica Mitchell.

## TABLE OF CONTENTS

## EXECUTIVE SUMMARY

During the production of large-sized prestressed concrete bridge girders it has been observed that vertical cracks may develop near the midspan of the girders during the curing process if the girders are left on the prestressing bed for an extended period of time before detensioning the strands. The cracks have been observed to initiate at the top flange of the girder and propagate downward in the depth of the section. In some cases, they have been observed to extend through the entire depth of the girder.

The reason for the cracking is attributed to restrained shrinkage and thermal effects during the curing period of the girders prior to release of the prestressing strands. During this period, concrete shrinkage is restrained by the prestressing strands, hold-down attachments, and friction between the girders and the casting bed. In addition, contraction of the exposed strands occurs between the girders due to rapid cooling after steam curing, creating extra tensile strains in the bonded concrete, which increases the likelihood of pre-release cracking.

The pre-release cracking problem is more likely to occur in long bridge girders with deep sections and large amounts of prestressing strands. In this case, the increased girder lengths lead to decrased free length of strands between the girders in the precasting bed, which with the increased strand area contribute to increased girder restraint forces.

Eighteen full-scale Mn/DOT Type 28M prestressed concrete beams, some of which incorporated manmade pre-release cracks of varying widths and depths, were tested to experimentally investigate the effects of the cracks on the performance of the beams, and to validate the results of the previous analytical study by Wyffels (2000). Issues investigated included the effect of pre-release cracks on the reduction in flexural crack initiation and re-opening loads and the possible subsequent reduction in fatigue life of the girders due to early flexural cracking and increased strand stress ranges.

Thirteen of the eighteen beams that were tested in this study incorporated 0.008 or 0.014 in. wide manmade pre-release cracks at either 6, 16 or 22 in. depths. All of the beams were tested under static loading to investigate the effects of pre-release cracks on concrete strains, flexural crack initiation and re-opening loads, overall beam stiffness and ultimate flexural capacity.

Following the static tests, three of the beams were subjected to cyclic testing in order to evaluate possible effects of the pre-release cracks on the strand stress ranges and fatigue life of the beams.

Experimental results obtained from the static tests validated the results of the analytical study. Different from the cases observed in the field, the pre-release cracks in the test beams did not close completely under the effects of beam self weight and prestressing force. In the single crack series beams, the pre-release cracks remained partially open at flexural crack initiation and re-opening loads. Consequently, for most of the beams the major part of the reduction in flexural crack initiation and re-opening loads was due to the reduced moment of inertia due to the pre-release cracks remaining partially open. However, there were also cases for which the effect of the reduced bottom fiber compressive stress on the flexural cracking load was larger than the effect caused by the pre-release crack remaining partly open.

The pre-release cracks were found to cause changes in beam strains around the crack locations. The changes included superimposed bottom fiber tensile strains below the pre-release crack, increased compressive strains near the crack tip, and reduced compressive strains at the top of the crack. Even though the effect decayed almost completely at a distance "*d*" away from the pre-release crack location, the reduced compressive strains below the cracks resulted in lower flexural crack initiation and re-opening loads of the beams incorporating pre-release cracks compared to the beams that did not have pre-release cracks.

The overall stiffnesses of the beams were also affected by the reduction in the moment of inertia of the pre-release crack section. However, following pre-release crack closure, the beams recover the stiffness comparable to that of the originally uncracked beams.

Although the reduction in stiffness of the beams disappear upon pre-release crack closure, the effects caused by the existence of pre-release cracks on beam strains during crack closure become "locked-in". This indicates that even if the pre-release cracks close completely on the precasting bed under the effects of beam self-weight and prestressing force, the strain distributions near the crack locations will be different than those of originally uncracked beams.

No significant effect of pre-release cracks was observed on the behavior of the beams near the ultimate capacity. This is because at the ultimate capacity of the beams the change in the strand stress due to the existence of pre-release cracks becomes negligible, and the top flange of

the section develops the full compressive strength of the concrete as the pre-release cracks closed.

Results from the cyclic testing of three beams, one without pre-release cracks and two with pre-release cracks, indicated that a beam that develops pre-release cracks is more likely to experience fatigue problems than a beam with no pre-release cracks. It was observed that the pre-release cracks tend to increase the strand stress range, and hence cause a reduction in the beam's fatigue life.

As an outcome of the study, guidelines are proposed for the assessment of girders that develop pre-release cracks during production.

# CHAPTER ONE
# INTRODUCTION AND LITERATURE REVIEW

## 1.1 Background

As high strength concrete becomes more popular, heavily reinforced sections with longer span lengths are being used for prestressed concrete bridge girders. During the production of these girders it has been observed that vertical cracks near the midspan of the girders may develop during the curing process if the girders are left on the casting bed for a long time without detensioning the prestressing strands (Ahlborn, 1998; Roller, 1993; Green, 1984). Cracks have been observed to begin at the top flange, and propagate downward in the depth of the section. In some cases they have been observed to extend through the entire depth of the section (Roller, 1993; Green, 1984). Following the release of prestressing strands the cracks may close completely due to the effects of prestressing force and girder self weight (Ahlborn, 1998; Roller, 1993; Green, 1984).

### 1.1.1 Statement of Problem

The reason for this type of cracking is attributed to restrained shrinkage and thermal effects that occur during the curing period of the girders prior to release of the prestressing strands (Ahlborn, 1998; Zia, 1993; Green, 1984). During the production of girders, shrinkage of concrete is restrained by the prestressing strands, girder hold-down points, and friction between the girders and the casting bed. In addition to this, contraction of the exposed strands between the girders due to rapid cooling after steam curing creates tensile strains in the bonded concrete, which promotes the development of pre-release cracks.

The problem of pre-release cracking is becoming more important as longer heavily reinforced girders are used. This phenomenon is illustrated in *Fig 1.1*.

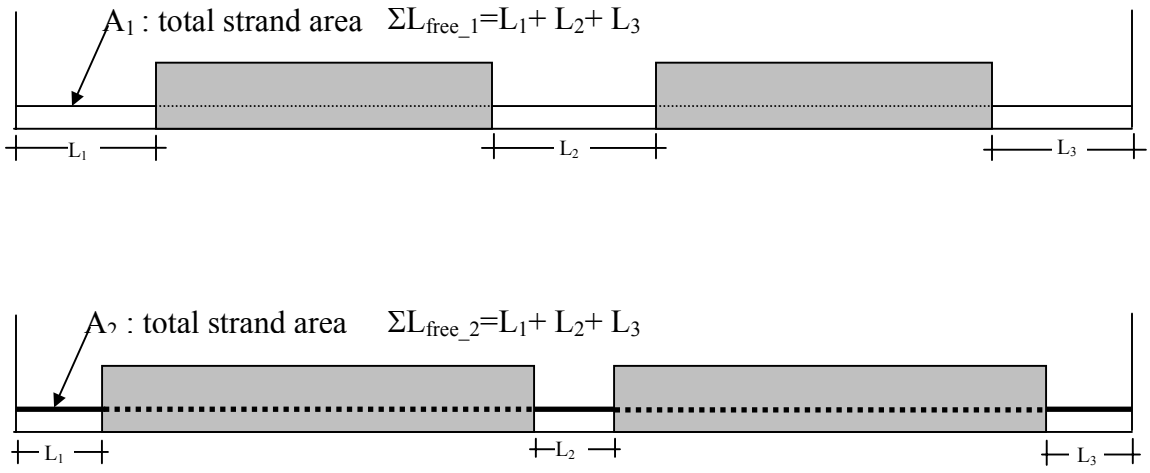


Figure 1.1 Effects of Increasing Girder Length and Strand Area

In the prestressing bed, the total shortening of the girders prior to release due to shrinkage and thermal effects must be accommodated by the elongation of the free length of strands between the girders:

$$\Delta_{free\_strand} = -\Delta_{girders} \tag{1.1}$$

The force that will develop in the strands due to $\Delta_{free\_strand}$ amount of elongation is:

$$\Delta P_{strand} = \Delta_{free\_strand} E_{steel} A_{strand} / L_{free} \tag{1.2}$$

where $E_{steel}$ is the modulus of elasticity of steel, $A_{strand}$ is the total area of the strands, and $L_{free}$ is the total length of the strands between girders.

Increases in girder length are typically accompanied by increases in strand area and decreases in the amount of free length of strands in the prestressing bed. The longer length girders will typically experience larger changes in length, $\Delta_{girders}$, due to shrinkage and thermal effects, and consequently much larger restraining forces, $\Delta P_{strand}$. The increased strand area, $A_s$, increased girder shortening, $\Delta_{girders}$, and decreased free length of strands, $L_{free}$, all contribute to increased girder restraint forces, and consequent increased likelihood of pre-release cracks.

In the reported cases where pre-release cracks have been observed to occur, the cracks closed completely following the release of the prestressing strands due to the effects of the prestressing force and the self weight of the girder (Ahlborn, 1998; Roller, 1993; Green, 1984). The action of the girder to close the cracks causes the stretching of the bottom fiber of the girder,

which results in reduced compressive stress at the bottom of the beam at the local region below the pre-release crack. As a result, the load required to initiate the flexural cracking in the girder would be reduced. The effect of the local reduction in the flexural cracking capacity of the girder may cause fatigue and corrosion problems in the strands.

### 1.1.2 Literature Review

There is a limited amount of information available in the literature on pre-release cracks. This section consists of a review of some of the studies related to pre-release cracks and fatigue of prestressed concrete girders.

#### 1.1.2.1 Studies Related to Pre-Release Cracks

*Ahlborn, French and Shield (1998):*

Two long-span high-strength prestressed concrete girders were fabricated and tested by Ahlborn et al. in a study to evaluate the use of high strength concrete in prestressed bridge girders and the adequacy of AASHTO 1993 provisions. During the production of the girders, pre-release cracks were observed to develop in one of the girders.

The girders were Mn/DOT 45M sections with a span length of 132 ft 9 in. Each girder was prestressed with forty-six 0.6 in. diameter Grade 270 strands initially stressed to 71% of their ultimate strength. The two girders had different concrete mix designs with measured 28-day compressive strengths of 12,100 psi and 11,100 psi, respectively. The girders were cast in the same bed simultaneously. One of the girders (Girder II) reached the required release strength before the other girder (Girder I). Formwork for Girder II was removed, and the girder was left on the casting bed without releasing the strands until Girder I gained the required release strength. There was a 6 hour difference between the time the forms for Girder II were removed and the strands were released. During this time, pre-release cracks developed in Girder II while no cracking was observed in Girder I. In total, fifteen cracks were detected. The pre-release cracks were localized in the middle 40% of the span length. The cracks extended from the top flange towards the bottom. The average crack depth was between 30 to 35 in. (the beams were 45 in. deep), even though there were cracks as shallow as 6 in. Crack widths were estimated on the order of *0.005 in.* to *0.025 in.* at the top of the beam. All of the cracks closed completely following strand release.

Results from the static testing of the beams indicated a reduction in the flexural cracking capacity of Girder II relative to Girder I. The predicted cracking moments were 3,020 k-ft and 2,840 k-ft, respectively for Girders I and II. The measured cracking moment for Girder I was 2,560 k-ft. Using the ratio between the predicted and measured cracking moments for Girder I, the expected cracking moment for Girder II was determined to be 2,410 k-ft. The cracking moment of Girder II was measured to be 2,020 k-ft during testing.

The distance to the nearest pre-release crack was documented in Ahlborn's dissertation (1998) for the first five flexural cracks that developed during testing of Girder II. All five flexural cracks were within 16 in. (35% of girder depth) of a pre-release crack.

It was stated by the authors that the difference between the expected and measured flexural cracking moments for Girder II was due to the existence of pre-release cracks in this girder. A geometric compatibility theory was developed by Shield (Ahlborn [1998]) to determine the effects of the closure of pre-release cracks on girder stresses and camber. The theory used the geometry changes required to close the pre-release cracks in the girder to predict the changes in camber and strains from the uncracked girder.

The results from Ahlborn's study prompted the first phase of the current research project, which included an analytical investigation of the problem.

*Wyffels, French and Shield (2000):*

Wyffels et al. conducted an analytical study to investigate the effect of pre-release cracks on girder stresses and camber. The first part of the study included a parametric study to determine expected strand stress ranges in cracked sections. Six girder designs with different concrete strength, girder type, girder spacing and strand size were investigated. For each design, the strand stress range was determined considering three different section properties: uncracked, partially cracked and cracked. The results of the parametric study indicated that there was a concern regarding steel fatigue for cracked and partially cracked section properties.

Their study also included a finite element investigation of girders with pre-release cracks. The finite element models involved girders incorporating both single and multiple pre-release cracks with different crack size and crack spacing.

Results from the finite element study indicated that stress changes occurred at the location of the pre-release cracks relative to beams with no cracks. Larger stress changes occurred for deeper and wider cracks. The length over which the cracks had an impact was limited to a distance equal to the depth of the girder on each side of the pre-release cracks. The area where the stresses changed due to a pre-release crack was dependent on the size of the crack. Regarding multiple pre-release crack interaction, the authors stated that the models involving multiple cracks behaved similarly to the models involving a single crack. When the cracks were spaced closely such that the affected stress areas overlapped, the effect of the cracks was the superposition of the effect from each individual crack.

Additional finite element models of the girders tested by Ahlborn et al. (1998), one of which developed pre-release cracks, were prepared to compare the analytical results to the experimental data. Results from the models were in good agreement with the measured girder behavior.

*Roller, Russell, Bruce, and Martin (1993):*

In a study to investigate the long-term performance of prestressed high strength concrete bridge girders, four 70 ft long 54 in. deep bulb-tee prestressed concrete girders were tested by Roller et al. Each girder had thirty ½ in. diameter Grade 270 strands initially tensioned to 75% of ultimate strength. One of the girders (Girder 4) was fabricated separately than the other three girders (Girders 1, 2, and 3). The concrete mix used in Girder 4 was different than the other girders. The 28-day cylinder strengths were 9,800 psi, 9,600 psi, 9,900 psi and 8,800 psi for Girders 1, 2, 3, and 4, respectively. Girders 1,2, and 3 were steam cured, while Girder 4 was cured under waterproof tarps. After removal of the forms, "a large crack" was observed near midspan of all four girders. The cracks were full-depth cracks, and were not visually detectable after strand release.

Girders 1 and 2 were tested in flexure to failure. Girder 3 was subjected to a static load for a duration of 18 months. Girder 4 was subjected to 5 million cycles of fatigue loading. During flexural tests, a new flexural crack occurred before the existing pre-release crack re-opened in Girders 1 and 3. In Girders 2 and 4, on the other hand, the pre-release cracks re-opened from the bottom prior to the development of any new cracks. The ratio of measured to

predicted cracking moments was 1.00 for Girder 1, 1.01 for Girder 2, 0.95 for Girder 3, and 0.90 for Girder 4. The ratios of measured-to-predicted ultimate moments were 1.13, 0.95, 1.13 and 1.08, respectively for Girders 1, 2, 3, and 4. The relatively low measured ultimate load for Girder 2 was attributed to lateral buckling of the beam near the end of testing.

After dissection of the failure region, it was noted that 4 of the strands were fractured in Girder 4. There was no necking in some of the fractured wires, indicating that the fractures occurred during the fatigue test. The strand fractures occurred at the location of the existing pre-release crack.

It was stated by the authors that:

> "…precast concrete fabricators will need to make some changes in the normal production regime in order to consistently produce high strength concrete girders."

*Muller and Dux (1994):*

Muller and Dux tested 37 prestressed concrete beams in a study to examine the fatigue behavior of beams with inclined strands. Among 37 beams, 15 of them had 5/16 in. diameter straight strands, seven of them had 5/16 in. diameter deflected strands, and 15 of them had 1/2 in. diameter deflected strands. The beams were 12.8 in. deep section 17 ft in length. All the beams were subjected to static testing to induce flexural cracks to the lowest tendon level prior to cycling testing. One of the beams with 5/16 in. diameter deflected strands cracked at 28.1 kips, while the typical cracking loads of the rest of the beams in the same series were between 31 and 32.4 kips. It was documented that "minor top surface" cracking occurred during production in the beam that had the lower flexural cracking load. It was also documented that the ultimate load of this beam was not affected by the existence of this crack.

*Green, Cookson, and Johnson (1984):*

To evaluate the effect of pre-release cracks on performance of prestressed concrete beams, Green et al. conducted tests on a series of bridge beams. Some of the beams tested had cracks that occurred during manufacture while other beams from the same cast did not develop pre-release cracks.

The beams were 38 in. high inverted T-sections prestressed with twenty-six 0.6 in. diameter seven wire strands, initially tensioned to 47.2 kips. The casting length of the beams was 69.9 ft with 20 in. free length of strands between the beams. The design concrete strength was 7600 psi. Five identical beams (Beams A, B, C, D, and E) were cast in the prestressing bed. Cracking prior to detensioning was detected in three of the beams (Beams A, C, and E). Crack widths up to *0.04 in.* were measured at top of the beams prior to detensioning. Most of the cracks were full-depth cracks with much smaller width at the bottom of beams. Most of the cracks occurred near the beam ends. After transfer of the prestressing force, the cracks closed.

Three of the beams, one with pre-release cracks (Beam A) and two without pre-release cracks (Beams B and D) were subjected to static tests. During the initial tests, the beams were loaded under four-point bending until the stress at the top flange was half of the concrete strength (3800 psi) . At this load, the calculated bottom fiber stress was 550 psi compression. No difference between the stiffnesses of the beams was observed during the initial tests. The beam that had pre-release cracks (Beam A) was further tested to produce 145 psi tensile stress at the bottom fiber. None of the pre-release cracks in the constant moment region re-opened during this test. After testing, the beams that had developed pre-release cracks (Beams A, C, And E) were rejected, while the other two uncracked beams were incorporated in a bridge. The beams that were rejected were subjected to further testing after a 6 in. deck was cast. Two of these beams (Beams A and C) were used to investigate flexural behavior while the third one was used for investigation of shear behavior.

In one of the beams that was subjected to flexural testing (Beam C), there was only one pre-release crack that was located approximately 12 in. from one end of the beam. During load tests, the pre-release crack in this beam was outside the test span. During testing of Beams A and C, flexural cracks were detected near the load points at the end of similar load increments. In the beam with pre-release cracks in the constant moment region (Beam A), a new flexural crack was detected prior to the existing pre-release cracks became visible again. The second and third visible flexural cracks were at the location of the pre-release cracks. It was concluded from these results that:

> "originally cracked sections had achieved a flexural tensile strength equivalent to that of originally uncracked sections."

The third beam that developed pre-release cracks during manufacture (Beam E) was subjected to tests to evaluate the effect of cracking on shear performance of the beam. Each end of the beam was tested independently. No significant difference was observed between the originally cracked and uncracked sections during these tests.

Permeability tests were performed on one of the beams with pre-release cracks (Beam A) to determine the difference between the permeability of the originally cracked sections and the uncracked sections. The method used to measure the permeability included drilling of holes that were approximately 1.2 in. deep and 0.26 in. in diameter. These holes were then filled with water, which was connected to a supply in a capillary tube. The time that it took the water to travel 1.97 in. in the tube was used as a measure of the permeability. In total, nine holes were drilled at sections with and without pre-release cracks. In one of those locations, water traveled significantly faster than others. From the results of the permeability tests, it was concluded that autogenous healing took place, and the permeability of originally cracked sections became essentially the same as that of uncracked sections. The probable reason for the increased permeability at one location in the top of the beam was reported to be incomplete autogenous healing at that location because of lower compressive stress at that level.

It was concluded by the authors that the beams that developed pre-release cracks may be accepted to be used in bridges if the following conditions are satisfied:

1. The beams should be load-tested before an age of 28 days with the maximum compressive stress less than half of concrete strength at that time. During these tests, there should be no visible cracking at the originally cracked locations. and the load-deflection curves should be linear. In addition, 90% of the deflection should be recovered after the first two load cycles.
2. For the shear check, the beams should be tested under the load that produces bending moment corresponding to the maximum design shear. The beams should remain uncracked through these tests.

*Zia and Caner (1993):*

Zia and Caner conducted a study to evaluate the pre-release cracking problem in prestressed concrete AASHTO girders. Their study consisted of several parts including a

national survey, a field study to measure the concrete properties and temperatures occurring during fabrication, and an analytical study to determine girder stresses before transfer of prestress.

In the first phase of the study, a questionnaire was prepared and sent to twenty-one prestressed concrete producers across the country. The authors summarized the responses of the sixteen producers who returned the survey:

1. "The strength of the concrete used by these producers ranged 4,500 to 7,000 psi in one day, and 7,500 to 9,000 psi in 28 days."
2. "Fourteen of sixteen producers have experienced the cracking problem at least twice in a year."
3. "The cracking problem was most common in long-span AASHTO Type IV girders."
4. "Six producers also experienced similar cracking problems in double tees and long piles."
5. "Ten producers believed that the cracking was due to temperature changes during production."
6. "Eight producers believed that a large drop in ambient temperature before detensioning was the cause of the cracking problem."
7. "Other possible reasons for the cracking problem were also suggested by the producers. They included insufficient amount of exposed strands in the casting bed, thin web joined with thick flanges, temperature variance along the casting bed, concrete shrinkage, curing rate of concrete, and length of curing time."

The second phase of the study included field investigations of Type III and Type IV AASHTO girders at three different prestressing plants. Girder and ambient temperatures were measured during fabrication. In addition, concrete cores were taken from both cracked and uncracked sections of previously rejected girders to determine the effect on the compressive strength of the concrete. The failure mode of both groups of cores was determined to be similar, even though the average compressive strength of the cracked cores was slightly lower than that of the uncracked cores.

A computer program was written to determine the stress developed across the girder section when subjected to temperature variations. Two different temperature variations through the girder depth were considered: uniform temperature variation and linearly varying temperature. Several cases were studied including different girder types, girder span lengths, and total strand area, under various temperature changes. For each case, the minimum required exposed tendon length to avoid concrete cracking was determined. It was stated that in terms of the stresses developed in the concrete, the case with linearly varying temperature was more critical than uniform temperature variation. Depending on the results from the analytical study, the authors indicated that the minimum required tendon length between the girders was 28% of the girder length.

It was suggested that the North Carolina Department of Transportation should develop guidelines to be followed for the acceptance of girders that develop pre-release cracks during production. According to the authors' recommendations, girders should be accepted if the cracks do not extend into the bottom flange. If there are two or more full depth pre-release cracks spaced at a distance less than the depth of the girder, the girder should be rejected.

The authors had the following conclusions:

1. The cause of pre-release cracks is due to restrained thermal contraction of the girders.
2. The cracking problem can be minimized by increasing the length of exposed strands between the girders. Reducing the cooling period and thus minimizing the temperature drops as much as possible would help reduce the likelihood of cracking.
3. As the pre-release cracks close following the transfer of the prestressing force, if enough moisture is supplied, autogenous healing can take place and the concrete can restore the original strength.
4. Fatigue of a girder that developed pre-release cracks is not a concern provided that the maximum nominal tensile stress is limited to $6\sqrt{f_c'}$ (in psi).

#### 1.1.2.2 Studies Related to Fatigue of Prestressed Concrete Girders

*Paulson, Frank and Breen (1983):*

Paulson et al. conducted a study to evaluate the fatigue behavior of prestressing strand in air. Their study included a review of the literature on fatigue of prestressing strand, and presentation of strand fatigue test results that they performed.

They tested 62 in-air strand specimens. The stress ranges that they used were between 22 ksi and 81 ksi, with minimum stresses varying between 75 ksi and 165 ksi. Based on the data obtained from their tests and the data from previous studies, they developed the following relationship for the fatigue of strand as an isolated element:

$$LogN = 11.0 - 3.5LogS_r \qquad (1.3)$$

with a fatigue limit of 20 ksi. Where $N$ is the number of cycles and $S_r$ is the strand stress range in ksi.

They also compared their model with previous fatigue data involving testing of prestressed concrete beams that were flexurally cracked before testing. No correlation existed between the recommended fatigue model and the data from the beam tests. They stated that the determination of the strand stress at a cracked section is the "weak link" in prestressed concrete fatigue. The methods used by different researchers to determine the strand stress range were not consistent, which increases the uncertainty of the data available in literature.

Regarding the applicability of their recommended model to evaluate the fatigue life of prestressed concrete girders, the authors indicated that the fatigue of prestressing strand as an isolated element cannot be directly related to the fatigue of prestressed concrete beams.

The variation in fatigue behavior of the samples was expressed by the authors as follows:

> "Tests conducted on samples of strand representing various manufacturers indicate significant variation among manufacturers. A similar variation was observed in the fatigue performance for two samples of the same product produced by the same manufacturer."

*ACI Committee 215 Report (1997):*

The ACI Committee 215 Report provides information regarding the repeated loading of concrete structures. The information given in the report was based on a review of a large number of studies conducted on this subject. In the part of the report discussing the fatigue of prestressed concrete beams, it was stated that determination of critical stresses in prestressing tendons is quite complex. Because flexural cracking must occur in these members before fatigue of reinforcement can be critical, determination of critical stresses must involve the analysis of cracked sections.

The following statement was made regarding the applicability of the fatigue data obtained from the strand-in-air tests to bridge girders:

> "Concern has been expressed over the applicability of the information to full sized members. Where comparisons have been made, it was found that the observed life of test beams could be substantially less than expected from S-N curves of the tendons alone. Differences were attributed to the difficulty of accurately determining stress in a tendon in a beam, and also to the local effects in the vicinity of a crack. In addition, the probability of a wire fracture in a tendon due to fatigue may be greater in a large beam than in a small specimen tested in air."

The differences in factors such as the loading rate, temperature effects, prestress losses, etc. between the laboratory tests and the bridge girders under service makes the application of the experimentally obtained fatigue data to actual structures controversial. It was stated that the high frequency loading used during laboratory tests caused cyclic creep of concrete, which resulted in a gradual increase in steel stress range and beam deflection. The relatively smaller loading rate in service applications would not normally cause cyclic creep.

The Committee recommended the maximum strand stress range to be $0.06f_{pu}$ based on a cracked section analysis. This limit corresponds to *16.2 ksi* for Grade 270 prestressing strand.

*Overman, Breen and Frank (1984):*

Overman et al. tested eleven full-scale prestressed concrete girders to determine the fatigue strength of the girders. The study by Overman et al. also included an extensive literature review of fatigue of prestressed concrete beams. Strand stress ranges were reported in only seven of the seventeen studies described by Overman et al. in their report. Results from these seven studies summarized by Overman et al. are explained below.

Among the eleven beams Overman et al. tested, eight of them were Texas Type C, and three of them were AASHTO-PCI Type II. The girders were 48 ft long, and had slabs cast composite with the girders. All of the beams, except Beam#7, were tested statically to flexural cracking prior to cyclic loading. The results from cyclic tests are shown in *Table 1.1* in order of

decreasing fatigue life. The table includes the measured strand stress ranges as well as the stress ranges computed determined using the program PBEAM.

The authors indicated concern about fatigue problems in prestressed concrete girders. It was stated that in the prestressed bridge girders subjected to repeated loading that produces $6\sqrt{f_c'}$ nominal tensile stress, fatigue failure of prestressing strands can occur at less than 3.0 million cycles.

Based on the results from this study as well as previously obtained data, which is described below, the authors stated that the following relation recommended by Paulson et al. (1983) can be used to predict the fatigue life of prestressed concrete girders with an endurance limit of 10 ksi:

$$LogN = 11.0 - 3.5LogS_r \qquad (1.4)$$

It was also indicated that prestress losses directly influence the strand stress range, and an accurate assessment of girder fatigue life requires a realistic estimate of prestress losses. The authors stated that strand stress ranges can be approximately calculated with available programs such as PBEAM, using partially cracked section analysis.

As mentioned above, the study by Overman et al. also included an extensive literature review of fatigue of prestressed concrete beams. Results from seven of the seventeen studies described by Overman et al., for which the strand stress ranges were reported, are as follows:

*i.* *Ozell and Ardaman (1956)*: Static and fatigue tests were performed on eight prestressed concrete beams. The beams were 19 ft long with 6 in. by 8 in. rectangular cross sections prestressed with two 7/16 in. strands. Five of the beams failed during fatigue testing. Ozell and Ardaman reported that all of the wire breaks occurred at flexural crack locations. As shown in *Table 1.2*, the strand stress ranges were between 18 ksi and 80 ksi with corresponding fatigue lives of 940,000 cycles and 126,000 cycles, respectively.

*ii.* *Nordby and Venuti (1957)*: Twenty-four static and fatigue tests were performed on beams with 12 ft length and 6 in. by 4.5 in. rectangular cross section. Three of the beams had prestressing steel fractures. The steel stress ranges in these beams were 23.9 ksi, 23.9 ksi and 29.4 ksi. The corresponding fatigue lives were 136,000 cycles, 186,000 cycles and 842,000 cycles, respectively (*Table 1.3*). The difference between the first two and the third

beams was the concrete mix design used. Nordby and Venuti concluded that cracking should not be allowed in beams subjected to repeated loading.

*iii.* *Ozell and Diniz (1958)*: The program involved fatigue testing of six 19 ft long prestressed concrete beams with 8 in. by 10 in. rectangular section prestressed with two ½ in. diameter strands. Strand stress ranges in the failed beams were between 32.5 ksi and 76 ksi with the fatigue lives of 2,273,000 cycles and 186,000 cycles, respectively, as shown in *Table 1.4*. Ozel and Diniz stated that the cracks in the beams act as "stress raisers" and caused fracture of prestressing wires at those locations.

*iv.* *Warner and Hulsbos (1962)*: Six 10 ft long prestressed concrete beams with 6 in. by 12 in. rectangular cross sections prestressed with three 7/16 in. diameter strands were tested. Three of the beams were tested under varying load ranges. The strand stress ranges in the beams tested with the constant load range and the corresponding fatigue lives are listed in *Table 1.5* in order of decreasing fatigue life. Regarding the effect of cracks on the strand stress ranges, Warner and Hulsbos stated that the steel stress increased significantly at crack locations and attained a maximum value at the widest crack. The authors explained the change in strand stress range during fatigue testing as "The response of a prestressed concrete beam may be expected to vary considerably as a result of the application of fatigue loading. This variation is probably due to creep effects, changes in the concrete stress-strain relation, and progressive bond failure between the tension steel and surrounding concrete in the vicinity of the tension cracks."

*v.* *Ozell (1962)*: Six full-scale (26 in. deep 40 ft long) prestressed concrete I-beams with ½ in. diameter strands were tested. The beams did not have a slab. The main purpose of the study was to determine the effects of bends in draped strands on the fatigue life of the beams. All of the beams were flexurally cracked prior to fatigue loading. The loads were such that the nominal bottom fiber stresses varied between 8.7 and $13.0\sqrt{f_c'}$ during fatigue testing. Five of the beams failed during fatigue testing. The calculated strand stress ranges and the fatigue lives of the beams are listed in *Table 1.6.*

*vi.* *Abeles, Brown and Hu (1974)*: Fifty-two prestressed concrete beams were tested. Three different specimen geometries were used: 12 ft 4 in. long beams with 12 in. by 6 in. rectangular section, 12 ft 4 in. long beams with 10 in. by 6 in. rectangular cross section, and

13 ft 9 in. long beams with 9 in. by 4 in. rectangular section. The beams had ¼ in. diameter prestressed and nonprestressed strands. Stress ranges and fatigue lives of the twenty-three beams tested under constant load are listed in *Table 1.7* in order of increasing stress range for six different groups of beams.

*vii.* Rabbat, Karr, Russell and Bruce (1978): Six 48 ft long AASHTO-PCI Type III I-girders (36 in. deep) were tested under cyclic loading. Prior to being subjected to fatigue tests the girders, which had cast-in crack-formers, were loaded to promote flexural cracking. Three of the beams were cycled to $6\sqrt{f_c'}$ nominal bottom fiber concrete stress, while the remaining three were cycled to zero nominal bottom fiber stress. No failure was observed in the beams tested under zero bottom fiber stress. Testing of these beams was stopped after 5 million cycles. The strand stress ranges and the fatigue lives of the beams are given in *Table 1.8*.

Harajli and Naaman (1985):

In a study to investigate the effects of partial prestressing ratio and reinforcing index, Harajli and Naaman tested twelve sets of 9 ft long prestressed concrete beams with 9 in. by 4.5 in. rectangular cross sections. Each set included two beams; one of them was tested under static load to ultimate, and the other one was tested under cyclic load. The minimum and maximum loads during cyclic tests were 40% and 60% of the ultimate load capacity of the static specimen, respectively.

Among the twelve beams tested under fatigue loading, three of them were fully prestressed, three of them were not prestressed, and six of them were partially prestressed with two different partial prestressing ratios. Two different strand diameters, 3/8 in. and 5/16 in. with ultimate strengths of 270 ksi and 250 ksi, respectively, were used. Crack-formers were used in all of the beams, and steel strains were measured with strain gages at crack-former locations. During the fatigue tests, each beam was cycled up to 5 million cycles or failure, whichever occurred first. All six partially prestressed and three non-prestressed beams survived 5 million cycles of loading, while the three fully prestressed beams failed earlier. The bottom fiber concrete stresses, the measured strand stress ranges and the fatigue lives of the fully and partially prestressed beams are shown in *Table 1.9*. As seen in the table, larger strand stress ranges were measured as

fatigue testing progressed. The possible reasons for this phenomenon are the reduction in the effective prestress resulting from strand slippage, and stress redistribution due to cyclic creep of concrete. The authors indicated that no strand slip was observed during the tests and that the stress range increase is mainly due to cyclic creep of concrete. Authors explained the behavior of the beams during fatigue testing with the following statement:

> "The failure of one wire was generally accompanied by a sudden jump in the residual deflection of the load-deflection hysteresis loop, a reduction in stiffness, an increase in the area enclosed within the hysteresis loop…. In the first few hundred cycles there is relatively sharp increase in deflection and crack width with increasing number of cycles, followed by a second portion with a steady state increase up to 80%-90% of fatigue life. Finally, the third portion corresponds to a sharp increase in deflection and crack width leading to failure. This third portion was clearly observed for the beams that failed during cycling."

It was concluded that increased strand stress range together with the fretting of the wires due to opening and closing of the cracks caused the prestressing strands to fracture at the location of flexural cracks.

*Muller and Dux (1994):*

Muller and Dux studied the fatigue behavior of beams with inclined strands. They tested 37 prestressed concrete box beams; 15 of them with 5/16 in. diameter straight strands, 7 of them with 5/16 in. diameter deflected strands, and 15 of them with 1/2 in. diameter deflected strands. The beams were 12.8 in. deep box sections 17 ft long. All the beams were subjected to static testing and cracked to the lowest tendon level prior to cycling testing.

Calculated strand stress ranges were used to make comparison among the beams. The authors explained the reason for computing the stress ranges rather than measuring the strand stresses as follows:

> "Extensive strain gaging would have been needed to ensure that reinforcement was instrumented precisely where the initial damage was to occur. The option of using crack-formers was rejected to allow natural

> cracking to arise….it is argued later that accelerated failure was in part due to combined flexure and extension of strands occurring locally at cracks, and this implies that measurement of the strain range in one wire of a strand would not be sufficient to define the average strain range in the strand. It was decided therefore to calculate strain ranges in each strand using measured material properties and the principles of strain compatibility and equilibrium."

*Table 1.10* presents the strand stress ranges and fatigue lives of the beams with straight strands. The only difference among the different sets of beams shown in the table is the strand diameter.

#### 1.1.2.3 Summary

It can be concluded from the results of the studies reported above that the pre-release cracking problem has been observed in long span prestressed concrete girders with deep sections. The researchers agree that the reason for pre-release cracking is due to the restraints that the girders are subjected to in the prestressing bed prior to release. Results of some of the studies indicated that the pre-release cracks have negligible effect on girder behavior as a result of autogenous healing which caused the concrete to regain the original strength. It should be kept in mind that the pre-release cracks mentioned in the studies by Roller (1993), Zia (1993), and Green (1984) were full-depth cracks. Different from the partial-depth pre-release cracks, closing of full-depth pre-release cracks does not require bending of the beam. Whereas, in the study by Ahlborn (1998) the bending action of the beam to close the pre-release cracks was suspected to be the reason for the reduced flexural cracking capacity. This hypothesis was validated by the analytical work done by Wyffels (2000). In the case of full depth cracks, on the other hand, the action of the girder to close the cracks may cause the loss of some part of the prestress in the strands at crack locations. Depending on the amount of crack, this local loss of prestress should cause a certain reduction in the flexural cracking load of the girder.

Regarding strand fatigue, strand stress range in a beam increases dramatically at the flexural crack location. The increased stress range together with the fretting of the wires during load cycles causes prestressing strands to fracture at the location of flexural cracks.

## 1.2 Objective and Scope

The objective of this research was to experimentally investigate the effect of vertical pre-release cracks on the performance of prestressed concrete girders and to validate the results of the analytical study by Wyffels (2000). The issues investigated were the effect of pre-release cracks on the reduction in flexural cracking load and the possible subsequent reduction in fatigue life of girders due to increased strand stress ranges. As an outcome of the study, recommendations were developed to assist in the decision to accept or reject girders that developed vertical pre-release cracks during fabrication. If cracked girders are accepted without any evaluation, fatigue problems and corrosion of strands during their service life may occur due to early cracking caused by pre-release cracks. On the other hand, if girders which would exhibit ordinary service performance are rejected, this would result in negative economic consequences.

Finite element models of girders with pre-release cracks were prepared with the program ABAQUS to investigate the behavior of girders with pre-release cracks. The models were used to perform a parametric study to optimize the test specimen design and instrumentation. Nineteen full-scale prestressed concrete Mn/DOT 28M girders were fabricated. Two beam lengths, 20 ft and 30 ft, were used. Fourteen of the beams incorporated manmade pre-release cracks with 0.008 or 0.014 in. nominal widths and 6, 16 or 22 in. nominal depths. Eighteen of the beams, eleven of which were 20 ft and seven of which were 30 ft long, were tested under static loading. Eight of the 20 ft beams subjected to static testing had single pre-release cracks, while the remaining three were uncracked. Among the seven 30 ft beams tested under static loading, four of them had multiple pre-release cracks, one of them had single pre-release crack, and two of them were uncracked. Three of the 20 ft beams, two with pre-release cracks and one with no pre-release cracks, were subjected to cyclic testing following the static tests.

The issues investigated with the static tests were the effects of pre-release cracks on concrete strains, flexural crack initiation and re-opening loads, overall beam stiffness, and ultimate flexural capacity. The effects of pre-release cracks on the strand stress range and fatigue life of the beams were evaluated with the help of the cyclic test results.

## 1.3 Organization of the Study

Chapter Two describes the pilot study conducted to determine a procedure for producing cracks in the beams and to investigate the accuracy of finite element models in predicting the behavior of small-scale beams with pre-release cracks.

Chapter Three is a description of the finite element models prepared to optimize the specimen design and instrumentation.

In Chapter Four, a detailed description of the beams is given, including the design, fabrication, instrumentation and testing of the beams.

Chapter Five includes the static and cyclic test results and discussion.

Chapter Six contains the conclusions, and Chapter 7 provides recommendations to be used as acceptance criteria for girders with pre-release cracks.

# CHAPTER TWO
# PILOT STUDY

A pilot study was conducted to determine the most suitable way of producing manmade pre-release cracks in the beams and to investigate the accuracy of finite element models in predicting the behavior of small-scale beams with pre-release cracks produced by these crack-formers. Manmade cracks were incorporated in the test specimens to facilitate comparison of the results between the analytical and experimental studies. In this way, cracks with the same geometry as the ones in the finite element models were created in the test beams at the desired locations.

The pilot study mainly included two phases: crack simulation and flexural testing of small-scale post-tensioned specimens. In this chapter, only the results obtained from the testing of the small-scale post-tensioned beams will be presented. The information about the crack simulation phase of the pilot study as well as the modeling, construction, and instrumentation of the post-tensioned beams can be found in Appendix A.

## 2.1 Small-Scale Post-Tensioned Beams

Three small-scale post-tensioned beams with pre-release cracks were constructed and tested to investigate the accuracy of the finite element model in predicting the behavior of the cracks and the beam itself. Finite element models were also prepared to optimize the beam dimensions, amount of post-tensioning force, and the pre-release crack dimensions. The test beams were 11 ft long with 10 ft clear span and loaded with three-point bending. Each beam had two pre-release cracks with the same crack width (0.01 in.) but different crack depths (4 in., 5 in., or 6 in.) as shown in *Fig. 2.1*. After casting and curing the concrete, each beam was post-tensioned using one 1 in. diameter high strength threaded rod. The post-tensioning force was measured using a load cell. The beams were externally instrumented with strain gages near the bottom surface and with LVDTs over the pre-release cracks. The design, construction, instrumentation, and testing of the beams are documented in Appendix A.

### 2.1.1 Testing and Test Results

The beams were tested in three-point bending with the load applied at midspan. In this configuration, the maximum positive moment and hence the maximum bottom fiber tensile strain occurred below the load point, i.e., at the midspan. Therefore, with this type of loading the first flexural crack would be expected to develop at the midspan if the pre-release cracks did not have any effect. The ultimate aim of these pilot tests was to verify the finite element study result which predicted that the first flexural cracking would occur below the deeper pre-release crack even though the tensile strain due to loading was not maximum there.

The beams were subjected to a displacement controlled loading with a rate of 0.025 in/min. The load was monotonically increased until a stabilized flexural crack pattern was obtained. Because the post-tensioning rod was not bonded to the concrete in the beams, fewer cracks with larger widths were expected to develop than would occur in beams with bonded reinforcement. In all three beams only three flexural cracks occurred with crack widths as large as 0.1 in. After the propagation of the flexural cracks stabilized, the loading was stopped and the beams were unloaded.

As predicted by the finite element analyses, the first of the three flexural cracks occurred below the deepest pre-release crack, the second flexural crack occurred below the shallower pre-release crack, and the third flexural crack occurred at the midspan. For each beam, the load at which these three flexural cracks occurred was recorded. The characteristics of the flexural cracks below the pre-release cracks and those at the midspan were different. For all three beams the flexural crack at the midspan had several branches. The branches became inclined as the crack approached the mid-height of the beam as depicted in *Fig. 2.2*. Some of the branches were almost horizontal. This might be due to the effect of the neoprene pad that was used to spread the actuator load in the beam. Because the size of the pad was large, the actuator load was transferred to the beam as a uniformly distributed load over the pad area, which changed the path that the compressive load followed, and caused tensile strains in the direction of the depth of the beam at approximately mid-depth. On the other hand, the flexural cracks below the pre-release cracks were relatively straight and vertical as a result of the reduced compressive strain below the pre-release cracks due to the closure of the cracks, as shown in *Figs. 2.3* and *2.4*. The strain changes that the closing of pre-release cracks cause in the beam are explained in Chapter 3. The

flexural cracks that occurred below the pre-release cracks stabilized at a distance of approximately 2 in. below the tip of the pre-release cracks when the loading was stopped. The pre-release cracks were observed to close completely after the formation of flexural cracks. Following the unloading of the beams, the pre-release cracks nearly came back to their original widths while the flexural cracks closed completely.

#### 2.1.1.1 Flexural Cracking Loads

The data collected from the strain gages were used to determine the load at which each flexural crack initiated. *Figure 2.5* shows the strain readings from the strain gages placed below the 5 in. deep pre-release crack on beam PT1, plotted against load. The relative location of the gages is also shown in the figure. Note that all loads referred to in this chapter are the loads applied by the actuator. The total load carried by the beams was equal to the actuator load plus the self-weight of the beams. As shown in the figure, the section where gage SG10 was located was less stiff than the other sections. In other words, for the same load, the tensile strain recorded by SG10 was more than the strain recorded by other gages. This is because of the tensile strain concentration that occurred below the pre-release crack due to the closing of the crack as the load increased.

Although the values of the strains recorded by strain gages may not accurately reflect the average strains at the gage location, because the gages used in these beams were only 10 mm in length (too small to adequately average the strain over concrete paste and aggregate), the strains were useful in determining the cracking loads. When a flexural crack occurs, the gages close to the location of the crack show a sudden reduction in tensile strain. After this sudden tensile strain relief, the measured strain in the vicinity of the crack remains constant as loading continues. This repeatable behavior can be used to determine the cracking loads. The cracking load for the beam PT1 was determined to be 4.9 kips from the readings of gage SG9 in *Fig. 2.5*. Gage SG10 also indicated this cracking load with a jump in the tensile strain followed by strain relief. It should be noted that the cracking loads identified in *Figs. 2.2*, *2.3*, and *2.4* are the loads at which these cracks were visually observed during the load tests. These loads are larger than the cracking loads determined from the strain gage data, because after the formation of the cracks more load needed to be applied to the beams so that the cracks became visible.

The cracking loads for all three beams were determined from the strain gage readings as described above and are tabulated in *Table 2.1*. The cracking loads predicted by the finite element models are also included in the table. As mentioned earlier, the flexural crack with the lowest cracking load always occurred under the deepest pre-release crack, the flexural crack with the next highest cracking load always occurred under the shallower pre-release crack, and the flexural crack with the largest cracking load always occurred at midspan as predicted by the finite element models. As seen in the table, the predicted cracking loads were in good agreement with the measured loads. For example, for the beam PT1, the finite element model predicted a 47% reduction in the cracking load from a beam that had no pre-release crack (5.0 kips versus 9.5 kips). The measured cracking loads for this beam indicated a 51% reduction (4.9 kips versus 9.9 kips). For beams PT2 and PT3 the correlations between the predicted and measured cracking loads were not as good as for the case of PT1. This might be due to the difference in pre-release crack geometry in these beams (See Appendix A for documentation on construction of the beams).

#### 2.1.2.2 Pre-Release Crack Closure

Closure of the pre-release cracks was monitored by LVDTs placed across the cracks as the beams were loaded. A typical plot of load versus pre-release crack closure for the 5 in. deep pre-release crack of beam PT1 is shown in *Fig. 2.6*. As loading continued, the slopes of the curves decreased which indicated a reduction in the stiffness due to the formation of a flexural crack below the pre-release crack. The load at which this occurred is shown by the horizontal dashed line in the figure. It should be noted that for this particular beam, the flexural cracking load indicated by the LVDTs was the same as that determined from the strain gage readings. With further increase in load, the stiffness of the section increased, indicating the closing of the pre-release crack. The two sides of the pre-release crack, which were apart from each other at the beginning of the test, started to come in contact as loading continued. At this point the concrete cross section at the crack location increased by the closing of the pre-release crack, and overcame the concrete section lost by flexural cracking, and the stiffness of the section exceeded the initial stiffness. At the level of each LVDT, the pre-release crack closed completely at the load where the slope of the curve belonging to that particular LVDT no longer changed. After this load, the displacements measured by the LVDTs were only due to the straining of concrete.

As shown in the figure, the final slopes of the curves for the three LVDTs were different. This was an expected result, because the LVDTs were at different heights. LVDT readings were due to the strains at that section and the strain was proportional to the distance from the neutral axis when the crack closed. LVDT 10 was located near the neutral axis of the section therefore, after the pre-release crack closed completely at this level, there were negligible strains and LVDT10 did not read any displacement. This phenomenon is shown by the vertical portion of the load versus displacement curve of LVDT10. LVDT12 was located at the top of the section and it had the largest distance to the neutral axis. At this level of the section, the value of compressive strain in concrete after the complete closure of the pre-release crack was the largest. As a result, LVDT12 measured displacements even after the pre-release crack closed completely, as indicated by the final portion of the load versus displacement curve of this LVDT.

*Figure 2.7* shows a comparison of the closing behaviors of 4 in. and 5 in. deep pre-release cracks in beam PT1. The displacements measured by LVDT12, which was measuring the closing of the 5 in. deep crack had a smaller initial slope than the displacements measured by LVDT9. This resulted, because there was less concrete below the 5 in. deep crack than the 4 in. deep crack, and hence the section with the 5 in. deep pre-release crack had a smaller moment of inertia. Also, marked on the figure are the regions where flexural cracking occurred. It is clear that the flexural crack below the deeper pre-release crack occurred earlier than the one below the shallower crack. When the pre-release cracks closed completely, the displacement measured by LVDT9 was larger than the displacement measured by LVDT12. This suggests that even though the crack-formers used to make these two cracks had the same width, the final width of the 4 in. deep pre-release crack was larger than that of the 5 in. deep crack. In the figure it is also seen that the slopes of the curves after the complete closure of the pre-release cracks were different. This was because of the difference in the stiffness of the sections after the complete closure of the pre-release cracks. As mentioned earlier, the distance between the end of the flexural cracks and the tip of the pre-release cracks was constant (i.e. approximately 2 in.) for all pre-release crack depths in all three beams. This means that the flexural crack below the 4 in. deep pre-release crack was longer than the flexural crack below the 5 in. deep pre-release crack. As a result, the section with 5 in. deep pre-release crack had a larger concrete area, and hence a larger stiffness than the section with the 4 in. deep pre-release crack after the complete closure of both pre-

release cracks. This was the reason that the load versus displacement curve of LVDT12 had a larger stiffness than that of LVDT9 after the pre-release cracks closed completely.

# CHAPTER THREE
# FINITE ELEMENT ANALYSIS

Two-dimensional finite element models were created with ABAQUS software to optimize specimen design. The aim was to determine the effects of pre-release cracks on the girder stresses and the flexural cracking load of the proposed test girders. The effect of pre-release crack size, geometry and interaction was investigated with models involving a single crack, and models involving three cracks. The models consisted of simply-supported beams having Mn/DOT 28M cross sections with pre-release cracks in them. There were three groups of models created: single crack models, multiple crack models, and three-point bending models. The following sections describe the model descriptions and results obtained from each of these models, separately.

## 3.1 Single Crack Models

Models of 20 ft long beams with a single pre-release crack placed at the midspan were used to investigate the effect of the size and geometry of pre-release cracks on girder stresses and the cracking load of the girders. A model with identical geometry but with no pre-release crack was also prepared to compare the results to those obtained from the models incorporating a crack.

### 3.1.1 Model Description

The models were 28 in. deep I-shaped cross sections spanning 19 ft. 2 in. between simple supports. The total length of the models was 20 ft, and on both ends, support conditions were defined at the nodes 5 in. away from the ends. The concrete beam was modeled using CPS8R two-dimensional solid elements. CPS8R elements are 8-node biquadratic reduced integration plane stress elements. Because the models had I–shaped cross sections, the width of the elements at different depths of the cross section differed. The triangular areas between the web and flanges in the Mn/DOT 28M sections needed to be modified in the ABAQUS models because the width of these two-dimensional elements had to be constant. To account for the changes in the width of the cross section, nine element sets with different element widths were created. These element sets with different widths were connected to each other at the element boundaries. *Figure 3.1*

shows the cross section of the Mn/DOT 28M section together with the section used in the ABAQUS models. As shown in the figure, the triangular areas in the Mn/DOT 28M section were replaced by series of rectangular areas. The dimensions of the rectangular areas were adjusted such that the cross-sectional area of the model was the same as that of the Mn/DOT 28M while providing a moment of inertia of the model similar to that of the original cross section. The sectional properties of the Mn/DOT 28M and ABAQUS model are given in *Table 3.1*.

In the models, the sizes of the elements were different depending on the location of the element in the model. Generally, a finer mesh was used near the pre-release crack location to be able to capture the local abrupt stress changes around the crack and to observe the closing of the pre-release crack at different stages of loading. To save time and memory space during the analyses, the length of the elements was increased gradually away from the pre-release crack location while keeping the depth of the elements at 1 in. The length of the elements in the portion between the midspan and 20 in. away from midspan was 0.5 in. This length was increased to 2.5 in. along the next 50 in. portion of the model. In the last 50 in. portion, the length of the elements was 5 in., resulting in the largest aspect ratio of 5. The same distribution of element lengths was used on both sides of the midspan.

The prestressing strands inside the beams were modeled with T2D2 linear truss elements placed in one layer at a distance of 2 in. from the bottom of the beams. These linear elements were connected to two nodes and could transfer only axial loads between the nodes. The total area of the prestressing strands of 0.612 $in^2$ was assigned to one line of truss elements because the beams were modeled as two-dimensional, and there was only one set of nodes in the width direction of the beams. The prestressing force was introduced into the models with an initial stress assigned to these truss elements. Because the reduction in the prestressing force due to the elastic shortening of concrete was taken care of in the models during the first step of the analysis, the value of initial stress given to the truss elements was such that the value of prestress after the first analysis step (self-weight and prestressing force applied only) would give the desired value of prestress after transfer. In the models, 202.5 ksi of prestress was introduced to the truss elements, which resulted in a compressive stress of 970 psi at the midspan bottom fiber after the application of prestress and the self weight of the girder.

The pre-release cracks were created using unidirectional gap elements (GAPUNI) between the nodes on the two sides of the crack. Each GAPUNI element had an initial separation distance equal to the pre-release crack opening at that location. As the crack closed, the length of the GAPUNI elements became smaller and when the crack closed completely, the GAPUNI elements enabled the transfer of compressive stresses across the crack. The meshing of the pre-release cracks in Mn/DOT 28M sections is shown in *Fig. 3.2*. In the figure, only the half of the cross section is shown due to symmetry. Pre-release crack geometry and crack dimensions are discussed in Section 3.1.2.

The stress-strain model defined for concrete had a bilinear elastic part with two different moduli of elasticity followed by a perfectly plastic plateau. The focus of the project was the beam behavior until the first occurrence of flexural cracking (i.e., the load at which the bottom fiber concrete stress reached the modulus of rupture of concrete). For a beam without a pre-release crack, the concrete would be expected to remain elastic throughout the cross section to this loading condition. A concrete model with a plastic part was used because for the case of the beams with pre-release cracks, as the pre-release crack closed, the stresses in the vicinity of the crack tip exceeded the yield strength of concrete. The concrete stress-strain relationship that was defined in the ABAQUS models is shown in *Fig. 3.3*. Superimposed on the same figure is the stress-strain curve obtained from concrete cylinders cast with the test specimens and tested at 28 days. A linear stress-strain relation with a modulus of elasticity of 29,000 ksi was used for the steel strand. Because the stress in the prestressing strands remained within the elastic limit, there was no need to define a plastic portion in the steel stress-strain curve.

The boundary conditions imposed on the models were restraint of both the horizontal and vertical degrees of freedom at the left support, and restraint of only the vertical degree of freedom at the right support. These restraints were defined at the nodes that were located 5 in. away from the ends of the beams at the bottom row of nodes to correspond with the center of bearing.

There were three types of loads applied to the models. These were the prestressing force, self-weight of the models, and point loads. In the first analysis step only the prestressing force and the self-weight of the models were introduced. The total prestressing force was 123,930 lbs, which resulted from 202.5 ksi stress given to the truss elements with 0.612 $in^2$ area. The value of

the self-weight was 299 lb/ft. Starting from the second step, two point loads were applied in an incremental manner with 2000 lb increments at each step.

The location of the point loads on the models was selected such that the pre-release crack would be in the constant moment region. As shown in *Fig. 3.4*, the point loads were positioned 30 in. away from the pre-release crack on either side. The distance between the pre-release crack and the point loads was chosen to be more than the depth of the cross section to eliminate any effect of the stress concentration from load points on the closing behavior of the crack.

### 3.1.2 Pre-Release Crack Geometry

Two different pre-release crack geometries were investigated. Cracks with "rectangular" and "tapered" cross sections were modeled. Even though the cracks observed in the field had cross sections that were closer to a V-shape, it was not feasible to fabricate a manmade perfectly V-shaped crack. For this reason, cracks with rectangular geometry were used initially in ABAQUS. The crack geometry was later modified to a tapered cross section to better represent the cracks that would be both realistic and practically producible in the test beams. Most of the analyses were done with the models involving rectangular cross section cracks. Some of these results were validated with models involving tapered cracks. *Figure 3.5* shows the rectangular and tapered crack geometries used in the models.

#### 3.1.2.1 Rectangular Cross Section Cracks

To study the effect of pre-release crack dimensions, rectangular cracks with four different crack widths and ten different crack depths were modeled. Crack widths were between 0.006 in. and 0.014 in., and crack depths were between 6 in. and 24 in. The opening of the rectangular cracks was equal to the designated width of the pre-release crack at the top and that width was maintained through the crack depth to the nodes just above the crack tip. From that point to the crack tip a triangular shape was imposed so that the crack had zero opening at the tip.

During the analyses it was observed that the pre-release cracks started to close from the top of the section. This was because of the rectangular crack geometry used in the models. In addition to this, pre-release cracks did not close completely in any of the models prior to flexural cracking. The models involving pre-release cracks with smaller depths and larger widths had larger resistance to crack closure. In the model with the 5 in. deep and 0.014 in. wide crack, the

pre-release crack remained completely open at the flexural cracking load. This resistance to pre-release crack closure was due to the large eccentricity of the prestressing force. In the models, prestressing force was applied through the truss elements located only two inches from the bottom of the models. In girders that are in service, the location of the center of gravity of prestressing strands is usually higher (i.e. the strand eccentricity is usually smaller). The reason that the location of the prestressing strands in FE models was lower was due to a technical difficulty encountered during the modeling phase. When the tip of the pre-release cracks in the models was coincident with or deeper than the strand level, ABAQUS could not execute the input file. In cases where cracks cross through the prestressing strands, a bond/slip model would be required to describe the behavior at the strand-concrete interface. If the strands had been placed at a higher level in the model to reduce the eccentricity and hence resistance to pre-release crack closure, then the depth of the deepest pre-release crack that could have been modeled would have been reduced. That would have further limited the range of pre-release crack depths to be investigated in the study.

The combinations of crack widths and depths used in the rectangular crack models are given in *Table 3.2*. For each crack width and depth combination shown in the table, a beam with a single pre-release crack at midspan was modeled. A beam with no pre-release crack was also modeled and results from this model were used to determine the effect of the presence of the pre-release crack in each case. For each model, the externally applied point loads required to make the bottom fiber stress equal to the modulus of rupture of concrete was determined. In the rest of this chapter this load is termed the "flexural cracking load". This was the value of each point load that the beam carried in addition to its self-weight when the stress in the element that was located at the bottom of the model reached the tensile strength of concrete, which was taken to be 650 psi. The flexural cracking loads of the models determined this way are tabulated in *Table 3.3*. As shown in the table, the cracking loads of the models that had pre-release cracks were less than the cracking load of the model with no pre-release crack. The last column of the table contains the percent reduction in the flexural cracking load of the girders from the uncracked model. The reduction in the flexural cracking load was calculated as:

$$\%reduction = \frac{P_{cr-pre} - P_{cr-u}}{P_{cr-u}} \times 100 \qquad (3.1)$$

where $P_{cr\text{-}pre}$ is the flexural cracking load of the pre-release crack model being considered, and $P_{cr\text{-}u}$ is the flexural cracking load of the uncracked model.

The reduction in the flexural cracking load was due to the reduction in the stiffness of the pre-release crack section. When the pre-release crack was open, the loads applied to the model were carried by part of the section below the pre-release crack at the midspan section. Because the stiffness of this "partially cracked" section was smaller than the stiffness of an uncracked section, the same load caused more tensile strains at the bottom of the pre-release crack models at the midspan than uncracked models. The extra tensile stresses at the bottom of the beam due to this local reduced stiffness caused the beams with a pre-release crack to crack under lower loads than the beam with no pre-release crack. As the load on the model increased, the pre-release cracks closed as a result of the bending of the cracked section. Closure of the pre-release crack caused an increase in the compressive stress on the elements located around the crack tip.

*Figure 3.6* shows the stresses after the first analysis step in the ABAQUS model involving a 0.014 in. wide, 16 in. deep crack. Because only self-weight and the prestressing force was applied to the model in the first analysis step, the pre-release crack did not close in this step. The stress distribution shown in *Fig. 3.7* was for the same model, but at the end of the seventh analysis step, where the pre-release crack started to close at an applied load of 14,000 lb at each load point. As shown in the figure, the stress changes were local to the pre-release crack location. The stress in the elements away from the pre-release crack location converged to those of the uncracked model. The amount of stress change was dependent on the size of the pre-release crack. Larger stress changes occurred with deeper and wider cracks. Because with a deeper crack, the stiffness of the uncracked part of the section below the crack is smaller. If the crack is wider, it requires more load to close the crack. In this case, more load is carried by the cracked section, which resulted in larger stress changes from an uncracked beam.

The change in the reduction of flexural cracking load with the pre-release crack depth is shown in *Figs. 3.8* through *3.11* for various crack widths. The reductions in the flexural cracking load were calculated using Equation (3.1). As shown in the figures, the reduction in flexural cracking load increases with an increase in pre-release crack depth for all crack widths modeled. This change was almost linear for smaller crack widths. As the crack width became larger, the change with the crack depth deviated from the linear behavior. For example, in *Fig. 3.11*, which

is for a 0.014 in. wide pre-release crack, the rate of change in reduction of flexural cracking load with crack depth was larger for crack depths of 5 in., 6 in., and 7 in. These were the depths for which the pre-release crack was located in the stepwise portion between the top flange and the web of the cross section. So, for these crack depths, the widths of the part of the section corresponding to the pre-release crack were different for different crack depths.

In *Fig. 3.10,* which is for 0.010 in. wide pre-release crack, a similar deviation from the linear behavior is shown for the crack depth of 6 in. This was the only 0.010 in. wide crack located in the part of the section where the width of the cross section was changing with the depth of the cross section. It is seen from the figures that the reduction in the rate of change for the 0.010 in. wide crack is less than the reduction in the rate of change for the 0.014 in. wide crack. Moreover, for the models with 0.006 in. wide cracks the rate of change was almost constant, even for the crack depth of 6 in. (*Figure 3.8*). This suggests that the change in reduction of the flexural cracking load with pre-release crack depth is sensitive to the changes in the width of the cross section of the model if the crack is located in the part of the section where the width of the section is changing. This phenomenon is more pronounced for the models involving wider pre-release cracks. This behavior is probably due to changing of the moment of inertia of the cracked section. As the load on the beam increased, the pre-release crack was forced to close, which resulted in a continuous increase in the moment of inertia of the cracked section. When the pre-release crack is located in the part of the section where the width of the section is changing, then the change in the moment of inertia as the crack closed is not only due to change in the depth of the crack. In this case, the width of the part of the section below the pre-release crack is also changing as the crack closed, which contributes to the change in the moment of inertia, and hence the change in reduction of flexural cracking load.

The reduction in flexural cracking load plotted against the pre-release crack width for different crack depths is shown in *Fig. 3.12*. As shown in the figure, there is a linear trend between the reduction in flexural cracking load and pre-release crack width. For the models with deeper cracks the change was perfectly linear. For the cases with shallower cracks, the rate of reduction started to decrease as the crack became wider because in these cases, the larger portions of the cracks remained open. This decrease in rate is clearly seen on the curve for the 6 in. deep pre-release crack. Among the crack depths shown in the figure, the 6 in. deep pre-release

crack was the only crack that remained completely open at the flexural cracking load. This curve would have been horizontal if the reduction in flexural cracking loads for pre-release cracks wider than 0.014 in. had been plotted. This means that the reduction in flexural cracking load would have been the same for the 6 in. deep crack for all pre-release crack widths larger than 0.014 in. This is because of the fact that the moment of inertia of the cracked section does not change during loading if the crack remains completely open. Therefore, as long as the pre-release crack remains completely open during loading, any change in the crack width does not cause a change in the moment of inertia of the section, and the flexural cracking loads corresponding to these different pre-release crack widths will be the same.

#### 3.1.2.2 Tapered Cracks

The results of tapered pre-release crack models were compared to the results of the models with rectangular cracks. Two different crack widths (0.008 in. and 0.014 in.) at three different crack depths (6 in., 16 in. and 22 in.) were modeled (*Table 3.4*). The geometry of the tapered pre-release cracks used in the ABAQUS models is shown in *Fig. 3.13*. In these models, the crack opening at the top represented the designated crack width. This width was maintained for a certain depth and then decreased linearly across two consecutive nodes whereafter the reduced width was maintained for a certain depth. This procedure was repeated several times until the tip of the crack where the width narrowed to zero over the last two consecutive nodes.

The closing behavior of the tapered pre-release cracks was somewhat different than the closing behavior of the rectangular cracks. As in the case of rectangular cracks, the tapered pre-release cracks started to close from the top. In addition to this, the tapered cracks closed around the locations where the width of the crack changed. This behavior is shown in *Fig. 3.14*, where the stress distribution around the 0.014 in. wide and 16 in. deep pre-release crack at the end of the seventh analysis step is given. The stress distributions for the other tapered pre-release crack models were similar. As shown in the figure, the stress distribution around the tapered pre-release crack was similar to the stress distribution obtained in the case with rectangular pre-release crack (*Figure 3.7*), except for the stress concentrations near the bottom part of the crack. These stress concentrations resulted because of the closing of the tapered pre-release crack at the locations where the width of the crack changed. It should also be noted that the part of the section below the pre-release crack where extra tensile stresses occurred as a result of the closing

of the cracks extended over a longer length of the beam in the case of the tapered pre-release crack.

The flexural cracking loads of the tapered crack models together with the percent reduction in the flexural cracking load from the uncracked model are tabulated in *Table 3.5*. The percent reduction in the flexural cracking load was calculated with Equation 3.1. When the values in this table are compared with those in *Table 3.3*, for the rectangular crack models, it is evident that the tapered crack geometry had a larger effect on the reduction in flexural cracking load. In spite of the differences, both crack models followed similar trends regarding the reduction in flexural cracking load with pre-release crack depth and width.

## 3.2 Multiple Crack Models

Multiple crack models were used to investigate the effect of the interaction of multiple pre-release cracks on girder stresses and flexural cracking loads. In these models, *rectangular* cross section pre-release cracks were used and the width and depth of the cracks were kept constant at 0.014 in. and 16 in., respectively. The parameters that were changed were the number of pre-release cracks and the spacing between the cracks.

### 3.2.1 Model Description

These models had the same cross section as the single crack models. Concrete beams, prestressing strands, and pre-release cracks were modeled in the same way as described in Section 3.1.1 for single crack models. Other than the number of cracks, the only two differences between these two sets of models were the lengths of the models and the position of the loading points. The length of the models was increased to 30 ft (spanning a distance of 29 ft 2 in.) to accommodate the placement of the multiple cracks. A summary of the properties of the multiple crack models is given in *Table 3.6*.

As mentioned above, these models were for the investigation of the case when there were multiple cracks interacting with each other. For this purpose, two models with three pre-release cracks in them were prepared. In these models, the pre-release cracks were widely spaced such that the areas over which the cracks had effect on girder stresses did not interact with each other, or closely spaced such that the areas did overlap. Two additional models, one with no pre-release

crack and one with a single pre-release crack placed at the midspan were also prepared to compare the results.

The models were loaded in four-point bending with the pre-release cracks in the constant moment region as in the case of the single crack models. For widely spaced cracks, the distance between the cracks was 60 in., which was more than twice the depth of the cross section of the model. As shown in *Fig. 3.15*, the loads in this model were applied to two of the nodes located at the top of the model. The load points were 30 in. away from the two outer pre-release cracks. For the closely spaced crack model, the distances between the cracks were 20 in., which was less than the depth of the cross section. In this model, the positions of the load points were the same as in the widely spaced crack model so that the constant moment regions for both models remained the same.

### 3.2.2 Results of Multiple Crack Models

The effect of the spacing of pre-release cracks was investigated with the models. The results are given in *Table 3.7*, which tabulates the flexural cracking loads and the percent reduction in flexural cracking loads of the models for the single and three pre-release cracks relative to the uncracked model. The percent reduction in the flexural cracking loads in this table was calculated with Equation 3.1. As shown in the table, the flexural cracking load of the model with a single pre-release crack was 46% lower than that of the uncracked model. It should be noted that for the same pre-release crack dimensions (0.014 in. wide and 16 in. deep) the reduction in the flexural cracking load of the single crack model was 43% for the 20 ft long beam (*Table 3.3*). The difference in results was due to the different self-weight moments as a result of the different span lengths between the single crack and multiple crack models.

In the widely spaced crack model, the distance between the cracks was 60 in., which was more than twice the depth of the model. Results from the single crack models indicated that the stress changes due to the presence of a pre-release crack occurs over the length which is approximately equal to the depth of the model on each side of the crack. According to this, the pre-release cracks spaced at 60 in. should not interact with each other. This behavior was confirmed in the widely spaced crack model. As seen in *Table 3.7*, the flexural cracking loads of the single crack model and the widely spaced crack model were the same.

*Figure 3.16* shows the stresses in the three widely spaced crack model at the end of the seventh analysis step. As shown, the cracks did not interact with each other. In addition to this, because all three cracks in the widely spaced crack model were in the constant moment region and the moment due to self-weight of the model was small compared to the moment due to the applied loading, the tensile stresses on the elements below each pre-release crack reached the tensile strength of concrete during the same load increment.

In the closely spaced crack model, the distance between the cracks was reduced to 20 in. This distance was less than the depth of the model, suggesting that the affected stress areas of the cracks would overlap and interact with each other. As seen in the table, the flexural cracking load of this model was less than those of the other models. The interaction between the three cracks is also seen in *Fig. 3.17,* which shows the stresses in the model at the end of the seventh analysis step. The total superimposed tensile stresses on the element below the middle pre-release crack was the summation of the tensile stresses at that location caused by each of the three cracks separately. In this model, even though all three cracks were in the constant moment region, the element below the middle pre-release crack reached the tensile strength of concrete before those below the other two pre-release cracks. This resulted because the middle crack was affected by the other two cracks while the outer cracks were each being affected by the middle crack only. As indicated in *Fig. 3.7*, the length of the beam where the 0.014 in. wide, 16 in. deep rectangular pre-release crack was effective on the beam stresses was approximately 21 in. on either side of the crack. Because the pre-release crack spacing in the three closely spaced model was 20 in., the effect of the interaction between the cracks was not too dramatic. If the cracks had been spaced more closely, the effect would have been more pronounced.

## 3.3 Three-Point Bending Study

The aim of the three-point bending study was to show the effect of pre-release cracks on the flexural cracking load of the girders with a different type of loading. The effect that pre-release cracks have on the position where the first flexural crack occurs on the beam was also investigated. The width and depth of *rectangular* pre-release cracks used in these models were 0.014 in. and 16 in., respectively.

### 3.3.1 Model Description

Two 30 ft models with Mn/DOT 28M cross section were used in the three-point bending study. Modeling of concrete beams, prestressing strands, and pre-release cracks were done in the same way as single crack models, and multiple crack models (Sections 3.1.1 and 3.2.1). Different from the other two groups of models, these models were loaded in three-point bending with the load applied at the midspan as shown in *Fig. 3.18*. One of the models was uncracked to serve as a benchmark and the other had two pre-release cracks placed 60 in. away from the midspan on either side. The aim of this study was to show that the first flexural crack would occur below the pre-release cracks, even though the section of maximum moment, and hence the tensile strain was at midspan. A summary of the properties of these models is given in *Table 3.8*.

### 3.3.2 Results of Three-Point Bending Study

The results from the three-point bending models are given in *Table 3.9*. Written in the brackets under the cracking loads are the positions where the first flexural cracks occurred in the models. As shown in the table, the flexural cracking load for the model without pre-release cracks was 33,500 lb. In this model, flexural cracking first occurred at the midspan. This was expected because these models were loaded in three-point bending, so the maximum bending moment occurred at the midspan. The second model had two pre-release cracks, placed 60 in. away from the midspan on either side. The cracking load for this model was 28,000 lb. In this model, tensile stress in the elements below the pre-release cracks reached the tensile strength of concrete before the element at the midspan even though the moment due to loading was maximum at the midspan. Moments due to the applied load at the locations of the pre-release cracks and at the midspan were proportional to the distances between these locations and one of the supports. As shown in *Fig. 3.17*, those distances were 115 in. and 175 in., respectively. This means that the ratio of the moments due to applied loading at the locations of pre-release cracks and at the midspan was 115 / 175 = 0.66. Because the moment due to self-weight of the model was negligibly small compared to the moment due to the applied loading, the same ratio can be used for the total moments. Even though the moment at the pre-release crack locations was 66% of the moment at the midspan, flexural cracking occurred below the pre-release cracks first. In the table, the percent reduction in the cracking moment of the pre-release crack model relative to

the uncracked model was also given. Because the position of the flexural cracking was different in the two models, cracking moments at the locations of first flexural cracking were used for comparison, rather than applied cracking loads. The percent reduction given in the table was calculated as:

$$\%reduction = \frac{M_{cr-pre} - M_{cr-u}}{M_{cr-u}} \times 100 \qquad (3.2)$$

where $M_{cr\text{-}pre}$ is the moment at the location of pre-release cracks in the second model (the model with the pre-release cracks) when the applied load was 28,000 lb, and $M_{cr\text{-}u}$ is the moment at the midspan in the first model (the model with no pre-release crack) when the applied load was 33,500 lb.

# CHAPTER FOUR
# FULL-SCALE BEAMS

Nineteen full-scale prestressed concrete Mn/DOT Type 28M girders were fabricated and tested to experimentally investigate the effect of pre-release crack depth, width and crack spacing on local stresses and flexural cracking load of the girders. The results obtained from the experimental study were used to validate the analytical results obtained by Wyffels and those described in Chapter 3. The possible effect of the presence of pre-release cracks on the fatigue life of the girders was also investigated in the experimental part of the study. There were three groups of beams: single crack series beams, multiple crack series beams, and a three-point bending beam. Manmade pre-release cracks were incorporated in the test specimens to control the crack dimensions and locations to facilitate placement of instrumentation and the comparison between the experimental and finite element study results. Finite element models were utilized for the optimization of the beams, including beam lengths, amount of prestressing force, pre-release crack dimensions and locations. The beams were fabricated at a local prestressing yard and transported to the University of Minnesota Department of Civil Engineering Structures Laboratory, where the static and cyclic testing was done.

## 4.1 Design of the Beams

Finite element models were used to optimize the specimen design. The aim was to investigate the effect of pre-release crack geometry and crack spacing on local girder stresses and flexural cracking load of the girders with the minimum number of test specimens. The cross section and lengths of the beams were selected such that the production of the beams would be possible using standard forms at a local prestressing yard, and the testing could be done economically. The Mn/DOT 28M cross section was selected because it was the smallest I-section produced by the prestressing plant where the beams were fabricated. The cross-sectional dimensions for Mn/DOT 28M are shown in *Fig. 4.1*.

### 4.1.1 Design of Single Crack Series Beams

Beams with a single pre-release crack were used for the investigation of the effect of changes in pre-release crack depth and width on beam stresses and cracking load of the beams. These beams were 20 ft long and they had a single pre-release crack placed at the midspan. A span of 20 ft was chosen because it was the minimum span that both provided the required distance between the pre-release crack and the load points so that they were not interacting, and a shear span-to-depth (*a/d*) ratio of three. *Figure 4.2* shows the pre-release crack, load point and support locations in the single crack series beams. As shown in the figure, the distance between the pre-release crack and load points was 30 in., which was approximately equal to the depth of the cross section. According to the results of the analyses described in the previous chapter, this distance was required to avoid any effect that the stress concentration due to load points may have on the closing behavior of the pre-release crack. With the Mn/DOT 28M section being used, an 84 in. shear span was required to have an *a/d* ratio of three so that the effects due to shear would be minimal. An additional 6 in. of length was provided at both ends of beams to facilitate the placement of the beams in the testing frame. As shown in *Fig. 4.2*, each beam had four 0.6 in. diameter straight strands placed 2 in. from the bottom of the section. The original design specified the use of 0.5 in. diameter strands, but due to a difficulty encountered during placement of instrumentation on the 0.5 in. diameter strands while the beams were being constructed, 0.6 in. diameter strands were utilized in the beams. To account for the increased strand area, the 0.6 in. diameter strands were tensioned to a lower initial stress than the 0.5 in. diameter strands would have been. This way, the total prestressing force applied to the beams remained the same.

In practice, pre-release cracks typically close almost completely following the release of the prestressing strands due to the effect of prestressing force and self-weight of the girders. However, in the test specimens the pre-release cracks were not predicted to close completely under only the prestressing force and the self-weight of the model. This was because of the extreme eccentricity of the prestressing force used in the specimens. The reason for using such large eccentricity in the specimens was because of the problems encountered during the finite element modeling of the beams, as explained in Section 3.1.2.1.

The stress at the top of any section in the model consisted of three components:

$$\sigma_{top} = -\frac{P}{A} + \frac{Pec}{I} - \frac{M_{self}\, c}{I} \qquad (4.1)$$

where negative sign signifies compression, and $P$ is the prestressing force, $A$ is the cross-sectional area, $e$ is the eccentricity of the prestressing force, $c$ is the depth of the neutral axis, $I$ is the moment of inertia of cross section, and $M_{self}$ is the moment at the section due to the self-weight of the model.

The low position of the prestressing strands in the beams yielded a large eccentricity of the prestressing force. The prestressing force with the large eccentricity caused reduced compressive stress at the top of the model. Because of the reduced compressive stress at the top of the model, the pre-release cracks did not close completely under only self-weight and prestressing force. In fact, in the cases with shallow pre-release cracks, the opening of the crack at the top of the section increased when the prestressing force and the self-weight was introduced to the model. This was predicted by the larger resistance to crack closure observed in models with shallow pre-release cracks (Section 3.1.2.1). To decrease the resistance of the beams against the closure of pre-release cracks, the beams were designed to be "lightly prestressed." The value of the total prestressing force applied to the beams was selected to be less than the value used in practice. This was the reason that there were only four prestressing strands in the beams. Although it changes with the length of the girders, in practice there would be more than four strands in the cross section. The initial value of the total prestressing force to be applied to the beams was 124,000 lbs.

Using the results obtained from the finite element study explained in Chapter 3, pre-release crack depths of 6 in., 16 in. and 22 in., and pre-release crack widths of 0.008 in. and 0.014 in. selected to be used in the test beams. These crack depths were representative of shallow cracks, mid-depth cracks and deep cracks observed in the field. *Figure 4.3* shows the depth of these cracks in the Mn/DOT 28M section. The shaded parts of the cross sections in the figure represent the pre-release cracks. Considering the pre-release crack widths of 0.005 in. to 0.025 in. reported by Ahlborn (1998), selected crack widths of 0.008 in. and 0.014 in. were a good representation of pre-release crack widths observed in field. The cross-sectional geometry of the crack-formers used to make pre-release cracks in the test beams is shown in *Fig. 4.4*.

*Table 4.1* shows the test matrix for the single crack series beams. The combination of pre-release crack depth and width used in each of the twelve single crack series beams is listed in the table. Each beam had a name as shown in the table. The letters and numbers in the names of the beams indicated different items. All names started with "*SC*" which indicated that they were a part of the single crack series study. The beams without pre-release cracks had "*UC*" next in their names. This indicated that they were the uncracked "control" beams in this seires. The following numbers 1, 2 and 3 in the names of uncracked beams indicated that the beam was the first, second or third uncracked beam, respectively. The first number in the name of the beams with pre-release cracks indicated the depth of the pre-release crack in that beam in inches. The second number indicated the width of the pre-release crack. This number was either *08* or *14*, indicating pre-release crack widths of 0.008 in. and 0.014 in., respectively. "*R1*" or "*R2*" indicated that the beam was the first or second repeat, respectively, of another beam with the same size pre-release crack. As shown in the table, there were twelve beams, six of which had different size pre-release cracks, three of which were repeat, and three of which were uncracked. The beams SC-UC-3, SC-16-14-R1 and SC-22-14-R2 were saved for the cyclic tests. The other beams were used to investigate flexural crack initiation and re-opening under monotonic loading. Depending on the results from the static tests, some of the tested beams were saved to be tested under cyclic tests in a cracked state.

The beams did not have any *longitudinal* reinforcement other than the prestressing strands. Transverse reinforcement in the beams included No. 4 epoxy coated, double leg steel stirrups. Stirrup spacing changed along the length of the beams as shown in *Fig. 4.5*. Except for the two stirrups placed at 4 in. from each load point, no stirrups were placed in the constant moment region.

### 4.1.2 Design of Multiple Crack Series Beams

The effect of multiple pre-release crack interaction on beam stresses and flexural cracking load was investigated with beams that were 30 ft long and had three pre-release cracks in them. *Figure 4.6* shows the position of the pre-release cracks, load points and support locations in these beams. There were either zero, one or three cracks placed in the constant moment region. *Table 4.2* shows the number of pre-release cracks and crack spacing used in the multiple crack series beams. The name of all beams starts with "*MC*" which indicated that the

beam belonged to the multiple crack series tests. The next group of letters and numbers indicated the number of pre-release cracks in the beam, "*UC*" indicating uncracked, "*1C*" indicating one crack, and "*3C*" indicating three cracks. For uncracked beams (MC-UC-1 and MC-UC-2), the numbers "*1*" and "*2*" indicated that the beams were the first and second uncracked beams, respectively. For the beams with three cracks, the next letter was for crack spacing. If this letter was "*W*", the cracks were widely spaced, and if it was "*C*", the cracks were closely spaced in the beam. Finally, if there was an "*R*" at the end of the beam name, this indicated that the beam was the repeat of another beam. As shown in the table, there were a total of six multiple crack series beams, two uncracked, one with a single crack, and three with multiple cracks. The pre-release cracks in one of the beams with three cracks (MC-3C-W) were widely spaced (*spacing>d*) such that there should be no interaction among the cracks. The remaining two beams (MC-3C-C and MC-3C-C-R) had closely spaced pre-release cracks (*spacing<d*) and were replicates of each other. Position of the pre-release cracks in the multiple crack series beams is shown in *Fig. 4.6*. It should be noted that the shear span-to-depth ratio in the multiple crack series beams was kept the same as that of the single crack series beams. The increased length of the multiple crack series beams was in the constant moment region to accommodate the placement of the three widely placed pre-release cracks which governed the length of the beams. The pre-release cracks in multiple crack series beams were 16 in. deep and 0.014 in. wide. The 16 in. deep cracks were chosen for the multiple crack series because they were easier to make than the 22 in. deep cracks, and they were anticipated to have larger effects on beam stresses than the 6 in. deep cracks. As shown in *Fig. 4.6*, the beams were prestressed with four 0.5 in. diameter prestressing strands, placed at 2 in. above the bottom of the beams and initially tensioned to 202.5 ksi (75% of the ultimate strength). As mentioned earlier, the strands in the multiple crack series beams were tensioned to a higher stress to accommodate the reduced strand area in these beams.

Similar to the single crack series beams, these beams did not have any designed longitudinal reinforcement in addition to the prestressing strands. However, during construction, No. 8 longitudinal bars were placed in the top flange of the multiple crack series beams along the shear span. The aim in placing these bars in the multiple crack series beams was to minimize flexural cracking observed near the ends of some of the single crack series beams following the transfer of the prestressing force (Section 4.2.1.7). Transverse reinforcement in the beams

included No. 4 epoxy coated, double leg steel stirrups. As shown in *Fig. 4.7*, stirrup spacing changed along the length of the beams, and no stirrups were placed in the constant moment region except for the two stirrups placed at 4 in. from the load points.

### 4.1.3 Design of Three-Point Bending Beam

A three-point bending beam setup was used in one of multiple crack series tests to show the effect of pre-release cracks on the flexural cracking load with a different type of loading than the one used for the other beams. As shown in *Fig 4.8*, this beam had two pre-release cracks placed 60 in. away from the midspan on both sides. This beam was designated 3P-2C indicating that it was loaded with three-point bending and had two cracks in it. The pre-release cracks in this beam were 16 in. deep and 0.014 in. wide. The beam was prestressed with four 0.5 in. diameter strands placed 2 in. above the bottom of the beam. The strands were initially tensioned to 202.5 ksi (75% of the ultimate capacity).

The mild steel reinforcement used in this beam was similar to the multiple crack series beams except for the position of stirrups (*Figure 4.9*).

## 4.2 Fabrication of the Beams

This section describes the steps followed during the construction of the test beams. The beams were fabricated at Elk River Concrete Products prestressing plant in Elk River, Minnesota. The construction was done with the cooperation of the plant personnel and University of Minnesota (UMN) personnel. The beams were fabricated in two different casts on a single prestressing bed with the second cast done six days after the first one. In the first cast, the twelve 20 ft span single crack series beams were fabricated. The second cast consisted of six 30 ft span multiple crack series beams and one 30 ft span three-point bending beam. During the fabrication of the beams, standard construction techniques were used, except for the placement of crack-formers between the segments of the steel forms. The construction of the beams included the following steps:

1. Tensioning and instrumentation of the prestressing strands.
2. Placement of the mild steel reinforcement.
3. Placement of the girder forms and crack-formers.
4. Casting of the concrete.

5. Removal of the crack-formers.

6. Removal of the girder forms.

7. Release of the prestressing strands.

Each of these steps is explained in detail in the following sections.

### 4.2.1 Fabrication of 20 ft Beams

Twelve 20 ft beams were cast simultaneously in a 311 ft long prestressing bed. The fabrication was done between November 8 and November 10, 2000. The layout of the beams on the prestressing bed is shown in *Fig. 4.10*.

#### 4.2.1.1 Tensioning the Prestressing Strands

The construction started with cleaning the prestressing bed of snow and scraping the ice from the surface of the bed. The beginning and ending location of each beam was marked on the bed before the placement of the prestressing strands. After 0.6 in. diameter seven wire Grade 270 prestressing strands were placed in the bed, vibrating wire strandmeters and electrical resistance foil gages were installed on the strands. Detailed information about the internal instrumentation put on the beams can be found in Section 4.3.1.

Prestressing of the four 0.6 in. diameter seven wire strands began at 1:40 pm and finished at 1:50 pm on November 8, 2000. A picture of the prestressing operation is shown in *Fig. 4.11*. The load to be applied to each strand was 31,610 lbs. with a required net strand elongation of 16.2 in. A temperature correction was applied, and these values were increased by 5% to account for the temperature difference between the strands and the fresh concrete. After the temperature correction, the value of the target load to be applied to each strand was 33,190 lbs with a net strand elongation of 17.0 in. The procedure used to prestress the strands included tensioning of each strand one at a time to the required elongation value, and checking the value of the applied load from the load cell attached to the hydraulic pump after the required elongation was reached. The total elongation value to which the strands were tensioned included two parts: the net required strand elongation, and the displacement due to seating of strands and chucks at the ends. The applied loads to each of the strands were 500 lbs, 750 lbs, 850 lbs and 1000 lbs more than the required values, respectively, making the total prestressing froce to be 135,860 lbs, and the average force in each strand to be 33,970 lbs. After the prestressing operation was completed,

plastic spacers were placed between the strands and the casting bed to prevent sag of the strands and to keep the strands at the desired locations. Then, the rest of the internal instrumentation including vibrating wire concrete gages, electrical resistance embedded concrete gages and electrical resistance foil strain gages were installed (Section 4.3.1).

#### 4.2.1.2 Placing the Mild Steel Reinforcement

Mild steel reinforcement placed in the beams included vertical double leg stirrups and confinement bars placed in the bottom flange around the strands as shown in *Fig. 4.12*. These two types of reinforcement were No. 4 epoxy coated Grade 60 steel. Placement of the mild steel reinforcement was done during the morning of November 9, 2000. Double leg shear stirrups and the confinement bars around the strands were tied together and to the strands at the locations that were previously marked on the strands.

#### 4.2.1.3 Placing the Girder Forms and Crack-Formers

The girder end forms were first installed. Because in practice it was not common to cast this many beams at once, the precaster did not have enough end forms for the twelve beams. Therefore, existing steel end forms as well as new end forms made from plywood by the plant personnel were used. Steel clamps bolted to the strands and wood braces were used to hold the end forms in place and to keep their orientation vertical. After all the end forms were placed, installation of the steel side forms began. Because crack-formers were going to be placed between the form segments at the midspan of the beams, there had to be a joint at these locations. The layout of form segments was determined such that two form segments met at the midspan of each beam.

The crack forming plates were placed between the form segments at the midspan of the beams after the forms were lifted into their places but before being bolted to each other and to the prestressing bed. Laminated stainless steel plates were used as crack-formers. The thinnest part of the plates was 0.002 in. and the thickest part was 0.014 in. Because the plates were so thin, they were easily bent, wrinkled or even torn. Special care was taken when handling the plates and placing them into their locations. As shown in *Fig. 4.13*, washers and steel shims were placed between the form segments to prevent the crack-formers from being compressed by the forms. After the depth of the part of the crack-former inside the forms was adjusted, the form

segments were bolted to each other and to the prestressing bed. After the bolts were tightened, the crack-formers were checked to make sure that they were loose enough so that they could be pulled out after the concrete set. The crack-formers were then lubricated with form oil.

#### 4.2.1.4 Casting the Concrete

The concrete casting operation began at 3:15 pm and finished at 4:30 pm on November 9, 2000. Concrete mixing was done at a batch plant on site. The concrete mix used in beams, which is documented in *Table 4.3* for the single and multiple crack series beams, was the standard mix used by the precaster. The mix had a water/cement ratio of 0.30, and a slump between 4.5 to 5.5 in. including the use of a superplasticizer. Each beam required approximately 1.5 cubic yards of concrete. A total of, 18 cubic yards of concrete was used for the twelve beams. *Figure 4.14* shows the casting operation. Special care was taken in placing the concrete around the crack-formers so as not to damage them. To achieve this, the forms were filled with concrete at the ends of each beam, and the concrete on both sides of the crack-former was consolidated with hand-held vibrators so that the concrete flowed towards the crack-former (*Figure 4.15*). In this way, the bending of crack-formers due to the unequal concrete pressure on the faces of the crack formers was minimized. *Figures 4.16 and 4.17* show the crack-formers inside the concrete. Casting of each beam was finished by screeding the concrete, and then casting of the next beam commenced. During casting of the beams, cylinder and modulus of rupture samples were taken by the UMN personnel. In addition, concrete cylinder samples were taken by the plant personnel. The plant personnel cured their cylinders overnight using the SURE-CURE Cylinder Mold System, and subsequently tested the cylinders to determine when the concrete reached the required release strength of 5000 psi.

#### 4.2.1.5 Removing the Crack-Formers

Removal of the crack forming plates began one hour after casting was completed. The last plate was pulled out of the concrete approximately one hour and 45 minutes after casting was completed. All plates were pulled out easily except for the crack-formers in beams SC-22-14, SC-22-14-R1 and SC-22-14-R2 (i.e., 22 in. deep by 0.014 in. wide cracks). As shown in *Fig. 4.18*, these crack-formers tore when pulling them out of the concrete, and some small portions of the plates remained inside the beams. These were the crack-formers that produced the deepest

cracks. So, the total pressure due to the concrete was largest on the bottom of those plates. The bottom 3.5 in. length of these plates was 0.002 in. thick, which was the smallest thickness used in the plates. *Figures 4.19* shows a close-up view of a pre-release crack during testing and *Fig. 4.20* shows the surface of a pre-release crack after testing when the beam was broken in two pieces at the pre-release crack location to examine the surface.

After all of the crack-formers were pulled out, the beams were covered with tarps for overnight curing.

#### 4.2.1.6 Removing the Girder Forms

After 14 hours of curing, tests of three of concrete cylinders cured using the SURE-CURE System indicated that the concrete strength was 4800 psi, close to the required release concrete strength of 5000 psi. The tarps over the beams and the forms were removed at this time. A picture of the beams taken after the forms were removed is shown in *Fig. 4.21*.

#### 4.2.1.7 Releasing the Prestressing Strands

The prestressing strands were flame-cut by oxy-acetylene torches. First, the outer two strands were cut in the order shown in *Fig. 4.22*. After the outer strands were cut between all of the beams, the two inner strands were cut following the same order. After all the strands were cut, flexural cracking near the ends of some of the beams was observed. As shown in *Fig. 4.23,* the cracks started at the top of the beams and propagated into the web. The location and depth of these cracks in the beams are given in *Table 4.4*. The reason for the cracking was believed to be due to tensile stresses caused by the prestressing force exceeding the tensile stress capacity of the concrete, because the positive moment due to self-weight of the beams was smaller towards the ends of the beams. In practice, prestressing strands are either draped or debonded near the beam ends to reduce the tensile stresses that develop at the top of the section. For the ease of construction, neither of these methods had been applied to the test specimens to reduce the tensile stresses near the beam ends.

After the strands were cut, the beams were moved to a storage are at the plant where they were kept until transported to the University of Minnesota Civil Engineering Department, Structures Laboratory to be tested.

### 4.2.2 Fabrication of 30 ft Beams

The 30 ft beams were cast six days after the 20 ft beams using the same prestressing bed. As shown in *Fig. 4.24*, there were seven 30 ft beams cast simultaneously. Fabrication of the beams was done between November 14 and November 16, 2000. The same basic procedure used during the production of 20 ft beams was used for these beams. In this section, only the differences in the fabrication of the 30 ft beams relative to that described for the 20 ft beams will be given.

Different from the 20 ft beams, 0.5 in. diameter Grade 270 seven wire strands were used in these beams. The total prestressing force was 132,480 lbs, resulting in an average strand force of 33,120 lbs.

Mild steel reinforcement used in these beams included longitudinal bars placed in the shear spans at the top of the cross section as well as double leg shear stirrups and confinement reinforcement placed around the strands, as shown in *Fig. 4.25*. Stirrups and confinement reinforcement were the same type as those used in 20 ft beams. The longitudinal bars were No. 8 epoxy coated Grade 60 steel and two of them were placed at each end of the beams to control cracking in the end regions.

In these beams, multiple crack-formers were placed between the girder forms. *Figure 4.26* shows the three closely-spaced crack formers placed between the girder forms.

A total of 16 cubic yards of concrete was used for the seven beams. The water/cement ratio of the concrete mix varied between 0.28 to 0.30 with a slump value between 3 to 5.5 in including the use of a superplasticizer. The concrete mix used in the beams is documented in *Table 4.3*.

Removal of the crack forming plates started approximately two hours after the concrete casting was completed, and this operation was completed in 30 minutes.

The average concrete compressive strength at the end of the 19-hour curing period was determined to be 6300 psi from the tests of three cylinders cured using the SURE-CURE System.

The prestressing strands were released using the same procedure explained in Section 4.2.1.7. The cutting order of strands at the ends and between the beams is illustrated in *Fig 4.27*. No flexural cracking was observed after transfer of the prestressing force to the beams.

## 4.3 Instrumentation of the Beams

The beams were instrumented internally during the production, and externally prior to load tests. This section describes the types of instruments used and the procedures followed during the placement of these instruments.

### 4.3.1 Internal Instrumentation

Internal instrumentation was placed during the production of the beams prior to concrete casting. There were four types of gages used to monitor the strand and concrete strains during the production and load tests.

#### 4.3.1.1 Electrical Resistance Strand Strain Gages

Foil type electrical resistance strain gages were bonded to the prestressing strands to measure the strand strains during the tensioning operation and during load testing of the beams. These gages were type FLK-1-11-5LT, produced by Tokyo Sokki Kenkyujo Co. Ltd. There were two groups of electrical resistance strand strain gages. The first group included six gages: three in the first cast (1SRP1, 1SRP2, 1SRP3), and three in the second cast (2SRP1, 2SRP2 and 2SRP3). The gages were placed near the vibrating wire strandmeters, which are described in Section 4.3.1.3. These gages were used to verify the level of initial prestressing force and to verify the strain readings from the vibrating wire strandmeters. They were bonded to the prestressing strands before they were tensioned. Location of these gages on the entire casting bed and in the cross section is shown in *Fig. 4.28*.

The second group of electrical resistance strand strain gages was to be used for measuring the strain in the prestressing strands during load tests. These gages were bonded on the strands after tensioning the strands. The typical location of these gages in the beams is shown in *Fig. 4.29*. As shown in the figure, in the beams with pre-release cracks, these gages were placed in the vicinity of the cracked section to be able to capture the changes in the strand strain due to closing of the crack. In addition, the finite element models predicted the flexural crack initiation to occur below the pre-release cracks; therefore by placing the gages in the vicinity of pre-release cracks, there was a possibility of measuring strand stress ranges at the flexurally cracked section during cyclic tests. The gages in the beams with no pre-release cracks were placed at the

midspan, as shown in the figure. *Figure 4.30* shows a picture of one of these gages after being bonded to the strand and covered with silicone sealant for water protection.

#### 4.3.1.2 Electrical Resistance Concrete Gages

The second type of gage installed during the production of the beams was electrical resistance strain gages embedded in the concrete. These gages, manufactured by Tokyo Sokki Kenkyujo Co. Ltd, were of type PML-60-2L. As shown in *Fig. 4.31*, they were placed between the prestressing strands after tensioning of the strands and before concrete casting. These gages were used to verify that concrete strains measured at the surface were the same as the internal concrete strains. The gages designated CRE1 to CRE4 in *Fig. 4.28* were PML gages. As shown in the figure, these gages were placed in only four of the 20 ft beams. They were placed 18 in. away from the midspan of the beams. As shown in *Fig. 4.31*, the gages were held in position by being tied to two of the prestressing strands.

#### 4.3.1.3 Vibrating Wire Strandmeters

Vibrating wire strandmeters Model 4410 manufactured by Geokon Inc, were used to measure strand strains during tensioning and to measure the prestress losses that occurred until the time the beams were tested. In the first cast, there were a total of seven strandmeters used. As shown in *Fig. 4.28*, three of these gages (SV3, SV4, SV6) were placed inside three different beams, and four of them (SV1, SV2, SV5, SV7) were placed on the free length of the strands between the beams. After release of the prestressing strands, the strandmeters that had been placed between the girders were removed to be used in the second cast, except for SV7, which was damaged during release of the strands. In the second cast, the three strandmeters (SV1, SV2, SV5) were placed between the beams.

The strandmeters were attached to the strands with the help of mounting brackets as shown in *Fig. 4.32*. In the first cast, 0.6 in. diameter prestressing strands were used so that the strandmeters could be mounted to the strands. In the second cast, strandmeters were used with 0.5 in. diameter strandmeters by placing duct tape around the strand before placing the mounting brackets, as the mounting brackets were made for 0.6 in. strand. The strandmeters were placed before tensioning of the strands at the locations shown in *Fig. 4.28*. Elongation of the strands was predicted and taken into consideration when placing the strandmeters so that they would be

positioned in their desired locations after tensioning. The desired location of the strandmeters placed inside the beams was 18 in. away from the midspan section.

#### 4.3.1.4 Vibrating Wire Concrete Gages

Each beam had one Model VCE-4200 vibrating wire concrete strain gage manufactured by Geokon Inc (denoted as "CV" in *Fig. 4.28*). These gages were placed between the strands at locations 18 in. away from the beam midspans as shown in *Fig. 4.33*. CV gages were installed inside the girders to determine the prestress losses.

### 4.3.2 External Instrumentation

After the beams were transported to the University of Minnesota Department of Civil Engineering Structures Laboratory, external instrumentation was placed on the beams before the individual load tests. Because the number of pre-release cracks were different in the single crack series and multiple crack series beams, the amount and location of the instrumentation were different in the two cast series.

#### 4.3.2.1 External Instrumentation of Single Crack Series Beams

External instrumentation put on single crack series beams included Linear Variable Differential Transducers (LVDTs), strain gages and crack detection gages. The aim of the external instrumentation was to monitor the beam deflections, closing of pre-release cracks, concrete strains, formation of flexural cracks, and opening of flexural cracks during the load tests.

*Beam Deflections*

Three LVDTs, one at each end of the beam and one at midspan, were used to measure the vertical midspan deflection of the beams. The location of these LVDTs is shown in *Fig. 4.34*. The LVDTs placed at beam ends had a range of ±0.5 in., and the one placed at the midspan had ±1 in. range. Three LVDTs were required to measure the midspan deflection, because the beams rested on neoprene pads at the supports and the deformations of these pads were included in the deflection readings collected by the midspan LVDT. The average support deflection, obtained by

taking the arithmetic average of the two support LVDTs, was subtracted from the readings of the midspan LVDT to obtain the net midspan deflection.

*Pre-Release Crack Closure*

Closing of pre-release cracks during load tests was monitored by LVDTs positioned over the cracks at different locations along the depth of the beam (*Figure 4.34*). The number of LVDTs used for this purpose was different for each beam depending on the depth of the pre-release crack. For the beams with a 16 in. or a 22 in. deep crack, LVDTs were placed at five different levels along the depth of the crack. For the beams with a 6 in. deep crack, there were four layers of LVDTs placed along the depth of the crack. Typical LVDT locations for the 22 in., 16 in., and 6 in. deep, 0.014 in. wide pre-release cracks in single crack series beams are shown in *Fig. 4.35*.

As shown in the figure, two additional LVDTs were placed next to the crack at the same height as the top and bottom level of LVDTs. These gages were used to identify the load at which the opposite sides of the crack at the level of these LVDTs came in contact. Theoretically, when the pre-release crack is open, concrete on opposite sides of the crack do not touch each other and the LVDTs placed next to the crack do not measure any displacement. When the crack closes and concrete on opposite sides of the crack come in contact, the LVDTs placed next to the crack begin to measure deformation that is due to compression of the concrete. This way the loads at which the pre-release cracks closed at the level of these LVDTs could be determined. This method did not work as well as expected, because the displacements measured by these LVDTs were very small, and as the beams were loaded, the closed part of the pre-release cracks affected the LVDT readings. These LVDTs started to indicate some displacements when the load on the beams reached certain values, even though the pre-release cracks were not closed at the levels of these LVDTs under those loads. These displacements were due to closing of the pre-release cracks at the locations near these LVDTs. The LVDTs placed over the cracks were found to be more reliable to determine the loads at which the pre-release cracks closed. *Figure 4.36* shows a 22 in. deep pre-release crack instrumented with LVDTs.

Two sizes of LVDTs were used. The LVDTs placed next to the pre-release cracks had a ±0.05 in. range. Among the LVDTs placed over cracks, some had ±0.05 in. and some had ±0.1 in. range. The resolution of these LVDTs was 0.1% of the full range of the LVDTs.

*Bottom Fiber Concrete Strain*

Concrete surface gages of type PL-60-11-5LT manufactured by Tokyo Sokki Kenkyujo Co. Ltd were used to measure the concrete strains at the bottom fiber of the beams. These gages were 60 mm in length and the strains recorded by these gages were the average of the strains along their 60 mm gage length. Using gages with such long gage lengths minimized the local effects of the concrete paste and aggregate on the surface strains. As mentioned in Section 4.3.1.2, electrical resistance concrete gages were embedded in the concrete during the fabrication of beams, and the strain readings from these embedded gages were compared with strain readings from the concrete surface gages to verify the reliability of surface strain readings. The external gages were glued to the bottom surface of the beams along the beam length, as shown in *Figs. 4.34* and *4.37*. *Figure 4.38* shows typical locations of these gages at the bottom surface of the cracked and uncracked beams. This was the gage configuration used in most of the beams, even though in some of the beams tested at the beginning of the testing phase, the configuration of concrete gages at bottom surface was slightly different. As shown in the figure, the gages were spaced evenly at a 4 in. spacing. Such close gage spacing along the entire constant moment region was necessary to capture the occurrence of first flexural cracking at the bottom surface. The spacing of the gages in the beams with pre-release cracks was not constant. Gages were placed at a 2 in. spacing around the pre-release crack location (midspan of the beam), and the spacing increased away from this location. From the results of the first static tests, the 2 in. gage spacing was determined to be an appropriate spacing to obtain the variation of concrete strain at the bottom surface in the vicinity of the pre-release crack.

*Concrete Strain through Beam Depth*

Concrete strains were measured through the depth of beams with the same type of gages used for the bottom fiber concrete strains (*Figure 4.34*). These gages were placed on the concrete surface at one side of beams along the depth. Locations of the gages among the beams were

different depending on the geometry of the pre-release cracks. Typical locations of these gages are shown in *Figs. 4.39, 40* and *41*. On the beams with a pre-release crack, the main aim of these gages was to determine the distribution of strain at the section next to the crack. As shown in the figures, the gages were placed more closely around the tip of the pre-release cracks to facilitate the measure of strain concentrations around the crack tip, indicated by the finite element study results. The gages placed next to the pre-release cracks were also used in monitoring the crack closure. When the crack was open, the gages next to the crack did not read any strain. Following the closing of the crack, the gages located around the closed part of the crack began to read compressive strains. This way, the closing behavior of the pre-release cracks was determined. *Figure 4.42* shows a 22 in. deep pre-release crack instrumented with concrete surface gages.

*Crack Detection*

Some of the beams were instrumented with crack detection gages of types CD-02-25A and CD-02-25A manufactured by Measurements Group, Inc. to capture the occurrence of the first flexural cracking during flexural crack initiation load tests (*Figure 4.34*). These gages were basically thin copper alloy wires bonded in a plastic matrix. They were bonded to the concrete surface with adhesive and connected to each other by soldering copper wires between the gages, as shown in *Fig. 4.43*. The resistance between the first and the last gages was monitored with a voltmeter during the cracking load tests. A crack that formed beneath a gage was supposed to fracture the gage and open the electrical circuit. Then, by checking the resistance across each individual gage, the location of cracking was determined. Crack detection gages were utilized only in the first nine tested beams, and not used in the other beams, because no unique correlation could be found between the flexural cracking loads obtained from these gages and the concrete surface gages at the bottom surface of the beams.

#### 4.3.2.2 External Instrumentation of Multiple Crack Series Beams

For multiple crack series beams, similar instrumentation was used as for the single crack series beams, except for some minor differences. Beam deflections were measured in the same way as the single crack series beams. The number and location of LVDTs used to monitor the pre-release crack closure were different. This was because of the limitations in the total number of LVDTs available. *Figure 4.44* shows the location of the pre-release crack LVDTs in the beam

with the three cracks that were closely spaced. This configuration of LVDTs was typical for other multiple crack series beams. *Figure 4.45* shows the pre-release crack LVDTs mounted on a beam with the three closely spaced cracks.

Multiple crack series beams were instrumented with concrete surface gages only at the bottom surface; no gages were placed along the depth of the beams. In *Fig. 4.46*, typical gage locations at the bottom surface of the multiple crack series beams are shown. The figure is for the beam with the three widely spaced cracks, and for the sake of clarity only half of the instrumentation is shown. The gages on the other half of the beam were placed symmetrically with respect to the midspan.

#### 4.3.2.3 External Instrumentation of Three-Point Bending Beam

The instrumentation used for the three-point bending beam consisted only of LVDTs; no strain gages were placed on this beam. There were three LVDTs (one at midspan and one at each end of the beam) to measure the net midspan deflection of the beam. In addition to this, there were four other LVDTs that were used to monitor the pre-release crack closure. Each crack was instrumented with two LVDTs placed across the crack at two different heights. The relative location of these LVDTs with respect to the pre-release cracks were the same as those in the multiple crack series beams, which are shown in *Figs. 4.44* and *4.45*. The flexural cracking load of this beam was only determined visually; no instrumentation was used to determine the flexural cracking load.

## 4.4 Testing of the Beams

Testing of eleven single crack (20 ft span), six multiple crack (30 ft span) and one three-point bending (30 ft span) beams was performed at the University of Minnesota Department of Civil Engineering Structures Laboratory between March 6, 2001 and March 17, 2002. When they were subjected to the first load tests, the beams were between the ages of 116 days and 496 days. During the testing program, several types of loading were applied. All of the beams were subjected to monotonically increasing load until flexural cracking occurred. Crack re-opening tests were performed following the cracking tests in order to determine the zero bottom fiber tension loads. Depending on the results from the cracking and crack re-opening tests, some of the single crack series beams were kept for future fatigue testing. Among the single crack series

beams that were not to be used for fatigue loading, three of them were loaded to ultimate failure. The rest of the single crack series beams not to be used for fatigue testing were tested to "near ultimate" state, in which the testing was stopped before the collapse of beams when a stabilized crack pattern was obtained. All of the multiple crack series beams, which were constructed to investigate the effect of multiple pre-release crack interaction, were only subjected to flexural cracking and crack re-opening tests. The three-point bending beam was subjected to the cracking test only.

### 4.4.1 Static Tests

#### 4.4.1.1 Static Tests of Single Crack Series Beams

The order of the tests applied to the single crack series beams was as follows:

1. Flexural crack initiation test (all beams)
2. Crack re-opening test (all beams)
3. Near-ultimate test (SC-UC-3, SC-06-08, SC-06-14, SC-16-14, SC-22-08, SC-22-14-R1)
4. Ultimate test (SC-06-08, SC-16-14, SC-2208)

For each beam, the dates at which these tests were conducted are given in *Table 4.5*. Each of these tests is discussed in detail in the following sections.

*Test Setup*

The testing frame, shown in *Figs. 4.47* and *4.48*, consisted of two steel columns, one short beam to connect the columns together and to hold the actuator, one spreader beam to distribute the load, and two floor beams to support the test specimens. Before cyclic testing, two diagonal braces were attached to the columns to prevent vibration.

The columns were W12 x 120, 20 ft tall and fixed to the strong floor of the laboratory with two 1-1/2 in. diameter threaded rods. The spacing between the centerline of the columns was 40 in., which was dictated by the hole pattern in the laboratory floor. A W16 x 77 cross member was bolted to the column flanges at 15 ft height. The hydraulic actuator was supported by this cross member. The load was distributed from the actuator to the beams with a 8 ft long W14 x 145 spreader beam bolted to the end of the actuator. Solid steel blocks of dimension 2.5 x 5 x 12 in. cks were attached to each end of the spreader beam at the locations of load points to

provide enough clearance between the test girders and the spreader beam to accommodate the top parts of stirrups extending out of the concrete. The test beams were supported on W27 x 94 beams bolted to the strong floor. The support beams themselves were stabilized by four 4 x 4 x ¼ tube section diagonal braces. The braces were bolted to the floor and to the support beams. The two diagonal braces used to stabilize the columns were added to the loading frame before starting the cyclic tests. The braces were W10 x 33, and bolted to column webs and to the floor. The test beams rested on 1 in. thick, 6 x 24 in.

High-grade neoprene pads of type 70A durometer placed on the support beams (*Figure 4.49*). To distribute the load to the beams evenly across the beam width, 1 in. thick, 3 x 12 in. 80A durometer high-grade neoprene pads were used between the beams and loading blocks (*Figure 4.50*).

The load was provided by a 220 kips capacity, ±5 in. stroke range, fatigue-rated hydraulic actuator manufactured by MTS Systems Corporation. The signal input/output to the actuator was performed by a MTS 407 Controller. Readings from the electrical resistance strain gages and LVDTs were collected electronically using the National Instruments model SCXI-1000 Data Acquisition System. Rate of data collection during the tests was 1 Hz.

*Flexural Crack Initiation Tests of Single Crack Series Beams*

Eleven 20 ft beams were tested under monotonically increasing loading to determine the load at which the first flexural cracking initiated. Eight of the beams had different size pre-release cracks in them while the remaining three were uncracked. The effects of different size pre-release cracks were investigated by comparing the beam strains.

The tests were performed under four point bending with a 60 in. long constant moment region and 84 in. long shear span. The clear span was 19 ft as shown in *Fig. 4.51*. Before the tests, all of the instruments except for the vibrating wire gages were connected to the data acquisition system and continuous data were acquired during testing. Data from the vibrating wire gages were collected manually with a GEOKON Model GK-403 readout box. The load versus actuator stroke data was also pen-plotted and monitored during the tests. During the tests, a careful visual inspection of the girders was done to identify the crack initiation visually as well as with the instrumentation.

Displacement-controlled loading was applied to all beams except for SC-22-14-R2 and SC-UC-1, which were the last two tested beams. Under displacement control, the load was applied at a rate of approximately 0.05 in/min until the load versus stroke plot indicated that the pads placed at the load points and supports were compressed (around 2-3 kips). At this point, the loading rate was decreased to 0.025 in/min. The loading rate was further modified and reduced to 0.0125 in/min when the applied load was close to the expected cracking load in an attempt to determine the flexural crack initiation load visually. The beams were unloaded at a typical rate of 0.1 in/min. For load-controlled tests, the loading rate was 3 kips/min at the beginning of the test, and was reduced to 2 kips/min after the neoprene pads were compressed. In the load-controlled tests, the beams were unloaded at a rate of 6 kips/min.

During the tests, load was monotonically increased from zero until a flexural crack was visually observed. In some of the beams with crack detection gages installed, the gage circuit opened indicating that a crack crossed the gages. In these cases, the loading was paused and the fractured gage was by-passed by connecting a wire across to the neighboring gages on both sides. Generally no crack was visually detected at this load, even though the crack gages indicated a crack had formed. The fracture of crack detection gages was decided to be due to the stretching of concrete. Because the cracking loads obtained by crack detection gages were not found to correlate with any other means of monitoring crack initiation, their use was suspended after the tests of the first seven beams.

When a crack was visually observed at the bottom surface of the beams, loading was paused, and the crack was marked on the beam. Generally, the cracks were small in length and width when they were first detected. After the flexural crack initiation, the loading was restarted and continued until the flexural cracks were easily noticeable with a naked eye so that the placement of LVDTs for crack re-opening tests would be easier and more accurate. The maximum load to which each beam was subjected during the flexural crack initiation test is given in *Table 4.6*. As shown in the table, the maximum applied loads during the flexural crack initiation tests were less than 67 kips, which was the upper load level used during the cyclic tests.

*Crack Re-Opening Tests of Single Crack Series Beams*

Each of the beams was subjected to a crack re-opening test following the flexural crack initiation test to determine the zero bottom fiber tension load. Testing dates for crack re-opening tests are given in *Table 4.5*. In some of the beams, crack re-opening tests were done immediately following the flexural crack initiation tests. When these beams were loaded to the maximum load during flexural crack initiation tests, the loading was paused at that load and instrumentation for the crack re-opening test was placed on the beams. Then, the beams were unloaded to zero load, and loaded back to determine the load at which the flexural crack re-opened. The maximum value of the load to which the beams were subjected during the crack re-opening tests was different for each beam, and was generally half of the maximum load applied in the flexural crack initiation test of that beam. For the rest of the beams, flexural crack initiation tests were completed by unloading the beams to zero load, and crack re-opening tests were performed the next day. Load rates used during crack re-opening tests were similar to those used in the flexural crack initiation tests.

The instrumentation used for crack re-opening tests included LVDTs that were placed over the flexural crack and next to the flexural crack at the bottom surface in the longitudinal direction of the beam, as shown in *Fig. 4.52*. If there was only one major flexural crack, then this crack was instrumented with two sets of LVDTs. If there was more than one flexural crack that had similar crack openings, then two of these cracks were instrumented with a set of LVDTs for each crack. The LVDTs used for this purpose had ±0.05 in. and ±0.10 in. ranges with a resolution of 0.1% of the full range. In addition to these LVDTs, data from the other external instruments placed before cracking tests were collected continuously during the tests.

*Near-Ultimate Tests of Single Crack Series Beams*

The results from flexural crack initiation and crack re-opening tests were used to determine which beams were to be candidates for the cyclic tests. Other beams (beams SC-UC-3, SC-06-08, SC-06-14, SC-16-14, SC-22-08, and SC-22-14-R1) were tested to near-ultimate, because the measured flexural crack initiation and re-opening loads for these beams were larger than the other beams. The other beams were kept for cyclic tests (Section 4.4.2).

The same loading setup used for flexural crack initiation and crack re-opening tests was used for these tests. The beams were subjected to monotonically increasing load with the same loading rates as used in the flexural crack initiation and crack re-opening tests up to the maximum loads listed in *Table 4.7*. Data from support and midspan LVDTs as well as concrete surface gages were collected during the tests. The beams were continuously inspected for cracking and the cracks were marked on the beams.

*Ultimate Tests of Single Crack Series Beams*

Three of the beams (SC-06-08, SC-16-14, and SC-22-08) were tested to ultimate. During testing, the load in the actuator was increased monotonically until the beam collapsed. The dates these tests were conducted are given in *Table 4.5*. From these tests, the ultimate flexural strength of the beams was determined. The test setup used for these tests was the same as that used for the other static tests. Before testing, all of the LVDTS were removed from the beams, and the strain gages were disconnected from the data acquisition system in order not to damage the instruments and other tools used for instrumentation and data acquisition when the beam collapsed. During testing, only the actuator load and stroke data were collected. The same data were pen plotted and monitored during testing.

#### 4.4.1.2 Static Tests of Multiple Crack Series Beams

Flexural crack initiation and crack re-opening tests were conducted on six multiple crack series beams between October 23, 2001 and December 13, 2001. *Table 4.8* shows the dates when each of these tests was conducted.

Because of the increased beam lengths for this test series, the loading frame used for the 20 ft single crack series beams could not be used for testing the 30 ft multiple crack series beams. Another existing frame in the laboratory was modified for testing these beams. This way, when the single crack series beams were being tested in one loading frame, multiple crack series beams were setup for testing in the other frame. The loading frame, shown in *Fig. 4.53*, consisted of a 600 kip capacity MTS Universal Testing Frame, one 18 ft long W14 x 145 spreader beam, and two sets of floor and support beam assemblies. To accommodate the hole pattern in the strong floor, a different support detail than the one used for the 20 ft beams was needed. As shown in *Fig. 4.54*, each support consisted of two 10 in. deep built-up floor beams, one W27 x

94 support beam, one tee bracket, and one 1 in. diameter threaded rod. The threaded rod, tee bracket and one of the floor beams were used to provide stability to the support beam. Different than the 20 ft beams, the 30 ft beams rested on two 1 in. thick, 6 x 24 in. 70A durometer high-grade neoprene pads, because of larger rotations expected at the beam ends (*Figure 4.55*).

During the tests, the load was provided by the ±3 in. stroke range 600 kip capacity Universal Testing Machine controlled by a Model 458.20 controller, both manufactured by MTS Systems Corporation.

The beams were tested using the same procedures used to test the single crack series beams (Section 4.4.1.1). *Figure 4.56* shows the location of supports and load points in multiple crack series beams. A maximum of 60 kip load was applied to all of the multiple crack series beams.

#### 4.4.1.3 Static Test of Three-Point Bending Beam

The beam TP-2C was tested for flexural cracking under three-point bending with the load applied at the midspan of the beam. The same loading frame used for testing the multiple crack series beams was used for testing this beam. Before testing this beam, the spreader beam attached to the crosshead of the testing machine was removed and the load was directly applied through the pin assembly shown in *Fig. 4.57*. As indicated in the figure, a 1 in. thick 6 x 12 in. 80A durometer high-grade neoprene pad was placed at the load point between the pin assembly and the beam.

The flexural crack initiation test of the beam was performed on December 14, 2001 (the fabrication date of this beam was November 15, 2000). The same loading procedure explained before for single crack and multiple crack series beams was followed during the test. First flexural cracking was observed at 35 kips of load at the midspan (below the load point). After formation of the second flexural crack below one of the pre-release cracks, which were located 60 in. on either side of midspan, the loading was stopped at 42 kips, and the beam was unloaded. No crack re-opening test was performed on this beam. In *Fig. 4.58*, the location of supports, load point, and pre-release cracks are shown.

### 4.4.2 Cyclic Tests

Three of the beams were subjected to cyclic loading under constant load amplitude to determine possible effects that the existence of a pre-release crack would have on the fatigue behavior of a girder. The testing date and load range information are tabulated in *Table 4.9*. As shown in the table, two of the beams had similar size pre-release cracks, while the other beam had no pre-release crack in it. The beams were subjected to flexural crack initiation and crack re-opening tests prior to cyclic testing. At the time the cyclic tests began, beam SC-22-14 was the beam with the smallest flexural crack initiation load. It was decided that this beam was the most critical beam with regards to strand stress ranges. Beam SC-UC-1 was one of three single crack series beams with no pre-release crack. This beam was subjected to cyclic testing in order to compare the results with those obtained from beam SC-22-14 and to determine the effects of the existence of the pre-release crack. Beam SC-22-14-R2 was the third beam subjected to cyclic testing. This beam was one of the replicates of beam SC-22-14, and was subjected to cyclic testing in order to validate the results obtained from beam SC-22-14.

As shown in *Table 4.6*, the maximum load applied during the flexural crack initiation and crack re-opening tests was higher than 67 kips, which was the upper load level used in the cyclic tests. The minimum load level during the cyclic tests was 39 kips. Information about the selection of the maximum and minimum load levels is given in the following section.

The same test setup used for static testing of single crack series beams was used for the cyclic tests. Two W10 x 33 diagonal braces were attached to the columns of the testing frame in order to reduce vibration. Load was provided by a 220 kip capacity fatigue-rated actuator manufactured by MTS Systems Corporation. The signal input/output for the first two cyclic tests (beams SC22-14 and SC-UC-1) was done with a MTS 407 controller, while a MTS Flextest IIm controller was used for the third test (beam SC-22-14-R2). The loading rate during the tests was varied between 1.25 Hz and 1.6 Hz.

At various stages of cyclic testing, the testing was stopped and static tests were performed. The static tests were done generally after 1,000, 5,000, 10,000, 50,000, and 100,000 cycles. After 100,000 cycles, static tests were done approximately at every additional 100,000 cycles. Before starting cyclic tests, the major flexural crack was instrumented with two LVDTs to monitor the change in crack width. One of the LVDTs was placed across the crack along the

longitudinal axis of the beam at the bottom surface, while the other LVDT was placed on one side of the beam at the level of the prestressing strands (2 in. from the bottom). In addition to these two LVDTs, three other LVDTs were used to measure the two support displacements and midspan deflection. During testing, data from all LVDTs were collected. This data was plotted with respect to time and actuator load to determine any degradation in the stiffness of the beam. Testing continued to a predetermined number of cycles or failure of the beam, whichever occurred first.

*Nominal Load Levels*

The main considerations in determination of the minimum and maximum load levels for cyclic testing were the strand stress range and the maximum nominal bottom fiber concrete stress. There were also secondary variables to consider when choosing the load range, such as the maximum strand stress, and the load that would cause the flexural crack re-opening. Because of the importance of the load range to the outcome of these tests, analyses were done with RESPONSE-2000 Reinforced Concrete Sectional Analysis Program (Bentz and Collins, 2000), and several options for load ranges to be used were determined. *Figure 4.59* shows the numerically-determined change of strand stress relative to the applied load on the beam.

When calculating the strand stress ranges, sectional properties corresponding to three types of conditions can be used; uncracked section, cracked section, and partially cracked section. The uncracked section analysis could realistically predict the strand stress range only if the beam remained uncracked, or if the cracks remained closed through the maximum applied load during cyclic testing. Fully cracked section analysis, on the other hand, overestimate the strand stress range, because it assumes that the applied load is carried by the fully cracked section after cracking occurs in the beam. In this type of analysis, the intermediate stages that correspond to propagation of the crack between the uncracked and the fully cracked conditions are not considered. The third approach, partially cracked section analysis, takes care of the intermediate stages between the uncracked and the fully cracked conditions by considering the changes in the cross-sectional properties as the crack propagates. In determining the nominal load levels for cyclic tests of the beams, partially cracked analysis results were used because they were deemed to better represent the conditions of the beams during cyclic testing. In the

RESPONSE-2000 analyses for the partially cracked condition, the tensile strength of the concrete was assigned to be zero so that flexural crack opened when the stress at that level reached zero.

The available literature points out that the two most important factors that affect fatigue life are the strand stress range and the maximum bottom fiber stress. For a given value of strand stress range, the maximum bottom fiber stress affects the fatigue life in two ways; as setting the maximum stress in the strand, and by determining if the applied load range includes crack re-opening. This behavior can be illustrated with *Fig. 4.59*. By keeping the strand stress range the same and changing the minimum and the maximum strand stresses, the required minimum and maximum load levels can be adjusted such that the flexural crack goes through re-opening while cycling between the minimum and maximum loads.

In determining the minimum and maximum loads to be applied, several different alternatives including different strand stress ranges and different maximum bottom fiber stresses (and hence different maximum strand stresses) were considered. Among these scenarios, the one shown in *Fig. 4.59* was chosen for cyclic testing of the beams. For the selected scenario, the minimum and maximum loads, and strand stresses at these loads are tabulated in *Table 4.10*. As shown in the table, the minimum and maximum loads were 39 kips 67 kips, respectively. The strand stress range corresponding to these load levels was calculated to be 23.4 ksi for a partially cracked section. The 67 kip maximum load corresponded to a nominal bottom fiber tensile stress of $6\sqrt{f_c'}$. With the minimum load level of 39 kips, flexural cracks were expected to undergo crack re-opening. For the same load range, the calculated strand stress range in an uncracked section was 2.8 ksi. It must be remembered that these calculated strand stress ranges were for a beam with no pre-release crack.

In the study performed by Wyffels (2000) at the University of Minnesota to investigate the strand stress ranges in typical Minnesota Department of Transportation Girders under an HS-25 truck load, the stress ranges were calculated for different parameters including concrete strength, girder type, span length, girder spacing and strand diameter. In this study the stress ranges were calculated considering three different section properties, uncracked, cracked, and partially cracked. According to these results, the 23.4 ksi strand stress range represented a live load that was 20% larger than the load used in Wyffels' study.

# CHAPTER FIVE
# TEST RESULTS

In this chapter, the results of the static and cyclic tests performed on the beams will be presented. First, the results from static and cyclic testing of the single crack series beams will be presented followed by the static test results of the multiple crack series beams. The chapter will close with the results of the three-point bending beam test.

All loads referenced in this chapter are loads applied by the actuator. For the beams loaded under four point bending, the load at each load point is half of this value. The total load carried by the beams is the load applied by the actuator plus the self-weight of the beams. Negative strain values indicate compressive strains.

To describe the beams, the naming system introduced in Sections 4.1.1, 4.1.2, and 4.1.3 will be used throughout this chapter.

## 5.1 Single Crack Series Beams

Eleven 20 ft long beams were tested; eight of which had different size single pre-release cracks while the remaining three had no pre-release cracks. The following sections present the results obtained from testing these beams.

### 5.1.1 Effective Prestress

The amount of effective prestressing force at the time of testing must be known to determine the predicted cracking and crack re-opening loads of the beams. The effective prestressing force can be determined either numerically or experimentally. Numerical determination of the prestressing force includes the determination of the total losses that occurred starting from the time that the strands were tensioned in the prestressing bed. The calculated loss is subtracted from the initial stress to which the strands were tensioned. This way, the value of the effective prestress at any time can be determined. The total prestressing loss at any time includes losses due to elastic shortening of the strands during strand release, relaxation of the steel, and creep and shrinkage of the concrete over time. Even though there are formulae available to determine the value of each loss component, due to the interdependent nature of the components, the losses predicted with these formulae may not give the correct value of the

losses. In addition to this, to obtain realistic results from these formulae, the environmental and loading conditions that the beam is subjected to over time must be known accurately.

Because of the shortcomings of the numerical methods, in this study, the effective prestress at the time of testing was determined experimentally. The method included exposing a small part of the prestressing strands by removing the surrounding concrete and cutting the strands after instrumenting them with strain gages. This procedure will be called "in-situ strand testing" hereafter.

Two of the beams (SC-UC-3 and SC-22-14-R1) were subjected to in-situ strand testing in order to determine the amount of prestress in them. Strand testing was performed after the beams were subjected to "near-ultimate" tests (Chapter 4). The maximum loads applied during near-ultimate tests were 105 kips and 90 kips, respectively, for beams SC-UC-3 and SC-22-14-R1. In each of these beams, two of the strands were exposed over a short length by removing the concrete at the corner of the bottom flange on both sides of the beam. The exposed portions of the strands were approximately 20 in. long and located between one of the load points and support as shown in *Fig. 5.1*. The distance from the beam end was approximately 50 in. This distance was selected to be larger than the transfer length, which was approximately 30 in. (50 times strand diameter) so that the prestress at this location would be the full effective prestress. The concrete surrounding the strands was removed by jackhammering. Each strand was instrumented with three FLK-1-11-5LT type strain gages. As shown in *Fig. 5.2*, the gages were bonded to three individual wires and oriented along the axis of the wires. To prevent any damage to the gages due to heat and unwinding of the strands during cutting, the strands were tied with reinforcement ties at several locations, and wet fabric was wrapped around the strands a short distance away from the gages as shown in *Fig. 5.3*. The strands were flame-cut with an oxy-acetylene torch. During cutting operations data was collected from the strain gages.

Strain readings recorded when the strands were cut are shown in *Figs. 5.4* and *5.5* for beams SC-UC-3 and SC-22-14-R1, respectively. The negative change in strain means that the gages underwent a reduction in tension following the strand cut. As explained above, two strands on each beam were instrumented with three strain gages each. There are two jumps in each figure, which correspond to the cutting of each strand. As shown in the figures, when a strand was cut, all three gages on that strand indicated approximately the same sudden strain decrease.

When the first strand was cut, the gages on the other strand showed a small strain decrease. This was because of the unequal compressive force along the width of the beam that occurred after one of the strands was cut, which resulted in out-of-plane bending of the beam. This out-of-plane bending caused compressive strain on the side of the beam where the strand was not yet cut. The small spikes in the strains that occurred immediately after the strands were cut were probably due to bending of the strands occurring as a result of the energy release when the strands were cut. As shown in the figures, after the second strands were cut, the strain values stabilized.

*Table 5.1* shows the change in strain values recorded by each strain gage. Shown in the same table are the average and the coefficient of variation of the strain values of the six strain gages in each beam. As shown in the table, the average strand strains were 3710 με and 3700 με with coefficient of variations of 3.6 % and 4.4 % for beams SC-UC-3 and SC-22-14-R1, respectively. To convert these strain values into effective strand stress, the modulus of elasticity documented by Lawver (1998) was used. In that study, a similar type of prestressing strand was instrumented with similar strain gages. The strain gages in the study by Lawver were placed on individual wires and oriented along the axis of the wires to find the relation between the strand stress and the strain along the axis of the wires. An "apparent modulus of elasticity" of 32,000 ksi rather than Young's modulus of 29,000 ksi for steel was documented.

Even though the modulus of elasticity reported by Lawver was used in all stress calculations from the measured strand strains, at a later stage in the project, 0.5 in. and 0.6 in. diameter strands used in the test beams were tension tested in order to verify the "apparent modulus of elasticity" reported by Lawver. Description of the procedure and results of the strand tension test can be found in Appendix B. The apparent modulus of elasticity values determined from these tests was 30,000 ksi for 0.5 in. diameter strand, and 31,100 ksi for 0.6 in diameter strand.

Using a modulus of elasticity of *32,000 ksi* and a strand strain of *3700 με*, the effective strand stress was calculated to be *118.4 ksi*. The strands in these beams were initially tensioned to 154 ksi. This resulted in a total prestress loss of *154-118.4=35.6 ksi*, or *35.6/154=23%*. The effective prestressing force was found to be 104,500 lb by multiplying the effective prestress (118.4 ksi) with the total strand area (4x0.22086 $in^2$).

Beam SC-UC-3 had a vibrating wire strandmeter and a vibrating wire concrete gage, and beam SC-22-14-R1 had a vibrating wire concrete gage placed inside the beam at the level of the strands during fabrication (Sections 4.3.1.3 and 4.3.1.4). For beam SC-UC-3, the strain readings collected from the strandmeter and the concrete gage indicated a total prestressing loss of *30.2 ksi* and *18.6 ksi*, respectively, between the time the strands were tensioned and the time the beam was brought into the laboratory for testing. The vibrating wire concrete gage in beam SC-22-14-R1, on the other hand, indicated a *22.3 ksi* prestressing loss. During calculation of the change in strand stress from vibrating wire concrete gage readings, the concrete strain immediately after concrete casting was assumed to be zero. The procedure to calculate losses from vibrating wire concrete gages is explained by Ahlborn (1998).

Strand strain changes in beams SC-UC-3 and SC-22-14-R1 calculated from the vibrating wire gage readings recorded at different stages during fabrication of the beams are given in Appendix C.

### 5.1.2 Static Tests of Single Crack Series Beams

Static test results of the single crack series beams were used to determine the effects that different size pre-release cracks had on beam strains, overall beam stiffness, flexural cracking, flexural crack re-opening and ultimate failure loads of the beams.

#### 5.1.2.1 Concrete Strains

Distribution of concrete strains along the depth and length of the beams were obtained from the electrical resistance gages placed on the concrete surface (Section 4.3.2.1). To ensure the reliability of strain readings obtained from these surface gages, embedded electrical resistance concrete gages were placed inside some of the beams during fabrication (Section 4.3.1.2). Strains measured by the internal and external gages compared well. Detailed documentation of the comparison of concrete strains measured by these two types of gages can be found in Appendix D.

*Concrete Strains through the Beam Depth*

Strain distributions through the depth of the section at several cross sections were measured for beams without pre-release cracks and for the beams with different size cracks.

These strain distributions were compared to determine the effect of the different size pre-release cracks.

*Figures 5.6* and *5.7* show the strain distributions due to the applied loading through the height of one of the beams with no pre-release crack. (Beam SC-UC-2) The former figure was for the midspan section and the latter was for a section 15 in. away from the midspan. Because the constant moment region extended 30 in. on either side of midspan, these two sections were subjected to the same amount of applied moment, and hence had the same strain profile. Even though the moments due to the self-weight of the beam were slightly different for these two sections, this effect is not seen on these plots, because the strains shown in these plots are due to the applied loading only. As seen in the figures, the neutral axes of the sections were 12 in. above the bottom of the beam. The neutral axis location was estimated to be 12.1 in. from calculations.

*Figures 5.8* and *5.9* provide a comparison between the calculated and measured strain profiles for beam SC-16-08. The strain profile in *Fig. 5.8* was obtained by plotting the calculated strain values for the elements with centers located 2 in. away from the cracked section. Locations of these elements with respect to the pre-release crack are indicated on the right side of the figure with small squares. The strain values used in this figure were from the model that had a V-shaped pre-release crack. *Figure 5.9*, on the other hand, shows the measured strains for beam SC-16-08. The gages used to measure these strains were centered 2 in. away from the pre-release crack on one side of the beam. The location of these gages with respect to the crack, and the crack geometry are indicated on the figure. During crack testing of this beam, no flexural cracking was observed visually until 25 kips. The strain profiles in these figures are given for the loads up to 20 kips so that the effect of flexural cracking on the measured strains is eliminated for comparison because finite element models did not take flexural cracking into consideration. When flexural cracking occurred in the test specimen during load tests, the strains measured by the strain gages were noticeably different than if there had been no cracking.

As seen from *Figs. 5.8* and *5.9*, the measured strain profiles for beam SC-16-08 were in good agreement with the predicted strain profiles. As shown in *Fig. 5.9*, the gages placed between 14 in. and 28 in. from the bottom of the beam did not measure any appreciable strain for the 4 and 8 kip loads. This was because the pre-release crack was open at the level of these gages

up to 8 kips. As the load kept increasing, the crack closed starting from the bottom and working toward the top, and the gages started to read compressive strains. The top of the crack remained open at 20 kips during testing. In the predicted strain profile shown in *Fig. 5.8*, on the other hand, the elements located between 16 in. and 28 in. from the bottom of the beam (i.e., top 12 in. of 16 in. deep crack) did not indicate any compressive strain under a 4 kip load. This means that the bottom 4 in. of the pre-release crack (between the depths of 12 in. and 16 in. measured from the bottom of the beam) was closed at 4 kips. When the load increased to 8 kips, the bottom 8 in. of the crack (between the depths of 12 in. and 20 in. measured from the bottom of the beam) was closed. The closing of the pre-release crack progressed as the load increased and the crack closed completely at 20 kips, as shown in the figure.

As shown in *Fig. 5.9*, at 4 kips, the neutral axis of the midspan section in the test beam was located approximately 5 in. from the bottom. This distance was almost 6 in. in the finite element model, because a larger portion of the pre-release crack was closed in the finite element model than in the test beam at that loading. Because the pre-release crack in the finite element model closed at a faster rate than the crack in the test beam, the neutral axis of the midspan section had moved up by a larger amount in the prediction than in the test beam at 20 kips.

When the strain profile in *Fig. 5.9* is compared with the one shown in *Fig. 5.10*, which is the measured strain profile of an uncracked beam for the same load increments, it is seen that there was a compressive strain concentration at the tip of the pre-release crack as the load increased. It is also seen that under the same load the tensile strain at the bottom of the beam with pre-release cracks was much greater than that of an uncracked beam (approximately 3 times as much at 20 kips). These strain changes were due to the reduction in the stiffness of the section at the pre-release crack location. At this section, the load was carried by the uncracked portion of the total cross section below the pre-release crack. The smaller stiffness of this cracked section resulted in larger tensile strains at the bottom fiber, and larger compressive strains at the crack tip than in the uncracked beam. The concrete at the top of the beam had reduced compressive strains relative to that of the uncracked beam because the pre-release crack remained open for some load levels. Compressive strain at the top of the beam could only increase after the pre-release crack closed almost completely.

*Figure 5.11* shows the same type of behavior observed for the beam SC-06-08 with the nominal 6 in. deep 0.008 in. wide crack. The strain distribution of the beam SC-UC-2, which was one of the beams that had no pre-release crack, is superimposed on the figure to make the comparison between the two beams easier. Even though the depth of the pre-release crack in beam SC-06-08 was small compared to the depth of the beam itself, the closure of the crack as the load increased caused increased tensile strains at the bottom of the beam, and increased compressive strains around the crack tip.

*Figure 5.12* shows the strain distribution for the beam SC-22-14 along the section 2 in. away from the pre-release crack under different loads as well as the strain distribution for the uncracked beam SC-UC-2. Locations of the strain gages with respect to the pre-release crack, and the pre-release crack geometry are indicated in the figure. The changes in beam strains due to the existence of the 22 in. deep and 0.014 in. wide pre-release crack are similar to those explained for beam SC-16-08. The reduced stiffness of the section at the pre-release crack location caused increased tensile strains at the bottom of the beam below the pre-release crack. Compressive strains around the tip of the crack increased due to the same reason. Because the depth of the uncracked portion of the section below the pre-release crack was only 6 in. in this beam, the beam had very small resistance to crack closure. Consequently, the 22 in. deep pre-release crack in the beam closed a large amount under small loads. As seen in the figure, the bottom 6 in. of the crack (between the depths of 6 in. and 12 in. measured from the bottom of the beam) was closed at 4 kips. This caused the depth of the section below the pre-release crack that carried the load to increase starting from the very early stages of loading. Due to this situation, the relative position of the part of the section where compressive strain concentration occurred with respect to the pre-release crack tip shifted up in this section compared to the case with the 16 in. deep pre-release crack. In beam SC-16-08, the part of the section where the compressive strain concentration occurred corresponded to the level of the crack tip (*Figure 5.9*). As shown in *Fig. 5.12*, this position was well above the level of the crack tip in beam SC-22-14. The same behavior is seen in *Figs. 5.13* and *5.14*, which show the strain profiles for the same beam (beam SC-22-14) predicted by finite element models using V-shaped and tapered pre-release cracks, respectively. The crack geometries and location of the elements for which the strain values were plotted are also indicated in the figures.

As shown in *Figs. 5.13* and *5.14*, the crack with a V-shaped geometry started to close from the crack bottom as the load increased. On the other hand, the crack with tapered geometry started to close from both the bottom and the very top of the crack. Comparison of the strain profiles in these two figures with the measured strain distribution shown in *Fig. 5.12* suggests that the geometry of the pre-release crack in the test beam was closer to a V-shaped crack rather than a tapered crack. An analysis of the results of the V-shaped and tapered crack models indicated that the pre-release cracks in the other beams also behaved more similar to the V-shaped models.

In *Fig. 5.15,* the strain distributions at the section 15 in. away from the pre-release crack are shown for beam SC-22-14. Strain distributions at the same section of an uncracked beam (beam SC-UC-2) are also plotted in the same figure. When the strain distributions in this figure are compared with those in *Fig. 5.12*, it is clear that as distance from the pre-release crack increases, the strain distribution approaches that of an uncracked beam, in other words, at a section far enough away from the pre-release crack, the effect of the crack on the girder strains is going to vanish.

The pre-release cracks in the beams closed from bottom to the top. Because of this, the top of the crack remained open longer than the bottom of the crack during loading. This behavior resulted in strain distributions such as the one shown in *Fig. 5.15*, where the strains at the bottom parts of the section are closer to the values in an uncracked beam than the strains at the top. As shown in the figure, the strains at the top of the beam with a pre-release crack were smaller than those in an uncracked beam even at a section 15 in. away from the crack, which suggests that the pre-release crack still had an effect on strains at this location.

The pre-release crack widths used in the test beams were selected to be sufficiently small to realistically represent cases observed in the field. One of the shortcomings of using such small crack widths was that any small change that undeliberately occurred in the geometry of the crack changed the strain profile. This is illustrated in *Fig. 5.16*, where the strain profile at the section 2 in. away from the pre-release crack in the beam SC-16-14 is plotted. The strain changes from an uncracked beam due to the existence of the pre-release crack for this beam were similar to the cases discussed earlier. The zigzags shown in the strain profiles between 16.5 in. and 25 in. depths measured from the bottom of the beam were probably due to irregularities in the crack

geometry localized in that region. These irregularities caused early contact of opposite sides along some portions of the crack face. These kind of defects are inevitable in producing manmade cracks of such small widths.

*Concrete Strains along the Beam Length*

As discussed in the previous section, the reduced stiffness at the pre-release crack location was determined to cause increased tensile strains at the bottom of the beam near the crack location. This behavior can be seen more clearly in the strain data from the gages placed on the bottom surface of the beams. *Figure 5.17* shows such data plotted with respect to gage distance from the centerline of the beam for beam SC-UC-2. This beam was one of the beams with no pre-release crack. The region where the bending moment was constant is also indicated on the figure. Because the strain readings were due to the applied load only, and did not include the effect of self-weight of the beam, the strain distribution along the length of the beam in the constant moment region was nearly uniform.

At 45 kips, flexural cracking occurred at the bottom surface of the beam. Occurrence of this cracking is evident by the constant tensile strain readings of the gage located 12 in. from the centerline with increasing load. When the flexural crack occurred, the tensile strains decreased in the vicinity of the crack, approaching zero on the crack surfaces. Because the strain gages used in the beams were 2.4 in. long, the strains measured by these gages represent the average concrete strains over a 2.4 in. gage length. Because of this, the decrease in tensile strains due to formation of a flexural crack appeared to be subtle, unless the gage was very close to the crack. Typically, flexural crack initiation was associated with constant tensile strain readings from the gages located near the crack with increasing load. This behavior is shown in *Fig. 5.17* for beam SC-UC-2; the occurrence of flexural cracking in this beam was indicated by constant tensile strain readings of the gage located 12 in. from the midspan.

In *Fig. 5.18*, bottom fiber strain distributions are shown for beam SC-22-14. The pre-release crack in this beam was 22 in. deep and 0.014 in. wide. The strain readings from the gages were plotted with respect to the distance of the gages from the pre-release crack section (located at centerline). Location of the constant moment region of the beam is also indicated in the figure. For comparison purposes, the data shown in *Fig. 5.17* were re-plotted in *Fig. 5.19* for the

corresponding load increments shown in *Fig. 5.18*. Comparison of strain distributions in *Figs. 5.18* and *5.19* indicate the effect that the pre-release crack had on bottom fiber concrete strains. There was a concentration in the tensile strain directly below the pre-release crack prior to flexural crack initiation. The effect of the pre-release crack decayed with distance from the cracked section, and the strains in the beam at further distance from the pre-release crack approached the strains in the uncracked beam. The strain profiles shown in *Fig. 5.18* for different loads appear to be getting closer to each other in the vicinity of the pre-release crack as the load increased. The strain profiles in this figure were plotted for 2 kip load increments. For each 2 kip load increment, the strain difference between the current and the previous strain profiles got smaller, indicating that the beam was getting stiffer during loading. This stiffening of the beam was due to the closing of the pre-release crack, and consequent increase in the local moment of inertia of the section with increasing load. Starting from 12 kips load, the gage located 2 in. away from the pre-release crack exhibited a negligible increase in strain with increasing load because a flexural crack formed near this gage at that load.

*Table 5.2* summarizes the effect of the presence of pre-release cracks on the measured bottom fiber strains. Strain readings from the gages located within 4 in. of centerline of the beam under 10 kip load are tabulated for all beams. The comparison was done at the 10 kip load level, because at this load all beams were flexurally uncracked. This way, the effect of flexural cracking on the measured strains was eliminated (Flexural cracking loads of the beams will be discussed in Section 5.1.2.3). In the table, the average bottom fiber strains of the beams with pre-release cracks were compared with the average bottom fiber strain of three uncracked beams. The last column in the table shows the percent increase in strain for each beam relative to the average strain at the same load for the beams with no pre-release crack.

The average of the percent increases in the three beams with 22 in. deep, 0.014 in. wide pre-release cracks (beams SC-22-14, SC-22-14-R1 and SC-22-14-R2) was 256% with a coefficient of variation of 14%. This increase was due to the reduced section stiffness at the location of pre-release cracks. This phenomenon was explained in the previous section. Because at the pre-release crack location the load is carried only by the uncracked part of the section below the pre-release crack, same amount of moment (and hence load) would cause larger strains in beams with pre-release cracks than in beams without pre-release cracks. Moreover, among the

beams with a pre-release crack, the beam with a deeper pre-release crack would theoretically undergo larger strains at the pre-release crack location than the beam with shallower crack. Because the width of the pre-release crack determines how long the pre-release crack will remain open (and hence how long the load will be carried by the section with reduced stiffness), it has an effect on the amount of strain increase, too. Under the same load, the beam with a larger pre-release crack width would have larger strains than a beam with a smaller crack width, provided that the pre-release crack depths are the same. As explained earlier, this effect caused by the existence of a pre-release crack decreases away from the crack location.

The increase in the bottom fiber tensile strains below the pre-release cracks caused the beams with pre-release cracks to undergo flexural cracking at much lower loads than the beams without pre-release cracks. It should be noted that the strain values given in *Table 5.2* were the strains due to the applied load only. Any strain change that occurred before the gages were placed on the beams was not included in these numbers. When correlating these strain values and the percent increase values to the flexural cracking loads, the strain changes that occurred before the testing of the beams, such as strain changes due to transfer of prestress, and creep and shrinkage during storage period, must also taken into consideration. If the pre-release crack had closed immediately upon strand release, the same behavior prior to pre-release cracks closure would have still been expected. In this case the only load that is carried by the section with reduced stiffness (due to the pre-release crack) would have been the self-weight of the beam. In such cases, the strain changes in beams with pre-release cracks from those of the uncracked beams due to reduced sectional stiffness would be "locked in", and the effect of pre-release cracks would stay present even if they closed following the release of the prestressing strands.

*Figures 5.20* and *5.21* show the bottom fiber strain distributions for beams SC-16-14 and SC-22-08, respectively. The same type of behavior explained above for beam SC-22-14 was observed for these beams. As seen by comparing *Figs. 5.18* through *5.21* the effect of pre-release cracks on bottom fiber strains became negligible at a distance of approximately 20 in. from the centerline of the beams. This behavior is illustrated in *Table 5.3*, where strain readings from the gages placed at 20 in. and further away from the centerline of the beams under 12 kip load are tabulated for these three beams relative to an uncracked beam.

The 12 kip load was selected, because this was the flexural cracking load for beam SC-22-14. Cracking loads for the other beams shown in the table were larger than 12 kips. This way, the effect of flexural cracking was eliminated on the data shown in the table. The last column in *Table 5.3* indicates the average strain values for each beam at locations outside of the influence of the pre-release cracks. The average strain values for beams SC-16-14 and SC-22-08 are almost the same as the average strain value for the uncracked beam, SC-UC-2. The average strain value for beam SC-22-14 is slightly larger than that for beam SC-UC-2, but the value is still within 10%. This suggests that the span length where these three pre-release cracks with different dimensions had an effect on bottom fiber girder strains was nearly the same. This length appeared to be approximately 20 in. on both sides of the pre-release crack. The 20 in. effective span length can also be seen by comparing the strain profiles shown in *Fig. 5.19* to those in *Figs. 5.18*, *5.20* and *5.21*.

Wyffels (2000) documented that the span length where the pre-release cracks were effective on the girder stresses was limited to the depth of the girder on both sides of the crack, based on a finite element study. In that study, a 4% stress change criteria was applied to determine the area where the stress state was changed due to a pre-release crack. The 20 in. effective span length determined from strain gage readings using 10% strain change criteria is consistent with Wyffels' result.

In *Fig. 5.22*, the bottom fiber strain distribution of beam SC-06-14 is shown. The depth of the pre-release crack in this beam was 6 in., which was the smallest crack depth used in the test beams. To make comparison easier, the strain distribution of an uncracked beam (SC-UC-2) is superimposed on the same figure. As shown in the figure, the same type of effect described earlier for the beams with 16 in. and 22 in. cracks existed in this beam, even when the depth of the crack was small compared to the depth of the beam. The 20 in. effective span length also seems to be valid for this beam too.

The following conclusions can be made regarding the effect of pre-release crack size on beam strains. Because they cause a smaller section to carry the load locally, longer cracks cause larger stress changes compared to a beam with no pre-release crack. For the same crack depth, more load is required to close a wider crack, which means that the load is carried by a smaller

section for a longer time. For this reason, a wider pre-release crack causes larger stress changes than a shallower pre-release crack, provided that the crack depths are the same.

#### 5.1.2.2 Pre-Release Crack Closure

Changes in beam strains resulting from the closing of pre-release cracks as the beams were loaded were explained in the previous sections. In this section, the closing behavior of the pre-release cracks having different size and geometry will be discussed.

During load testing of the beams, closure of pre-release cracks was monitored with LVDTs placed across the cracks at different levels through the crack depth (Section 4.3.2.1). In some of the beams, pre-release crack widths were measured at several locations using feeler gages prior to the load tests in an attempt to determine the original crack geometries. It was difficult to obtain reliable measurements because of the effect of local changes in the crack openings, such as those due to irregular crack surfaces or particles stuck inside the crack. For this reason, only the data obtained from the LVDTs placed across the cracks will be used to describe the closing behavior of the pre-release cracks.

*Figure 5.23* shows data from five LVDTs distributed over the depth of the pre-release crack in beam SC-16-14 plotted with respect to the applied load. The pre-release crack geometry and location of LVDTs through the crack depth are also indicated on the figure. As shown in the figure, LVDTs placed at higher levels through the crack depth indicated a larger amount of crack closure than the LVDTs placed at lower levels. This was an expected result, because the cracks had a tapered geometry, i.e., they were narrower at the bottom and wider toward the top (Section 4.2.1.3). The plots for all five LVDTs had different slopes, because the LVDTs were placed at different distances from the neutral axis of the section. The initial slope of the plot for each LVDT was inversely proportional to the distance from the neutral axis of the cracked section to the level of that LVDT. LVDT1 had the smallest distance to the neutral axis of the cracked section, and therefore had the curve with the largest initial slope. LVDT5 was the furthest LVDT from the neutral axis location and hence had the curve with the smallest initial slope. When the pre-release crack started to close, the plots were no longer linear. The stiffness of the section increased as the pre-release crack began to close, which resulted in an increased slope of the LVDT displacement versus load curves. This change in slope was more pronounced for the LVDTs closer to the closed part of the crack, but the slope of the other curves changed as well,

because of the increase in the overall stiffness of the cracked section. When the crack closed completely at the level of the LVDT, the plot for that LVDT became almost linear again, with a much larger slope. This behavior is explained in the following paragraph.

As mentioned in Section 4.3.2.1, the LVDTs were placed across the crack, and the gage length of the LVDTs was 2 in. Before closure of the crack, the displacement recorded by the LVDTs included the displacement due to closure of the crack and the displacement due to straining of the concrete along the gage length of the LVDT. As long as the crack was open, the former displacement was much larger than the latter. The displacement due to straining of the concrete along the gage length of the LVDTs was theoretically near zero, because when the pre-release crack was open, the opposite sides of the crack did not touch each other and the concrete was not subjected to any compressive strain. Indeed, the strain gages placed on the side of the beams at the section 2 in. away from the pre-release cracks at the level of these LVDTs indicated strains on the order of 20 με before the pre-release crack closed. A compressive strain of 20 με over a 2 in. gage length would result in a 0.00004 in. increase in the displacement reading of the LVDTs. This displacement is insignificant compared to the amount of crack closure shown in *Fig. 5.23*, and is beyond the resolution of the LVDTs. It is clear that the strains at the section 1 in. away from the pre-release cracks would be smaller than these strains. Therefore the displacements due to straining of concrete before the closure of the pre-release cracks were likely to be even smaller than 0.00004 in. After the crack closed and the two sides of the crack came in contact with each other at the level of the LVDT, all the displacement then recorded by that LVDT was due to straining of the concrete over the gage length of the LVDT. In *Fig. 5.23*, this stage is illustrated by the portion of the plots that is almost linear following the nonlinear portions. Because the gage length of the LVDTs was only 2 in., and there was no longer a crack within this gage length, the slope of the last portion of the plots was large compared to the initial slopes. As for the case of the initial slopes, slopes in this portion were inversely proportional to the distance between the LVDTs and the neutral axis. Because the crack was closed in the latter case, the slopes were inversely proportional to the distances from the neutral axis of an *uncracked* section. LVDT1 was placed only 2 in. from the neutral axis of the *uncracked* section, and had a plot that was almost vertical. LVDT5 was the furthest LVDT from the neutral axis and had the smallest slope.

Stiffness of the beam in the third portion of the plots, which occurred following the nonlinear portions, was larger than the initial stiffness, because the pre-release crack closed. In addition to this, displacements measured by the LVDTs in this third portion of the plots were only due to straining of the concrete over the gage length, as mentioned earlier. Because the measured displacements were small and the stiffness of the section got larger, the plots were almost linear in the third portion, even though the stiffness of the beam was still changing in this portion. This small nonlinearity existed until the pre-release crack closed completely from bottom of the crack to the top of the crack. Starting from that point, stiffness of the pre-release crack section remained the same until flexural cracking occurred.

In *Fig 5.23* closing of the pre-release crack at the level of each LVDT is indicated on the figure by circles. The reason for the closing loads for LVDT3 and LVDT4 being so close to each other was probably due to the change in the crack geometry at the level of LVDT3. It should be noted that, at 30 kips no flexural cracking was visually observed in this beam. Therefore, the curves shown in *Fig. 5.23* do not include any effect of flexural cracking.

*Table 5.4* shows the nominal and measured widths of the pre-release cracks at the level of LVDTs for beam SC-16-14. The nominal crack width values shown in the table are the thickness of the crack forming plate used during the fabrication of the beams at the locations corresponding to the LVDT locations in the test beam. The actual crack widths were different than the nominal values because of changes in pre-release crack widths that occurred during the transfer of prestress and during the storage period, and due to possible errors during fabrication. The measured crack width values listed in the table were obtained from *Fig. 5.23*. They were the crack closure values for each LVDT corresponding to the circles drawn on the figure. As mentioned earlier, these values included negligible displacements due to straining of the concrete within the gage length of the LVDTs. As shown in the table, the nominal and the measured crack widths were in relative good agreement. Even though the nominal crack widths at the levels of LVDT4 and LVDT5 were the same, the measured crack widths were quite different. As shown in the table, LVDT5 indicated a larger crack width than LVDT4. That is, the width of the pre-release crack in the beam increased toward the top, and hence the shape of the crack was close to a V-shape.

The fact that the geometry of the pre-release cracks in the beams was close to a V-shape is more clearly seen in *Fig. 5.24*. In this figure, the amount of crack closure at the level of each LVDT was plotted against the location of the LVDT from the bottom of the beam for beam SC-16-14. The location of the tip of the crack relative to the bottom of the beam was 12 in. It is shown that, for each load level the amount of pre-release crack closure increased nearly linearly up through the crack depth. On the previous figure it was shown that the pre-release crack closed completely at approximately 23 kips. Therefore, the plots for 25 kips and 30 kips in *Fig. 5.24* represented the case with a completely closed crack. Because the crack was completely closed, the difference between the LVDT readings at these two loads was due to the straining of concrete in the gage length of LVDTs, as mentioned earlier. Because the neutral axis of an "uncracked" section was at 12 in., the LVDT located at 14 in. indicated almost no displacement between 25 kips and 30 kips. On the other hand, the LVDT at the top of the beam had the largest distance from the neutral axis, and indicated the largest displacement between 25 kips and 30 kips, as expected.

*Figure 5.25* shows the closure of the pre-release crack for beam SC-06-08. This beam had a 6 in. deep crack, which was the shallowest crack used in the test beams. The plots in this figure had different characteristics than those in *Fig. 5.23*. As shown in the figure, slopes of the curves, and hence the stiffness of the section did not change as much as for the case of the other beams. This indicated that during loading, the pre-release crack in this beam did not close as much as the cracks in the other beams. This result was previously obtained from the finite element models and mentioned in Section 3.1.2.1. Beams with shallower pre-release cracks had more resistance against crack closure than beams with deeper cracks. The larger concrete area below shallower pre-release cracks provides larger flexural stiffness in the beams with shallower cracks.

*Figure 5.26* compares the closure of the 0.014 in. wide pre-release cracks of different crack depths. As indicated in the figure, the LVDTs were placed at the same location on the 6 in., 16 in. and 22 in. deep cracks. The plot for beam SC-06-14 did not show any change in slope, indicating that the crack remained open throughout the load levels shown in the figure. The fact that, at 30 kips, the displacements measured for beams SC-16-14 and SC-22-14-R1 were quite larger than the displacement measured for beam SC-06-14, which had the same nominal crack

width as the other two beams, indicated that the pre-release crack in beam SC-06-14 was still open at 30 kips. The smaller crack depth used in this beam also resulted in the largest stiffness of the cracked section compared to the other two beams in the figure. This was indicated by the steeper load versus crack closure plot.

In *Fig. 5.26*, the plots for beams SC-16-14 and SC-22-14-R2 were not as different from each other as one would expect intuitively. This was probably due to closure of the bottom parts of the crack in beam SC-22-14-R2 under very small loads, or under the effect of the prestressing force, only. LVDTs placed 3 in. and 6.5 in. from the bottom of the 22 in. deep pre-release cracks indicated that the cracks started to close at those heights at very low loads. This caused the 22 in. deep cracks to have the same effects under additional applied load as 16 in. deep cracks starting from very low load levels, as shown in the figure.

Comparison of the pre-release crack closures of the two beams with 16 in. crack depths, SC-16-14 and SC-16-08, is shown in *Fig. 5.27*. The locations of the LVDTs crossing the cracks on these two beams were the same. As shown in the figure, the pre-release crack width in beam SC-16-08 was larger than the crack width in beam SC-16-14, even though the nominal crack widths were 0.008 in. and 0.014 in., respectively. A similar discrepancy was observed in some of the other beams. This might be due to shrinkage and creep of concrete between the time the crack-formers were removed and the time the beams were tested.

Measured and predicted strain profiles across the beam depth being in good agreement with each other (Section 5.1.2.1) indicated that the pre-release crack depths attained in the test beams were similar to those in the finite element models. By considering this agreement and the above discussion about the crack widths, it could be concluded that in producing the pre-release cracks in the test beams, the degree of control on the crack depth was greater than the degree of control on the crack width.

*Figure 5.28* shows the closure of the pre-release cracks in the three beams with the same nominal crack width and depth, beams SC-22-14, SC-22-14-R1, and SC-22-14-R2. The crack-formers used in these three beams were identical. The plots shown in the figure were for the LVDTs that were placed at the same location on all three beams, as indicated in the figure. The sudden increase shown in the displacement reading for beam SC-22-14 around 16 kips was probably due to an external effect on the LVDT during testing. All three cracks seem to close at

the level of these LVDTs around 20 kips. During load testing, no flexural cracking was visually observed in these beams at 20 kips. As shown in the figure, the amounts of crack closures at 20 kips were different for the three beams, even though the nominal crack geometries were identical. This reaffirmed the variability in the degree of control on pre-release crack widths in the beams.

#### 5.1.2.3 Flexural Cracking Loads

The closing behavior of pre-release cracks and the effects that this caused on strains were discussed earlier in this chapter. The results suggested that as the load on the beams increased, the pre-release cracks were forced to close, and that the reduced moment of inertia at the cracked section caused changes in beam strains in the vicinity of the crack. These changes included extra tensile strains at the bottom of the beam below the pre-release crack, extra compressive strains around the crack tip, and reduction in compressive strains around the top of the crack. The extra tensile strains caused by the stretching of the bottom fiber of the beam to close the pre-release crack resulted in flexural cracking of the beam at lower loads than beams without pre-release cracks.

Three different methods were used to determine the flexural crack initiation loads. The formation of the first flexural crack could not be detected from the load versus deflection plot for any of the beams, because formation of the first crack did not affect the overall stiffness of the beams significantly. The different methods used to determine the cracking loads included visual observation, use of crack detection gages, and use of the bottom fiber strain data.

*Flexural Cracking Loads from Visual Observation*

Loads at which the first flexural crack was visually detected are tabulated in *Table 5.5*. In the table, rows containing data for the beams without pre-release cracks were shaded for ease in comparison. The average of the flexural cracking load of the three beams without pre-release cracks (beams SC-UC-1, SC-UC-2 and SC-UC-3) is 63 kips with a coefficient of variation of 8%. The corresponding values for the three beams with identical pre-release crack dimensions (beams SC-22-14, SC-22-14-R1 and SC-22-14-R2) are 37 kips and 20%, respectively.

The percent reductions in cracking load of the beams from the average cracking load of the beams with no pre-release crack are also given in *Table 5.5*. As shown in the table, visually

observed cracking loads of all the beams with pre-release cracks were smaller than those of the uncracked beams. The range in reduction in cracking load occurred was 29% to 60% with the largest reduction occurring in beam SC-16-08.

Also indicated in *Table 5.5* is the location of the first visually observed flexural crack for each beam. When the flexural cracks were first observed visually during the flexural cracking tests, they were hairline cracks extending only on the bottom surface of the beams. These cracks were not visible on the sides of the beams when they first appeared. In beam SC-UC-1, three cracks were detected at the bottom surface when the loading was paused at 67 kips. First flexural cracking in all the beams with pre-release cracks localized in a region at most 3 in. from midspan. (directly below the pre-release cracks) On the other hand, the location of first flexural cracking in the beams with no pre-release crack was spread in the constant moment region. The difference in the location of first flexural cracking between the beams with and without pre-release cracks was a result of the localized effects due to the existence of the pre-release cracks, as mentioned previously.

The use of visually observed cracking loads was not a reliable way of comparing the flexural crack initiation among different beams. This is because of the observer-dependence of the visually observed loads. The relatively large coefficient of variation (20%) between the visually observed cracking loads of the three identical beams (beams SC-22-14, SC-22-14-R1, SC-22-14-R2) is an indication of the observer dependence of these loads. Flexural crack initiation loads were smaller than these visually observed cracking loads.

*Flexural Cracking Loads from Crack Detection Gages*

As mentioned in Section 4.3.2.1, the beams were instrumented with crack detection gages in an attempt to detect the occurrence of flexural cracking during testing. Flexural cracking loads determined from these gages are listed in *Table 5.6*. Some of the beams did not have crack detection gages. The loads at which the flexural cracking tests were terminated are also listed in the table.

Flexural cracks were detected in beams SC-22-08 and SC-22-14-R1 when loading was paused following the fracture of one of the crack detection gages. That is why the visually

observed cracking loads for these two beams are the same as the cracking loads indicated by the crack detection gages.

In beams SC-UC-2 and SC-UC-3, when the crack detection gages indicated flexural cracking, no crack was visually detected. Flexural cracking in these beams was visually observed after the loading was restarted. This resulted in visually observed cracking loads being greater than the cracking loads indicted by the crack detection gages for these two beams.

Crack detection gages in beams SC-16-08 and SC-16-14 indicated flexural cracking after a flexural crack was visually observed. In beams SC-06-08, SC-06-14 and SC-22-14 crack detection gages did not fracture before testing was terminated.

As shown in *Table 5.6*, the data from the crack detection gages were incomplete and not as useful as data from visual observation. In addition to this, sometimes the cracking loads indicated by the gages were higher than the visual cracking loads and sometimes lower. For these reasons, it was decided that using cracking loads from the crack detection gages was not a reliable means of comparison.

*Flexural Cracking Loads from Bottom Fiber Strain Data*

The third method used to determine the flexural crack initiation loads included the use of strains measured by the gages placed at the bottom surface of the beams.

*Figure 5.29* shows the variation of tensile strains with the applied load for the gages placed on the bottom surface of beam SC-16-14. Location of the gages with respect to the pre-release crack is also indicated on the figure. As seen, there is a small non-linearity in the increase of the strains up to 15 kips. The reason that the change of strains was not exactly linear was because of the closing of the pre-release crack. As the load on the beam increased, the pre-release crack started to close from the bottom. This caused a continuous increase in the stiffness of the cracked section, resulting in a nonlinear load versus strain curve as shown in *Fig. 5.29*. For beam SC-16-14, a flexural crack was visually observed at 32 kips, and loading was paused at that load. The irregularities shown in plots after 30 kips were due to these subsequent loading pauses.

*Figure 5.30* shows the same strain data as *Fig. 5.29*, but for gages H10 and H11, only. As shown in the figure, starting around 15 kips, the strain readings of the two gages started to diverge from each other. Starting at this load, gage H11 indicated constant strain with increasing

load. This was due to tensile strain relief resulting from flexural cracking in the vicinity of the gage. Theoretically, the strain relief due to initiation of a flexural crack should cause a decrease in tensile strain in the vicinity of the cracks. Because the surface gages used in this study were 2.4 in. long, the strains indicated by the gages were the average strains over the 2.4 in. length. Because of this relatively long gage length, the local decrease in tensile strain in the vicinity of the flexural crack was not detected with the gages, unless the flexural crack formed very close to the gage. In most of the beams, formation of a flexural crack was indicated by constant strain with increasing load. Flexural crack initiation loads of the beams were determined assuming this behavior. For each beam, the flexural cracking load was determined to be the load at which this tensile strain relief was first detected from the gages.

The plots that were used to determine the flexural cracking loads using the procedures explained above are given in *Figs. 5.30* through *5.39*. The figures include the strain data from the strain gage that first indicated constant tensile strain together with the data from one of the neighboring gages. The cracking loads determined from each plot are also indicated on the figures. These are the loads at which the load-strain plots of the neighboring gages started to diverge from each other.

The behavior exhibited in the load versus bottom fiber strain plots (*Figures 5.30* through *5.39*) used to identify the crack formation did not exist in the data for beam SC-16-08. *Figure 5.40* shows the variation of bottom fiber tensile strain with the applied load for beam SC-16-08. As shown in the figure, up to 28 kips, none of the gages showed an abrupt change in bottom fiber strain such as seen in *Figs. 5.30* through *5.39*. During testing of this beam, loading was stopped at 28 kips when a flexural crack was visually observed. The change in the slopes of the curves that occurred between 10 kips and 15 kips was probably due to closing of the pre-release crack. As indicated in the figure, gages H6 and H14 were located 8 in. from the midspan section on either side, and hence they were affected from the pre-release crack closure by the same amount. The fact that the strain gages that were symmetric with respect to the pre-release crack indicated similar slope changes suggested that these slope changes were due to closure of the pre-release crack, rather than initiation of a flexural crack.

Formation of flexural cracking could also be identified from the plots of bottom fiber strain along the beam length. Such a plot is shown in *Fig. 5.41* for beam SC-16-14. As shown in

the figure, the gage located 2 in. from the pre-release crack section (gage H11) indicated approximately the same tensile strain for loads larger than 16 kips. As mentioned above, this constant tensile strain with increasing load was due to the formation of a flexural crack in the vicinity of the gage. In this figure, the strain distributions were plotted for 2 kip load increments for clarity. If they had been plotted for 1 kip load increments, the strain values for gage H11 would have been the same for all loads larger than 15 kips. This indicated that a flexural crack initiated near gage H11 at 15 kips.

Cracking loads determined with the use of bottom fiber strain data was tabulated in *Table 5.7* for all beams, except for beam SC-16-08. In the table, rows corresponding to the beams with no pre-release cracks (SC-UC-1, SC-UC-2 and SC-UC-3) were shaded to make the comparison easier. The average of the flexural cracking load of the three beams with no pre-release crack (beams SC-UC-1, SC-UC-2 and SC-UC-3) is 40 kips with a coefficient of variation of 24%. The corresponding values for the three beams with identical pre-release crack dimensions (beams SC-22-14, SC-22-14-R1 and SC-22-14-R2) are 13 kips and 13%, respectively. As shown in the table, flexural cracking load of one of the beams with no pre-release crack (beam SC-UC-2) is much smaller than those of the other two beams with no pre-release crack. This phenomenon will be discussed in Section 5.1.2.5.

The bar chart shown in *Fig. 5.42* provides a comparison of cracking loads obtained from bottom fiber strain data and visual observation for the beams. The first three bars represent the beams with no pre-release cracks. As shown, both observed and measured flexural cracking loads of the beams with pre-release cracks are significantly smaller than those of the beams without pre-release cracks.

*Predicted Flexural Cracking Loads*

Predicted cracking loads of the beams without pre-release cracks were calculated and compared with experimentally determined cracking loads. The following relationship was used to calculate the moment that caused flexural cracking in the beams,

$$\sigma = -\frac{P_{eff}}{A_g} - \frac{P_{eff} e_g c_g}{I_g} + \frac{M_{self} c_g}{I_g} + \frac{M_{applied} c_{tr}}{I_{tr}} \qquad (5.1)$$

where $\sigma$ is the bottom fiber stress at midspan (tension is positive), $P_{eff}$ is the effective prestressing force, $A_g$ is the cross-sectional area, $e_g$ is the eccentricity of the prestressing force, $c_g$ is the depth of the neutral axis of the gross section, $I_g$ is the gross moment of inertia, $M_{self}$ is the midspan moment due to self-weight of the beam, $c_{tr}$ is neutral axis depth of the transformed section, $I_{tr}$ is the transformed moment of inertia, and $M_{applied}$ is the midspan moment due to applied loading.

Using *Equation (5.1)*, the actuator load required to cause the bottom fiber stress to reach the modulus of rupture was back-calculated. The value of each parameter in this equation is given in *Table 5.8*. As shown in the table, the tensile strength of the concrete was taken to be 650 psi. This was the average strength determined from testing 6x6x24 in. modulus of rupture beams. The effective prestressing force used in the calculations was 104,500 lbs. This was obtained by multiplying the effective prestress determined from strand severing (Section 5.1.1) by the total strand area. Gross section properties were used to calculate the effect of the prestressing force and the self-weight, and transformed section properties were used to calculate the effect of applied load.

Using the quantities given in *Table 5.8*, *Equation (5.1)* gave a predicted applied moment of 2967 in-kips, corresponding to an actuator load of 70 kips.

The flexural crack initiation loads determined from the bottom fiber strain data were 47 kips and 44 kips, respectively for beams SC-UC-1 and SC-UC-3. The visually observed cracking loads for these beams were 67 kips and 57 kips respectively. A reason for some of the difference between the measured and calculated flexural cracking loads may have been due to the location of the prestressing strands in cross section. Even though the depth of the section was 28 in., the prestressing strands were located in one row located 2 in. from the bottom. This situation may violate the plane section assumption behind the formula used to calculate the flexural cracking load. In addition, distribution of the four prestressing strands along the width direction of the cross section might be the reason for the discrepancy between the calculated and measured flexural cracking loads. The bottom flange of the beams was 18 in. wide. Two of the four prestressing strands were placed 2 in. from ends of the flanges. The remaining two strands were placed 1 in. from the centerline of the bottom flanges on each side. (The cross section is shown in *Fig 4.1*) There were only four strands, and the smallest distance between the strands was 2 in.

and the largest distance was 6 in. This "unequal" distribution of the prestressing force in the bottom flange might be another possible reason for the beams to undergo flexural cracking at lower loads than calculated.

The discrepancy that existed between the calculated and experimentally flexural crack initiation loads obtained in this study was found to exist in other studies in literature. Results of the studies by Shanafelt and Horn, Shenoy et al., and Halsey et al. support the results obtained in this study.

In a test performed by Shanafelt and Horn on an AASHTO Type III prestressed concrete girder, flexural cracking was observed at a load of 55.1 kips. This load corresponded to a calculated tensile stress in the concrete of 2.7 or $4.5\sqrt{f_c`}$, which is less than the AASHTO-specified allowable tensile stress of $6\sqrt{f_c`}$. Considering the fact that flexural crack initiation load is in most cases smaller than the load at which the cracks become visible, it is clear that the actual bottom fiber concrete stress was smaller than the reported values of 2.7 or $4.5\sqrt{f_c`}$.

Shenoy et al. tested two 27-year-old prestressed concrete box beams. The predicted flexural cracking load of the beams was 30.1 kips. Even though it was stated in their paper that visually observed flexural cracking loads were 29 and 35.5 kips for Beams 7 and 4, respectively, the strain distribution across depth of Beam 7 was nonlinear starting at 11.8 kips. At 11.8 kips, the strain gage located on one side of the beam at 1.2 in. from the bottom surface of the beam indicated smaller tensile strain than the value expected for a linear distribution. This suggests that there was a flexural crack near that gage at 11.8 kips load, even though the predicted flexural crack initiation load of the beam was 30.1 kips.

In the study by Halsey et al., two 40-year-old prestressed concrete inverted T-beams were tested. The predicted flexural cracking load was 16.2 kips for Beam 1, and 16.4 kips for Beam 2. The experimental cracking loads were reported as 18.5 and 16.5 kips for Beams 1 and 2, respectively. The strain distribution across depth of Beam 2 was nonlinear at 10 kips. At 16.5 kips a flexural crack became visible on one side of the beam. Even though flexural cracking load was reported as 16.5 kips for Beam 2, it is evident that initiation of flexural cracking in this beam occurred at a lower load.

#### 5.1.2.4 Flexural Crack Re-Opening Loads

Following flexural cracking tests, the beams were subjected to crack re-opening tests in order to determine the load at which the flexural cracks started to re-open at the bottom surface of each beam. Theoretically, a flexural crack re-opens when the bottom fiber of the beam decompressed and the stress at the location of the crack reached zero. Different than the flexural cracking loads, crack re-opening loads do not depend on the tensile strength of the concrete. Crack re-opening loads determined for each beam were used to make comparisons among the beams regarding the effects of the existence of pre-release cracks.

Two different methods were used to determine the crack re-opening loads. These methods are discussed in the following sections.

*Flexural Crack Re-Opening Loads from Bottom Fiber Strain Data*

Data from the strain gages located on the bottom surface of the beams were used to determine the flexural crack re-opening loads. These gages were attached to the beams prior to flexural cracking tests, and only a few of them were damaged during the cracking tests. Therefore, they could be used to obtain the strain measurements during the crack re-opening tests. *Figure 5.43* shows the load versus bottom fiber strain plot of beam SC-06-14 during the crack re-opening test. As shown in the figure, the gage exhibited a bilinear response. The load at which the slope of the first linear portion changed was taken as the crack re-opening load for this beam. This bilinear response suggests that the gage was located near a flexural crack. During the first linear portion, the crack was closed and the strain at the bottom surface of the beam increased at a certain rate with the applied load. When the load was large enough to cause a zero bottom fiber stress, the flexural crack re-opened. At this moment, a sharp strain gradient occurred in the vicinity of the crack with the strain at the sides of the crack being zero. The reduced tensile strains due to this strain gradient resulted in a smaller amount of change in strain with the applied load than before.

Re-opening of the flexural cracks could be discerned from the strain gage data for only six of the beams. In *Figs. 5.43* through *5.48*, the plots that were used to determine the flexural crack re-opening loads using the procedure explained above are given. Each figure includes the data from the strain gage that was used to determine the flexural crack initiation load. These

gages were also the ones that first showed the change in initial slope during crack re-opening tests. The crack re-opening loads determined from each plot are also indicated on the figures.

It should be remembered that in most of the beams there was only one visible flexural crack when the flexural cracking tests were stopped. The reason that crack re-opening could not be detected from the bottom fiber strain data for all of the beams may have been due to the relative position of the flexural cracks with respect to the strain gages. If the gage was not close to the crack, it may not be affected by the re-opening of the crack, even if it was affected by the formation of the crack. In addition to this, the number of flexural cracks developed at the bottom surface of the beams at the end of flexural cracking tests was not the same. This could be another possible reason that re-opening of the flexural crack(s) could not be detected from the bottom fiber strain gages for some of the beams.

*Flexural Crack Re-Opening Loads from LVDT Readings*

Measurements from LVDTs were also used to determine the crack re-opening loads of the beams. As mentioned in Section 4.4.1.1, after the initial flexural cracking tests, the flexural crack(s) were instrumented with two LVDTs, one over the crack and one next to the crack. When the crack was closed, the two LVDTs were expected to measure the same amount of deformation due to straining of concrete only. When the actuator load reached the value large enough to overcome the existing compressive stress and produce zero stress at the bottom surface of the beam, a nonlinear load versus displacement behavior was expected to occur. When the crack started to re-open, displacement measured by the LVDT over the crack was expected to increase at a faster rate than the displacement next to the crack. Following re-opening of the crack, the displacement measured by the LVDT over the crack was mostly due to opening of the crack at the bottom surface. At the same time, the displacement measured by the LVDT that was next to the crack started to decrease because of the strain gradient in the vicinity of the crack.

Theoretically, the initial slopes of the plots for both near-crack and over-crack LVDTs should be the same, and when the crack would re-open, the two plots should diverge from each other. In the measured data, however, the initial slopes of the two plots were not the same for most of the beams. This was probably due to unequal gage lengths of the over-crack and near-crack LVDTs during crack re-opening tests. As a result, it was not possible to determine the load

at which the two plots started to diverge from each other for most of the beams. For this reason, measurements from only the near-crack LVDTs were used to determine the crack re-opening loads for most of the beams. For the cases where the near-crack LVDTs were not helpful, re-opening loads were determined by using measurements from the over-crack LVDTs. Ahlborn et al. (1998) documented that this method (determination of crack re-opening load from the divergence of the plots of near-crack and over-crack LVDTs) had been successfully used to determine the flexural crack re-opening load of two full-scale prestressed concrete girders.

*Figure 5.49* shows the load versus displacement plot of the LVDT placed *over* the first visually observed flexural crack on beam SC-UC-2. As shown in the figure, the initial slope of the plot changed at approximately 26 kips. This load was taken to be the crack re-opening load for beam SC-UC-2. The same data for beam SC-UC-1 is shown in *Fig. 5.50*. In this case, there was not a sudden change in the initial slope as in the previous beam. For this beam, the crack re-opening load was estimated to be 27 kips, which is the load at which load versus displacement plot first deviated from linearity, as shown in the figure. In *Fig. 5.51*, the load versus displacement plot of the LVDT placed *next to* a flexural crack on beam SC-22-14 is shown. For this beam, the same criterion was used to determine the crack re-opening load; the point where the initial slope of the plot changed was considered as crack re-opening, as shown in the figure.

Load versus displacement plots of the LVDTs placed *next* to flexural cracks in beams SC-UC-1 and SC-UC-2 did not show almost any nonlinearity. These plots are given in Appendix E. The reason that the LVDTs placed *next* to flexural cracks in beams SC-UC-1 and SC-UC-2 were not affected from the re-opening of the flexural cracks might be due to the LVDTs not being placed close enough to the cracks.

The plots used to determine the flexural crack re-opening loads using the procedures explained above are given in *Figs. 5.49* through *5.58*. Crack re-opening loads determined from each plot are also indicated on the figures.

The behavior that existed in the load versus LVDT displacement plots (*Figures 5.49* through *5.58*) used to identify the flexural crack re-opening was not observed in beam SC-16-08. *Figure 5.59* shows the load versus displacement plots for near-crack and over-crack LVDTs. As shown in the figure, neither of the LVDTs exhibited slope changes such as those shown in *Figs. 5.49* through *5.58*.

The flexural crack re-opening loads determined from the bottom fiber strain data and LVDT readings are listed in *Table 5.9*. As shown in the table, there is only a slight difference between the crack re-opening loads determined by the two methods, except for beam SC-22-08. The average of the crack re-opening load of the three beams with no pre-release crack (beams SC-UC-1, SC-UC-2 and SC-UC-3) determined from LVDT readings was 26 kips with a coefficient of variation of 2%. Crack re-opening loads of the three replicate beams with the identical pre-release crack geometry (beams SC-22-14, SC-22-14-R1 and SC-22-14-R2) were all 4 kips.

The flexural crack re-opening loads given in *Table 5.9* are plotted in the bar chart in *Fig. 5.60*. The chart illustrates the findings that were mentioned above; for the beams for which the crack re-opening load could be determined from both strain gages and LVDTs, these loads were in good agreement. Moreover, crack re-opening loads of the beams without pre-release cracks (beams SC-UC-1, SC-UC-2 and SC-UC-3) were all significantly larger than the re-opening loads of the beams with pre-release cracks.

*Predicted Flexural Crack Re-Opening Loads*

As in the case of cracking loads, predicted crack re-opening loads of the beams without pre-release cracks were calculated using *Equation (5.1)*. The values given in *Table 5.8* were used except the bottom fiber tensile stress was taken as zero in determining the crack re-opening load. Taking the left side of the equation as zero, $M_{applied}$ was calculated to be 1672 in-kips, which corresponded to an actuator load of 39 kips.

The average of the crack re-opening load of the three beams without pre-release cracks was determined to be 26 kips. The same discrepancy that existed between the measured and calculated crack initiation loads existed between the measured and calculated crack re-opening loads. The possible reasons for this discrepancy discussed earlier for cracking loads are valid for crack re-opening loads too.

### 5.1.2.5 Discussion of Special Cases Regarding the Bottom Fiber Strain Data

As explained earlier, the flexural crack initiation loads of the beams were determined to be the smallest of the loads at which one of the gages started to indicate a nearly constant strain with increasing load. Generally this abrupt strain change coincided with the point where the

load-strain plots of the two neighboring strain gages started to diverge from each other. In this case the flexural cracking load was easily observed from the plots. In some cases, on the other hand, the point of divergence of the plots did not coincide with the point where one of the gages indicated a sudden change in slope. For these beams the flexural crack initiation load could be taken as either the point of divergence or the point of abrupt slope change. SC-UC-1, SC-UC-2, SC-22-14-R1 and SC-22-14-R2 are the only beams where the points of divergence and abrupt slope change did not occur at the same time. Cracking loads determined from bottom fiber strain data of these four beams are discussed below.

Load versus bottom fiber strain plot of beam SC-22-14-R1 is shown in *Fig. 5.38*. As shown in the figure, strain in one of the gages (gage H10) remained constant starting from 20 kips. Before this constant strain occurred, the strain measured by the two gages diverged from each other starting from 15 kips. A similar situation occurred with beam SC-22-14-R2 (*Figure 5.39*) with a strain divergence at 12 kips, and constant strain at approximately 19 kips. That is, flexural cracking load of beam SC-22-14-R1 could be taken as either 15 kips or 20 kips, and flexural cracking load of beam SC-22-14-R2 could be taken as either 12 or 19 kips. The former loads correspond to the load at which the plots started to diverge from each other, while the latter ones were the loads at which the plots became vertical.

As explained earlier, crack re-opening loads of beams SC-22-14, SC-22-14-R1 and SC-22-14-R2, which were replicates of each other, were all determined to be 4 kips (*Table 5.9*). By considering that the crack re-opening of these three beams were the same and the cracking load of beam SC-22-14 was 12 kips, it is more likely that the cracking load of beams SC-22-14-R1 and SC-22-14-R2 were 15 kips and 12 kips, respectively, rather than 20 kips and 19 kips. SC-22-14-R1 and SC-22-14-R2 were the beams that had the deepest and widest pre-release cracks. If cracking loads for these beams were selected as 20 kips and 19 kips, which were the loads at which strain became constant, these two beams with the deepest and widest pre-release cracks would have cracking loads that were larger than the cracking loads of almost all the beams with pre-release cracks. This is not logical considering that the effects of deeper and wider pre-release cracks on bottom fiber strains were larger. Therefore, the cracking loads of beams SC-22-14-R1 and SC-22-14-R2 were estimated to be *15 kips* and *12 kips*, respectively, by considering the divergence of the strain plots as the sign of flexural crack initiation.

Similar behaviors were observed in beams SC-UC-1 and SC-UC-2 (*Figures 5.31* and *5.32*). As shown in the figures, the strain plots started to diverge from each other before one of the gages showed an abrupt change in slope. In beam SC-UC-1, the divergence occurred at 47 kips, while the slope changed suddenly at 54 kips. These values were 29 kips and 44 kips for beam SC-UC-2.

Flexural cracking loads for beams SC-UC-1 and SC-UC-2 were determined the same way as for beams SC-22-14-R1 and SC-22-14-R2; divergence of the plots of the two neighboring gages was decided to be the sign of flexural crack initiation. This resulted in flexural cracking loads of *47 kips* and *49 kips*, respectively, for beams SC-UC-1 and SC-UC-2.

The flexural crack re-opening load of beam SC-UC-2 was 27 kips. Re-opening load for beams SC-UC-1 and SC-UC-3, which were the replicates of beam SC-UC-2, were both 26 kips. This suggests that the *29 kips* cracking load for beam SC-UC-2 was actually the crack re-opening load, which means that the beam must have already undergone flexural cracking prior to the flexural cracking test.

Assuming beam SC-UC-2 was already cracked prior to the flexural cracking test, the average flexural cracking load of the beams without pre-release cracks was computed to be *46 kips* taking the average of cracking loads of beams SC-UC-1 and SC-UC-3, only.

*Effect of Type of Loading on Behavior of Bottom Fiber Strain Data*

During the cracking tests of the beams, displacement-controlled loading was applied except for beams SC-UC-1 and SC-22-14-R2, which were the last two specimens subjected to the flexural cracking test. The behavior of these two beams was different than those tested under displacement-controlled loading, as far as bottom fiber strain versus load plots are concerned.

During the formation of a crack in load-controlled testing, the load applied by the actuator remained constant while the stiffness of the beam changed due to cracking. Whereas in displacement-controlled testing, when there was a change in the stiffness of the beam, the load applied by the actuator reduces to maintain a constant displacement even as the stiffness reduces due to cracking. This difference between the two types of loading resulted in different behavior in bottom fiber strain versus load plots of the beams tested using different types of loading.

*Figures 5.61* and *5.62* show the change of bottom fiber strains with the applied load for beams SC-UC-1 and SC-22-14-R2, respectively. During testing of beam SC-UC-1, three flexural cracks were detected visually at 67 kips. These cracks crossed gages H4, H13 and H15. As shown in *Fig. 5.61*, these gages showed a sudden increase in tensile strain around 62 kips due to the flexural cracks passing across the gages. A similar behavior was observed for gage H4 in beam SC-22-14-R2 at 35 kips, as shown in *Fig. 5.62*. At 35 kips, a hairline crack passing beneath gage H4 was detected visually, and loading was paused. As shown in *Fig. 5.62*, gage H4 indicated a "jump" in tensile strain around 34 kips. When the loading was paused at 35 kips, gages H3 and H5, which were neighboring gages of gage H4, showed a sudden decrease in tensile strain. This sudden tensile strain relief was due to the formation of a flexural crack near the gages.

Even though the sudden increases or "jumps" that were observed in bottom fiber strains of the beams tested under load-control did not exist in beams tested under displacement-control, this does not imply that the flexural crack initiation load could be detected more easily in load-controlled testing than in displacement-controlled testing. The flexural crack initiation loads of beams SC-UC-1 and SC-22-14-R2, which were the beams subjected to load-controlled testing, were determined to be 47 kips and 12 kips, respectively, from the bottom fiber strain data, while the strain jumps occurred at 62 kips and 34 kips, respectively. This is due to the fact that the strain jumps occur when the flexural cracks reach a certain width, whereas the method used to determine the flexural cracking loads using the bottom fiber strain data yields the load at which the flexural cracks initiate originally.

#### 5.1.2.6 Overall Beam Stiffness

Load versus midspan deflection behavior of the beams measured during flexural cracking tests were plotted and compared with each other to discern any effect of the pre-release cracks. *Figures 5.63* and *5.64* show these plots. In the figures, plots for the beams with 0.008 in. and 0.014 in. wide pre-release cracks were compared to the uncracked beams separately. The deflections shown in these plots were the net midspan deflections. The support deflections due to compression of the neoprene pads used at the supports were averaged and subtracted from the readings of the LVDT that measured the amount of total deflection at the midspan. The points where a flexural crack was visually observed during testing of the beams (and loading was

paused) are indicated with solid circles in the figures. The behaviors explained below were valid until flexural cracking occurred in the beams; the effect of flexural cracking on the stiffness of the beams was not included in this discussion. It should also be noted that the beam deflections were dependent on the modulus of elasticity of the concrete at the time of testing. The measured modulii of elasticity at the beginning and end of the testing program differed by approximately 10%.

As shown in the plots, the beams with 16 in. and 22 in. deep pre-release cracks had bilinear load versus midspan deflection behaviors. In the first stage of loading, midspan deflection of these beams increased linearly. This portion corresponded to a state where the pre-release cracks were completely open. As loading continued, an increase in load no longer resulted in a proportional increase in midspan deflection, because the pre-release cracks started to close. Closing of the pre-release cracks during this stage resulted in a continuous change in the moment of inertia of the cracked section, and hence a nonlinear load versus displacement behavior. The loads at the start of crack closure (end of initial linear portion) determined from the load-deflection plots shown in *Figs. 5.63* and *5.64* are consistent with those obtained from the load versus pre-release crack closure plots (*Figures 5.23*, *5.26*, *5.27* and *5.28*). Following the nonlinear portion, the deflections started to increase linearly with increasing load, again. As shown in *Figs. 5.63* and *5.64*, almost no change was observed in the stiffness of the beams during this second portion. This almost linear response does not mean that the pre-release cracks were closed completely. They might have still remained partly open, but the closed part of the cracks was large enough to increase the stiffness of the section such that further closing of the crack did not cause a significant change in the overall stiffness of the beam.

As shown in *Figs. 5.63* and *5.64*, the beams with 6 in. deep pre-release cracks did not show as much stiffness change during loading as the beams with 16 in. and 22 in. cracks. This was because of the reason explained above; the original stiffness of these beams before loading was so large that the closing of the cracks did not cause much change in the stiffness. In addition to this, the beam with a shallower crack had more resistance to pre-release crack closure than the beam with a deeper crack, as explained before. Therefore, the 6 in. deep pre-release cracks did not close as much as other cracks during loading, which was another reason that the stiffness of the beams with 6 in. deep cracks did not undergo much change.

As shown in *Fig. 5.64*, the initial stiffness of the beams decreased with increasing pre-release crack depth for the 0.014 in. wide cracks. A similar behavior was observed in the beams with 0.008 in. wide pre-release crack, as shown in *Fig. 5.63* with the exception of the 22 in. deep crack. Another difference between the two figures is that in *Fig. 5.64*, the load versus deflection plots of the beams with 0.014 in. wide pre-release cracks remained fairly parallel to each other during testing. This was not the case for the beams with 0.008 in. wide crack. As shown in *Fig. 5.63*, for the 0.008 in. pre-release crack width, stiffness of the beam with a 22 in. deep crack increased more than the stiffness of the beams with 6 in. and 16 in. deep cracks. This suggested that the 22 in. deep pre-release cracks closed more than the other two cracks. This might have resulted from a smaller pre-release crack width in the beam with the 22 in. deep crack (beam SC-22-08) than the beams with the 6 in. and 16 in. deep cracks (beams SC-06-08 and SC-16-08).

The stiffness of the beams at the initial stage and the stage prior to flexural cracking are listed in *Table 5.10*. The stiffness values shown in this table were the slopes of the initial and prior-to-flexural cracking portions of the load versus midspan deflection plots obtained during the flexural cracking tests, such as those shown in *Figs. 5.63* and *5.64*. The slopes were determined by inserting trendlines to a group of data points and increasing the number of data points until the slope of the trendline changed.

In *Table 5.10*, rows corresponding to the beams without pre-release cracks were shaded to make comparison easier. Also shown in the table are the visually observed cracking loads and the maximum loads used to calculate the final stiffnesses. As shown, the maximum loads used were always smaller than the visually observed cracking loads to eliminate the effect of flexural cracking on the calculated stiffness of the beams. Load-deflection plots of the beams were not affected by the initiation of flexural cracks, until the cracks became visible. For this reason, the maximum loads used while calculating the slopes of load-deflection plots were taken to be the loads at which flexural cracks were visually observed.

The average initial and prior-to-flexural cracking stiffness of the three beams without pre-release cracks (beams SC-UC-1, SC-UC-2 and SC-UC-3) were 550 kips/in and 540 kips/in, respectively. The corresponding coefficients of variation were 11% and 12%. For the three beams with identical pre-release cracks (beams SC-22-14, SC-22-14-R1 and SC-22-14-R2), the

average initial and prior-to-flexural cracking stiffnesses were 170 kips/in and 450 kips/in, respectively, with the corresponding coefficient of variation values of 9% and 6%.

The difference among the stiffnesses of the beams without pre-release cracks was probably due to the change in the modulus of elasticity of the concrete, because the testing times of these beams were different. As indicated earlier, the measured modulii of elasticity at the beginning and end of the testing program differed by approximately 10%. Beam SC-UC-1 was subjected to a cracking test approximately 9 months later than beams SC-UC-2 and SC-UC-3.

The stiffness values in *Table 5.10* are plotted in the bar chart in *Fig. 5.65*. As shown in the figure, the initial stiffness of the beams with pre-release cracks was always smaller than the stiffness of beams without pre-release cracks. Due to closure of the pre-release cracks, the prior-to-flexural cracking stiffness of the beams with pre-release cracks increased and approached the stiffness of the beams without pre-release cracks. If the pre-release cracks had closed completely, then the prior-to-flexural cracking slopes of the beams with pre-release cracks should have reached the stiffness of the uncracked beam (assuming no flexural crack prior to pre-release crack closure). It is evident from the figure that the pre-release cracks in beams SC-16-14 and SC-22-08 may have closed completely before visually observed flexural cracking. The same behavior was observed in the load versus pre-release crack closure plots of these beams. Another result that is present in this figure is that the initial and prior-to-flexural cracking stiffness of the beams with 6 in. deep cracks were similar to each other. This was because of the previously explained behavior that shallow pre-release cracks closed less during loading.

#### 5.1.2.7 Near-Ultimate State Comparison

After flexural cracking and crack re-opening tests, six of the beams (SC-UC-3, SC-06-08, SC-06-14, SC-16-14, SC-22-08, and SC-22-14-R1) were tested to a “near-ultimate” state. In these tests the beams were loaded up to 90 kips. During testing, data from the strain gages and LVDTs were recorded and cracks were marked on the beams.

*Figure 5.66* shows a comparison of the load versus midspan deflection from these tests. As shown in the figure, there was no significant difference among the responses of the beams, except the initial stiffnesses, which were explained in the previous section. Even though there was a slight difference among the maximum midspan deflections, it seemed that there was no relation between the pre-release crack size and the maximum measured deflection. Independent

of the pre-release crack size, all beams had a significant change in the slope of the load-deflection curves at approximately 70 kips. At this load, new cracks formed at the bottom flange and propagated near the load points. *Figure 5.67* shows the typical crack pattern at near-ultimate state for beam SC-16-14.

*Figure 5.68* compares the observed crack pattern for beams with different size pre-release cracks as well as an uncracked beam. The numbers shown near the cracks indicate the load at which the crack propagated to that position. As shown in the figures, near-ultimate state tests created similar series of flexural cracks in these beams. For the beams with pre-release cracks (beams SC-06-14, SC-16-14, and SC-22-14) under the same load, the flexural cracks below the pre-release cracks were longer than the other flexural cracks. This was a result of the extra tensile strains that developed below the pre-release cracks due to reduced sectional stiffness prior to the pre-release crack closure.

#### 5.1.2.8 Ultimate Flexural Strength

After near-ultimate tests, three of the beams (beams SC-06-08, SC-16-14 and SC-22-08) were tested to failure to determine the ultimate flexural capacities. The test setup and procedure were discussed in Chapter 4. During these tests, only the actuator load and stroke data were collected.

Failure of the beams was crushing of the concrete in the top flange inside the constant moment region. *Figures 5.69* and *5.70* show the digitized video frames of the instant of concrete crushing in beams SC-16-14 and SC-22-08, respectively. As shown in the figures, the beams exhibited explosive compression failures due to crushing of the concrete. *Figure 5.71* shows an overview of beam SC-06-08 following the ultimate test. As shown in the figure, failure occurred in the midspan region. *Figure 5.72* shows a close-up view of the damaged region in beam SC-06-08. The part of the pre-release crack that remained undamaged is highlighted in the figure.

The measured ultimate loads of the beams are listed in *Table 5.11*. As shown, there was a marginal difference among the measured ultimate flexural loads of these three beams that had different size pre-release cracks.

*Predicted Ultimate Flexural Capacity*

The ultimate flexural capacity of a beam without pre-release cracks was calculated using strain compatibility and equilibrium. The procedure followed during the calculations is explained below.

The total strand strain at the ultimate state of the beam includes three components. The first component, $\varepsilon_1$, is the strain due to the effective prestress, $f_{pe}$, in the strand.

$$\varepsilon_1 = \varepsilon_{pe} = \frac{f_{pe}}{E_{ps}}$$

where $E_{ps}$ is the modulus of elasticity of the prestressing steel, which was taken as 32,000 ksi.

The second strain component, $\varepsilon_2$, is the strain to reach the decompression of concrete at the level of the steel.

$$\varepsilon_2 = \frac{1}{E_c}\left[\frac{P_e}{A_{net}} + \frac{P_e e^2}{I_{net}}\right]$$

where $E_c$ is the modulus of elasticity of the concrete, $P_e$ is the effective prestressing force, $A_{net}$ is the net cross-sectional area, $e$ is the eccentricity of the prestressing force, and $I_{net}$ is the moment of inertia of the net section.

The third component, $\varepsilon_3$, is the strain increment above decompression to failure. Failure is defined by crushing of the concrete at the ultimate compressive strain ($\varepsilon_{cu}$=0.003). This strain component can be computed from a linear strain distribution as follows:

$$\varepsilon_3 = \varepsilon_{cu}\left(\frac{d_p - c}{c}\right)$$

where $d_p$ is the distance from the extreme compression fiber to the centroid of the prestressing steel, and $c$ is the distance from the extreme compression fiber to the neutral axis.

The total strain at failure becomes:

$$\varepsilon_{ps} = \varepsilon_1 + \varepsilon_2 + \varepsilon_3$$

The corresponding steel stress, $f_{ps}$, at failure was obtained from the PCI Design Handbook (1999) Design Aid 11.2.5 using the following relations:

$f_{ps} = 28{,}500\,\varepsilon_{ps}$, if $\varepsilon_{ps} \le 0.0086$, and

$$f_{ps} = 270 - \frac{0.04}{\varepsilon_{ps} - 0.007}, \text{ if } \varepsilon_{ps} > 0.0086$$

A standard trial and error solution was required to determine the stress in the prestressing strand at ultimate, $f_{ps}$. This procedure can be summarized as follows: first a value for neutral axis depth is assumed. Using this assumed neutral axis depth and strain compatibility, $\varepsilon_3$ and hence the strain in the prestressing strand is determined. The stress-strain expression given above for the steel can be used to calculate the stress in the prestressing strand at ultimate, $f_{ps}$. Using this value, the total tension force in the steel, *T*, and assuming Whitney's stress block assumptions are valid, the total compressive force in the concrete, *C*, corresponding to the assumed neutral axis depth are evaluated. If these tension and compression forces are equal, equilibrium is satisfied and the method has converged. If not, the process is repeated with a new assumption for neutral axis depth. Once the total tension, and hence the compression, force is determined, the moment capacity of the section can be calculated as:

$$M_{ult} = T(d_p - \frac{\beta_1 c}{2})$$

where T is the total tension force in the steel, $d_p$ is the distance from the extreme compression fiber to the centroid of the prestressing steel, $\beta_1$ is a factor depending on concrete strength, and *c* is the distance from the extreme compression fiber to the neutral axis.

Using this procedure, the ultimate flexural capacity of the beams was calculated to be 134 kips. The numerical calculations are given in Appendix F.

Ratios of the measured ultimate loads to the predicted ultimate load are presented in *Table 5.11*. As shown in the table, the measured ultimate capacities were in good agreement with the predicted ultimate capacity.

### 5.1.3 Cyclic Tests

Results from the cyclic tests performed on three of the beams (SC-22-14, SC-22-14-R2 and SC-UC-1) are discussed in this section. Detailed information about the test setup and procedure including the nominal minimum and maximum load levels chosen for cyclic tests can be found in Section 4.4.2.

The beams were cycled in four-point bending between *39 kips* and *67 kips* (276 k-ft and 475 k-ft). The 67 kip load corresponded to a nominal bottom fiber tensile stress of $6\sqrt{f_c'}$ in a beam with no pre-release crack. A partially cracked section analysis predicted that this load range would produce a 23 ksi stress range.

The terms "flexural crack opening" or "flexural crack width" refer to the displacements measured by the LVDTs placed across the flexural cracks. These displacements include the crack opening displacement, as well as the displacement due to straining of concrete within the gage length of the LVDTs. Because the typical gage length of these LVDTs was in the range of 2-3 in., and they were placed in the vicinity of cracks, the latter part of the displacement was insignificant compared to the former part.

#### 5.1.3.1 Beam SC-22-14

This beam was one of the three beams that had the deepest and widest pre-release crack. The flexural cracking and flexural crack re-opening loads of the beam were determined to be 12 kips and 4 kips, respectively (Sections 5.1.2.3 and 5.1.2.4). These were the smallest cracking and crack re-opening loads obtained among the single crack series beams tested. The maximum load applied during the flexural cracking test of this beam was 46 kips. At 45 kips, one flexural crack was visually detected at the bottom surface of the beam below the pre-release crack. Following the flexural cracking test, the beam was subjected to a flexural crack re-opening test, where a maximum 10 kip load was applied. Upon cyclic loading, the beam lasted 5 million cycles with no significant degradation in stiffness.

*Figure 5.73* shows the crack pattern after 1 million cycles of loading. This crack pattern had stabilized at approximately 300,000 cycles and was almost the same as the crack pattern at the end of the cyclic test at 5 million cycles. As indicated in the figure, the major flexural crack was below the pre-release crack. All other flexural cracks were smaller than this major crack.

During the cyclic tests, the midspan deflection of the beam remained stable with increasing number of cycles. *Figure 5.74* shows that no degradation in the stiffness of the beam was observed through 5 million cycles. This figure does not include the permanent part of the deflection, which will be discussed below; all the deflections shown in the figure were the deflections that occurred during each individual static load cycle. The different plots in this figure are for the midspan deflections at different load levels during the intermittent static tests.

As shown, the selected load levels were 40 kips, 50 kips, 60 kips and 65 kips. The minimum and maximum loads during cyclic testing were 39 kips and 67 kips, respectively. The plots corresponding to different load levels being almost linear and parallel to each other indicated that the stiffness of the beam did not change significantly during 5 million cycles of testing. This behavior is also seen in *Fig. 5.75*, which shows the load versus midspan deflection at various stages of cyclic testing. The figure indicates that after a slight change during the first 5000 cycles, the stiffness of the beam remained fairly constant through the cyclic tests. The horizontal shifts of displacement between the curves indicate the permanent part of deflections. *Figure 5.76* shows the change of permanent deflections with the increasing number of cycles. The permanent deflection was the amount of deflection measured at the beginning of static load tests when there was no load applied to the beam. As shown in the figure, this deflection stabilized after approximately 50,000 cycles. There was a sudden increase in permanent midspan deflection around 4 million cycles.

The opening of the major flexural crack below the pre-release crack was also monitored during the cyclic test. *Figures 5.77* and *5.78* show the variation of this crack opening at various phases of testing. As shown in *Fig. 5.77*, the crack opening remained stable except for the sudden increase at approximately 4 million cycles. As mentioned in the previous paragraph, the same type of sudden change existed in the permanent midspan deflection at the same load cycle. These sudden increases might be due to the fracture of a wire of the prestressing strands. The fact that the crack opening and the permanent midspan deflection stabilized again after this jump, however, decreases the likelihood of this possibility. The sudden increase in flexural crack opening is seen in *Fig. 5.78* in the form of a relatively large difference between the plots at 3,000,000 and 4,052,000 cycles.

Because no sign of degradation was observed through 5 million cycles, the cyclic test was paused at this cycle. An approximately 5 in. long portion of one of the edge strands was exposed by removing the cover concrete at the location of the major flexural crack (below the pre-release crack), as shown in *Figs. 5.79* and *5.80*. A Hilti drill was used to remove the cover concrete. Then, the strand was exposed with the help of a chisel and a hammer. Even though special attention was paid to avoid damaging the strand, some of the wires were nicked accidentally during this operation. *Figure 5.81* shows the load versus midspan deflection plots

before and after the concrete cover around the major flexural crack was removed. The small difference between the two plots indicated that the removal of the concrete did not change the overall stiffness of the beam significantly. After the concrete was removed, five strain gages were glued on three different wires in the 5 in. exposed length of the strand, as shown in *Fig. 5.82*. The gages were positioned parallel to the axis of each individual wire. The beam was cycled again under the same load range after the strain gages were placed on the exposed strand. *Figure 5.83* shows the change in strand strain with load for all five strain gages during the first static loading after the gages were placed on the strand.

*Figure 5.84* shows the change of the strand stress range with the number of cycles after 5 million cycles. The strain values shown in this figure are the difference in strand strains at maximum and minimum loads, measured by the gages placed on the exposed strand. To convert the strains into the stress, a modulus of elasticity of 32,000 ksi was used. As mentioned in Section 5.1.1, this "apparent modulus of elasticity" value was documented by Lawver (1998), and it relates the strain along the axis of individual wires to the strand stress. At a later stage, the modulus of elasticity reported by Lawver was verified by the strand tension tests conducted on 0.5 in. and 0.6 in. diameter strands. These tests are described in Appendix B.

The maximum strand stress ranges obtained from this figure are listed in *Table 5.12*. As shown in the figure, the strand stress range values obtained from the five strain gages differed slightly. The reason for this was the location of the strain gages relative to the flexural crack. Strain gages closer to the flexural crack indicated larger strain changes. Because the largest of these strains was of concern for fatigue of the strand, the maximum strand stress ranges are listed in *Table 5.12*. The range in maximum strand stress ranges were 28.6 ksi and 55.2 ksi, respectively, at the beginning and end of 557,000 load cycles following the initial 5 million cycles.

One of the wires on the exposed strand were observed to be fractured 387,000 cycles after the beginning of the "post-5-million" cycles. There was a small nick on the strand surface at the location of this wire break. The last static loading done before the wire break was at cycle 5,244,000. At this cycle the maximum strand stress range was *35.3 ksi*. After the wire break, the maximum stress range in the remaining wires increased to *43.9 ksi*. There were two strain gages on the fractured wire, and the strain readings from these gages decreased to zero after wire

fracture, as shown in *Fig. 5.84*. There was another wire fracture observed after 5,428,000 cycles. After the fracture of the second wire, the maximum stress range on the remaining wires was measured to be *53.0 ksi*. There were no additional wire fractures until the test was stopped at 5,552,000 cycles. Because there were nicks on some of the wires, it was suspected that the strand stress ranges were affected by the reduction in wire area in the vicinity of the nicks. The fact that all five strain gages, placed on three different wires in the 5 in. length of the strand, measured similar strains indicated that the effect of wire nicks on the strain range was insignificant.

The stress ranges measured from the strain gages represent the lower bound of the stress range on the other strands at the same section, because of the degree of bond between the strands and the concrete. When a flexural crack forms in the beam, the bond between the strands and the surrounding concrete deteriorates in the vicinity of the crack, and a strand stress gradient occurs in this "debonded" length. Because some of the bond between the strand and the concrete was destroyed when the concrete was removed, the debonded length of the exposed strand was actually longer than that of the other three strands. This resulted in a smaller strain in the exposed strand, because the same amount of flexural crack opening was effective over a longer length of strand.

#### 5.1.3.2 Beam SC-22-14-R2

This beam was the replicate of beam SC-22-14, which had a 22 in. deep and 0.014 in. wide pre-release crack. Flexural cracking and flexural crack re-opening loads of this beam were 12 kips and 4 kips, respectively. During the flexural cracking test, this beam was subjected to a maximum load of 45 kips. At the end of the flexural cracking test, there were three visually detected flexural cracks at the bottom surface of the beam. The cracks were located in the region approximately 2 in. on either side of midspan. The longest and widest of these cracks was located below the pre-release crack. Cyclic testing of this beam was stopped after 2 million cycles due to excessive deformation and wire breaks.

During testing cycles, the major flexural crack was the one located below the pre-release crack. As cycling continued, the width of the flexural crack located approximately 12 in. north of the midspan section started to increase, and this crack became the major flexural crack. The crack pattern after 1 million cycles is shown in *Fig. 5.85*. The new major flexural crack is indicated as the "failure crack" in the figure. After 1.5 million cycles, a squeaking sound was

detected coming from the beam near this crack. At 1,880,000 cycles, it was noticed that the concrete below the pre-release crack on the east face of the beam was heavily damaged and started to spall, as shown in *Fig. 5.86*. During testing, the east face of the beam was not easily accessible because of another specimen in the laboratory. The cracks were monitored and marked on the west face of the beam. For this reason, this heavy damage may have occurred earlier, even though it was noticed after 1,880,000 cycles.

After 1.9 million cycles, opening of the major flexural crack at the bottom surface of the beam was approximately 3/32 in.(*Figure 5.87*). At this cycle, the flexural crack below the pre-release crack was almost completely closed. *Figure 5.88* shows the crack pattern at 2 million cycles. The numbers shown near the cracks indicate the number of cycles at which the crack propagated to that position. As shown in the figure, there was excessive cracking in the beam after 2 million load cycles.

Testing of the beam was paused at 2 million cycles, and one of the edge strands was exposed for a length of approximately 6 in. at the location of the flexural crack located below the pre-release crack. When the strand was exposed, two of the seven wires in that strand were observed to be fractured. Five strain gages were placed on three of the remaining five wires. These strain gages indicated strand stress ranges changing between only 4 ksi and 7 ksi during the first static loading. Compared to the strand stress ranges measured in the previous beam (SC-22-14) and also considering that two of the wires on the instrumented strand had already fractured, these stress range values seemed low. After 30,000 load cycles, testing was paused again, and the same strand was exposed at the location of the major flexural crack (12 in. north of midspan). All seven wires of the strand were observed to be fractured at this location. A close-up view of the fractured wires is shown in *Fig. 5.89*. Fracture of wires in this strand was the reason for the low strand stress range measured at midspan. The reason for measuring any strand stress at midspan was attributed to the bond between the wires and the surrounding concrete along the length of approximately 12 in. between the fracture and the gage location.

*Figure 5.90* shows the change of static centerline deflection of the beam. As shown, the centerline deflection of the beam remained essentially constant until approximately 1.9 million cycles. After this cycle, the stiffness of the beam deteriorated rapidly. The permanent midspan deflection plot in *Fig. 5.91* showed a similar behavior. The permanent deflection increased

slightly until approximately 1.9 million cycles, and increased rapidly thereafter. *Figure 5.92* shows the load-deflection behavior at various static load tests. The plots shown in this figure include both the change in midspan deflection due to the stiffness change and the permanent deflection. As shown in the figure, the midspan deflection at 67 kips was approximately 0.2 in. during the first static loading. This deflection increased to approximately 0.4 in. after 2 million cycles.

The change in permanent deflection between cycles 901,000 and 1 million in *Fig. 5.91* was probably due to fracture of two wires at the location of the flexural crack below the pre-release crack. As shown in *Fig. 5.88*, after 1 million cycles, horizontal cracks developed at the strand level, approximately 15 in. south of midspan. This type of horizontal cracking is a sign of bond failure between the steel and the concrete. This suggests that the strand debonded from the concrete on south side of midspan. Such cracking was not observed on north side of midspan during cyclic testing, suggesting that strand was still bonded to the concrete on this side. The reason that the strand may have had greater debonding on the north side of midspan than the south side was probably due to the existence of another flexural crack approximately 7 in. south of midspan.

As shown in *Fig. 5.88*, the flexural crack located approximately 12 in. north of midspan reached to the web of the beam, and propagated rapidly after 1 million cycles. This is illustrated by the increased slope of the load-permanent deflection plot after approximately 1.2 million cycles, as shown in *Fig. 5.91*. Stiffness of the beam deteriorated rapidly after approximately 1.9 million cycles. This rapid deterioration in beam response that led to failure of the beam was likely due to progressive fracture of the wires at the flexural crack located 12 in. north of the pre-release crack.

#### 5.1.3.3 Beam SC-UC-1

The third beam subjected to cyclic testing was beam SC-UC-1, which was one of the three beams that did not have a pre-release crack. Flexural cracking and crack re-opening loads of this beam were 54 kips and 27 kips, respectively. The maximum load that this beam was subjected to before the cyclic tests was 67 kips, which was applied during the flexural cracking test. At this load, three flexural cracks were visually detected at the bottom surface of the beam. The crack located approximately 20 in. away from the midspan section of the beam was longer

and wider than the other two cracks. This crack will be called the major flexural crack throughout the discussion in this section. New flexural cracks developed during the cyclic tests and the cracking pattern shown in *Fig. 5.93* was obtained after 1 million load cycles. Two million cycles of fatigue loading caused no discernable damage to this beam.

Static centerline deflection after various load cycles during cyclic testing is shown in *Fig. 5.94*. After the very early stages of testing, the response of the beam was stable except for the slight increase in deflection between the 500,000 and 1,000,000 cycles. This behavior is seen in *Fig. 5.95* in the form of a slight difference between the load versus midspan deflection plots obtained after 500,000 and 1,000,000 cycles. As shown in the figure, there was a relatively large change in the stiffness of the beam during the early cycles. The change in the slopes, and hence the stiffness of the beam, changed by a very small amount after 100,000 cycles. Indeed, the plots for static tests done after cycles 1,518,000 and 2,000,000 were on top of each other. This indicated that neither the stiffness of the beam changed, nor a permanent midspan deflection occurred between these cycles. The permanent midspan deflection plotted against the number of cycles is shown in *Fig. 5.96*. The permanent midspan deflections increased until approximately 1.4 million cycles, as shown in the figure.

*Figure 5.97* shows the variation of the opening of the major flexural crack with the number of cycles. The crack opening remained stable between approximately 50,000 and 1.4 million cycles. The sudden short jump at approximately 1.2 million cycles was probably due to an external effect to the LVDT or to the cables used for data acquisition during the intermittent static test. As shown in the figure, the crack opening stabilized again, after a slight increase between 1.4 million and 1.8 million cycles.

After 2 million cycles, the cyclic test was paused because the response of the beam had stabilized and no sign of structural distress was observed. Using the same procedure explained earlier for the other two beams, an approximately 5 in. long section of one of the edge strands was exposed at the location of the major flexural crack. Six strain gages were placed on three different wires along the 5 in. exposed length of the strand, and cyclic testing was continued. *Figure 5.98* shows the change of the strand strain with the load for the first static loading after the strain gages were placed on the wires. As shown in the figure, all six strain gages indicated the same amount of strain until approximately 26 kips. In this load range the flexural crack

remained closed. At 26 kips, the crack started to re-open and the strain gages on the strand started to indicate different strains, depending on the relative position of the gage with respect to the flexural crack.

Change of the measured strand stress range with the number of cycles (after 2 million cycles) is shown in *Fig. 5.99*. The corresponding strand strain ranges are also shown in the figure. As shown in the figure, strand stress range remained almost the same during approximately 0.6 million cycles of "post-2-million" cycles. *Table 5.13* shows the maximum strand stress ranges at various cycles. As shown in the table, the maximum strand stress ranges were approximately *20 ksi*.

No wire fracture occurred through 578,000 cycles following the "initial" 2 million cycles, and the cyclic test was stopped after 2,578,000 total load cycles.

#### 5.1.3.4 Discussion of Cyclic Test Results

The primary purpose of the cyclic tests was to evaluate the effect of the existence of pre-release cracks on the fatigue life of the beams. Three cyclic tests do not form a large enough sample size to draw definitive conclusions regarding the fatigue behavior of structures. The non-homogeneous nature of concrete, interaction among the prestressing strands and the concrete, level of prestress in the strands, and the susceptibility of test results to the cracking pattern developed during testing makes the fatigue problem even more complicated in prestressed concrete beams. These uncertainties show themselves in the form of large scatter in the fatigue data obtained by different researchers through the years (Paulson et al. (1983), Overman et al. (1984), and Muller and Dux (1994)).

The two parameters used to assess the condition of the beams during cyclic testing were the measured stiffness of the beams and the measured strand stress ranges. The former parameter implicitly includes the effects of the number of flexural cracks developed during testing and the widths of these cracks.

As shown in *Figs. 5.73*, *5.85*, and *5.93*, the crack pattern after 1 million cycles of fatigue loading were similar in all three beams. During fatigue testing, beam SC-UC-1 experienced stiffness degradation. Even though the rate of degradation was small, there was a noticeable change in the stiffness of this beam between cycle 1000 and 100,000, as shown in *Fig. 5.95*. The slight increase in midspan deflections with the increasing number of cycles shown in *Fig. 5.94* is

a result of this stiffness degradation. Beams SC-22-14 and SC-22-14-R2 did not show this stiffness degradation. The load-deflection plots at several cycles shown in *Figs. 5.75* and *5.92* remained parallel to each other through 1.5 million cycles, except for the stiffness changes occurring at the very early cycles. The difference in the response of the beams was likely due to the existence of pre-release cracks in beams SC-22-14 and SC-22-14-R2. In these beams, the flexural cracks below the pre-release cracks propagated up to the level of the pre-release crack tip, and joined with the pre-release cracks, during the early cycles of testing. This means that there was a through-depth crack at midspan of these two beams. During loading, these through-depth cracks opened from the bottom of the beams up to the level where the stress due to the applied load was zero. On the other hand, there was no such crack in beam SC-UC-1, which did not have a pre-release crack. As fatigue loading continued, the flexural cracks in this beam propagated towards the top of the beam, and caused reduction in the stiffness of the beam, but never developed into through-depth cracks. Propagation of the flexural cracks in this beam might be due to weakening of the concrete resulting from large number of load cycles.

Strand stress ranges measured after exposing the strands in beams SC-22-14 and SC-UC-1 are useful in terms of quantifying the effect of the existence of pre-release cracks, even though the stress ranges were measured after 5 million cycles in beam SC-22-14 (*Figure 5.74*, *Table 5.12*), and after 2 million cycles in beam SC-UC-1 (*Figure 5.99*, *Table 5.13*). The average of the maximum strand stress ranges measured between cycles 2,000,000 and 2,578,000 in beam SC-UC-1 was *20.4 ksi*. In beam SC-22-14, the maximum strand stress range was measured as *28.6 ksi* during the first static loading after initial 5 million cycles of loading. The maximum strand stress range increased to *33.3 ksi* 32,000 cycles later, and stabilized between 33.3 ksi and 35.3 ksi during the following 200,000 cycles. As explained earlier, these stress ranges were measured at the location of the major flexural crack in both beams. Unfortunately, no meaningful data can be obtained from the measured strand stress ranges on beam SC-22-14-R2, because there were already seven fractured wires when the strand stress ranges were measured in this beam.

The fact that beam SC-22-14-R2 withstood only 2 million fatigue cycles, while the replicate of this beam, beam SC-22-14, lasted 5 million cycles with no significant damage could be explained by the random nature of fatigue tests as discussed above. During cyclic tests, the bottom flange of beam SC-22-14-R2 was heavily damaged at the location of the pre-release

crack. In this beam, there were two fractured wires below the pre-release crack and seven fractured wires approximately 12 in. away from the pre-release crack in the exposed strand after 2 million load cycles. This damage, which led to failure of beam SC-22-14-R2 was likely due to the effect caused by the existence of the pre-release crack.

The above results provide an indication that a beam that develops pre-release cracks is more likely to experience fatigue problems than a beam with no pre-release cracks. In this particular study, the beams were subjected to cyclic testing in the cracked state with the maximum load being 67 kips. If the maximum load were less than 67 kips, then the beam with no pre-release crack would have been subjected to cyclic testing in the uncracked state, while the beam with the pre-release crack would still have been in the cracked state. In this case, the difference between the strand stress ranges of the two beams would have been larger than observed in the test beams.

## 5.2 Multiple Crack Series Beams

Six multiple crack series beams spanning 29 ft were subjected to static tests. Two of these beams had no pre-release crack, one of them had one pre-release crack placed at midspan, and three of them had three pre-release cracks placed symmetrically with respect to midspan in the constant moment region. Among the beams with three pre-release cracks, cracks were widely spaced in one of them and closely spaced in the other two. A detailed description of the beams was presented in Chapter 4. Results obtained from testing of these beams are presented in the following sections.

### 5.2.1 Effective Prestress

Two of the multiple crack series beams (beams MC-UC-1 and MC-1C) were subjected to strand testing in order to determine the value of effective prestress. The procedure included exposing a small part of two of the four prestressing strands in each beam, and flame-cutting the strands after placing strain gages on the individual wires. This procedure is explained in detail in Section 5.1.1 for the single crack series beams. The maximum load that beams MC-UC-1 and MC-1C were subjected to prior to strand testing was 60 kips, which was applied during the flexural cracking tests.

*Figures 5.100* and *5.101* show the strain readings recorded during the strand-cut in beams MC-UC-1 and MC-1C, respectively. The negative change in strain means that the tension in the strands was released after the strand cut. As shown in the figure, each beam had six strain gages placed on two strands. The behavior observed from the strain readings was the same as that obtained in the strand testing of beams SC-UC-3 and SC-22-14-R1, which was discussed in Section 5.1.1.

*Table 5.14* shows the change in strain values for each strain gage after the strain values stabilized following the strand cut. In each beam, two of the gages indicated strain change values that were quite different than the other four gages. The cells containing strain readings from these two gages for each beam are shaded in the table. The reason for reading less strain change could be due to misorientation of the gages with respect to the axis of the individual wires on which the gages were placed. Any strain gage orientation other than along the axis of the wires would result in smaller strain. Therefore, the reason for smaller strain readings of gage South3 in beam MC-UC-1 and gages South2 and South3 in beam MC-1C might be due to misorientation of the 1 millimeter gages. As shown in *Table 5.14*, average strain changes obtained from four strain gages were 5970 με and 5500 με for beams MC-UC-1 and MC-1C, respectively. The coefficient of variation values were 3.2 % and 2.7 % respectively. To convert the strain values into effective strand stress, an "apparent modulus of elasticity" of 32,000 ksi documented by Lawver (1998) was used. As mentioned in Sections 5.1.1 and 5.1.3, at a later stage, the modulus of elasticity reported by Lawver was verified by the strand tension tests conducted on 0.5 in. and 0.6 in. diameter strands. These tests are described in Appendix B.

The effective strand stresses for beams MC-UC-1 and MC-1C were calculated to be *191.0 ksi* and *176.0 ksi*, respectively. These stress values corresponded to total effective prestressing forces of 116,300 lb and 107,200 lb, respectively.

### 5.2.2 Concrete Strains and Pre-Release Crack Closure

In this section, closing behavior of the pre-release cracks and changes in bottom fiber concrete strains along the length of the beams will be discussed.

*Figure 5.102* shows the bottom fiber concrete strain plotted with respect to the distance of the strain gages from the centerline of the beam for beam MC-UC-2. The constant moment

region extended 90 in. on either side of centerline, as indicated on the figure. This beam had no pre-release crack, and hence the strain due to the applied load at the bottom of the beam was constant along the constant moment region. The strain changes that occurred at 40 kip load were indications of flexural cracking at the bottom surface.

In *Fig. 5.103*, the bottom fiber strain distribution of beam MC-1C is shown. Even though this beam had one 16 in. deep and 0.014 in. wide pre-release crack placed at midspan, the strain distribution for this beam was not significantly different than the one shown in *Fig 5.102*, which was for the beam without pre-release cracks. The reason that the pre-release crack in beam MC-1C did not have an effect on the bottom fiber strains may have been due to the size of the pre-release crack in this beam being much smaller than anticipated. This event is more clearly seen when the strain distributions in *Figs. 5.104* and *5.105* are compared. *Figure 5.104* shows the bottom fiber strain distribution for beam SC-16-14. This beam belonged to the single crack series beams (*20 ft long*), and had one 16 in. deep and 0.014 in. wide pre-release crack placed at the midspan (same as beam MC-1C). *Figure 5.105* shows the bottom fiber strain distribution for beam MC-1C (*30 ft long*). This figure contains the same data as *Fig. 5.103*, but plotted for the same load increments shown in *Fig. 5.104*.

Even though the beams SC-16-14 and MC-1C both had the same size pre-release crack placed at midspan of the beams, as shown in *Figs. 5.104* and *5.105*, the bottom fiber concrete strain distributions were quite different. Beam MC-1C behaved as if there was no pre-release crack in it. The reason for this behavior is likely because the actual width of the pre-release crack in beam MC-1C was much smaller than the width of the crack in beam SC-16-14. *Figure 5.106* shows the displacements measured by the LVDTs placed across the pre-release cracks in beams SC-16-14 and MC-1C. In the figure, beam *SC-16-14* is indicated as "*20 ft*", and beam *MC-1C* is indicated as "*30 ft*". The pre-release cracks in these two beams were intended to be identical with 16 in. depth and 0.014 in. width. As shown in the figure, under the same load, closure of the pre-release crack in beam SC-16-14 was much larger than closure of the crack in beam MC-1C.

The displacements and strains measured during the load tests reflect the response of the beams due to the applied load only without any effect of self-weight. The moment arms in the single crack (*20 ft long*) and multiple crack (*30 ft long*) series beams were the same. Even though the self-weights of the two types of the beams were different, the moment due to self-weight of

the beams was small compared to the moment due to the applied load for both types of beams. The additional self-weight moment on the multiple crack series beams (*30 ft long*) due to the longer span length was 214 in-kips, which corresponded to a 5 kip actuator load on the single crack series beams (*20 ft long*).

In *Fig. 5.106*, at 40 kips, pre-release crack closure at the top of the 20 ft beam was approximately *0.021 in*. This value was approximately *0.003 in*. for the 30 ft beam (For the sake of illustration, the pre-release crack closure values were compared at the same load for both series of beams without considering the difference between the self-weight moments). Similar ratios exist between the crack closures of the 20 ft and 30 ft beams at different levels through the depth of the crack, as shown in the figure. It is evident from this that the width of the pre-release crack in beam MC-1C (30 ft) was much smaller than width of the crack in beam SC-16-14 (20 ft) at the time of testing.

In addition to the difference in the amounts of crack closure, shapes of load versus amount of crack closure plots for 20 ft and 30 ft beams were also different. As shown in *Fig. 5.106*, the plots for the 20 ft beam were bilinear with significantly different slopes. The change of the slope in these plots was due to stiffness increase resulting from closure of the pre-release crack. This type of slope change is not seen in the plots for the 30 ft beam. This was because of the fact that the increase in the stiffness of the beam due to closure of the crack was very small compared to the initial stiffness of the beam. This suggests that the pre-release crack in beam MC-1C closed by a small amount during the load test.

The bottom fiber strain distributions shown in *Fig. 5.107* are for beam MC-3C-C, which had three pre-release cracks that were closely spaced. As indicated on the figure, one of the pre-release cracks was placed at midspan and the other two were placed 20 in. from midspan on either side in the constant moment region. Similar to beam MC-1C, the existence of the pre-release cracks in beam MC-3C-C had almost no effect on the bottom fiber concrete strains; the beam behaved as if there were no pre-release cracks. This was likely due to the width of the pre-release cracks in this beam being much smaller than the anticipated crack widths.

*Figure 5.108* shows the closing of the pre-release cracks in beam MC-3C-C. For comparison purposes, the load versus crack closure plot of beam MC-1C iss also plotted in the same figure. In the figure, “Crack2” represents the pre-release crack at the midspan, and

"Crack1" and "Crack3" represent the other two pre-release cracks. As shown, all three cracks exhibited similar closing behaviors. Even though the amounts of closure of the pre-release cracks in beam MC-3C-C were slightly larger than crack closure in beam MC-1C, they were on the same order of magnitude. This indicates that, before the load tests, the width of the pre-release cracks in beam MC-3C-C was much smaller than the crack widths in 20 ft beams.

Distribution of bottom fiber strain for beam MC-3C-W is shown in *Fig. 5.109*. This beam had three pre-release cracks, one of which was placed at the midspan and the other two were placed 60 in. on both sides of midspan. Different from the other multiple crack series beams, the pre-release cracks had an effect on bottom fiber strains in this beam. As shown in the figure, the bottom fiber tensile strains locally increased in the vicinity of the pre-release crack sections. Because the distance between the pre-release cracks (60 in.) was larger than two times the depth of the beam (56 in.), the span lengths where each pre-release crack was effective did not interact with each other. The reason that the pre-release cracks in beam MC-3C-W affected the bottom fiber strains while the cracks in other multiple crack series beams did not, was likely due to the pre-release cracks in beam MC-3C-W being wider than the cracks in the other multiple crack series beams. *Figure 5.110* shows the closing of the pre-release cracks in beam MC-3C-W. In the figure, "Crack1" represents the pre-release crack located 60 in. east of midspan (-60 in.), "Crack2" represents the pre-release crack at midspan, and "Crack3" represents the pre-release cracks located 60 in. west of midspan (+60 in.). Load versus pre-release crack closure plots of beam MC-1C is superimposed on the same figure. As shown, under the same load, closings of the pre-release cracks in beam MC-3C-W were larger than closing of the crack in beam MC-1C.

For the multiple crack series beams, measurements of the pre-release crack widths before and after the transfer of the prestressing force were done with a feeler gage. These measurements indicated that the widths of the pre-release cracks in the multiple crack series beams before and after the prestressing strands were released were smaller than the anticipated crack widths.

There were two possible reasons for the pre-release crack widths in multiple crack series beams being much less than the crack widths in the single crack series beams. One of the reasons is the larger self-weight moment in the multiple crack series beams due to longer span length. Because the span length in the multiple crack series beams (29 ft) was approximately 1.5 times larger than the span length of single crack series beams (19 ft), the midspan moment due to self-

weight of the beams was approximately 2.3 times larger. The larger moment caused the pre-release cracks in the multiple crack series beams to close more than the cracks in single crack series beams. This closure of pre-release cracks occurred before load testing of the beams. Because the feeler gage measurements indicated that the crack widths in the multiple crack series beams were already smaller before the transfer of the prestressing force, difference in self-weight moments cannot be the only reason for the difference in crack widths between the two groups of beams. In addition to this, the moment due to self-weight of the beams was not believed to be large enough to cause such big changes in pre-release crack openings.

The other possible reason for the difference in pre-release crack openings between the single crack and multiple crack series beams may be due to a difference that may have occurred during fabrication of these two sets of beams. The beams were fabricated at the same plant using the same construction techniques. The single crack series beams were fabricated six days earlier than the multiple crack series beams. The concrete mix used for the two series of the beams was the same except for the amount of superplasticizer. The concrete mix for the single crack series beams included, 130 oz/cuyd of superplasticizer. The amount of superplasticizer used in the multiple series beams was 150 oz/cuyd. In spite of this difference in the amounts of superplasticizer used, the concrete slump for the two series of beams was similar. The times when the crack-formers were removed after concrete pouring were similar for both sets of beams. Another difference that occurred during fabrication of the beams was the maximum concrete temperature during the curing period. The maximum concrete temperatures were approximately 140 ºF and 185 ºF for the single crack and multiple crack series beams, respectively. The reason for different concrete temperatures was due to the externally applied temperature to the multiple crack series beams during overnight curing.

### 5.2.3 Flexural Cracking Loads

This section presents the results of the flexural cracking tests performed on the multiple crack series beams.

The cracking loads determined by visual observation during the flexural cracking tests of the beams are listed in *Table 5.15*. As shown in the table, flexural cracking loads of the 30 ft. long beams with single and multiple pre-release cracks were similar to the cracking loads of the 30 ft. long beams without pre-release cracks, except for beam MC-3C-W. The reason for the

negligible difference in flexural cracking loads among all but one of the beams was attributed to smaller actual pre-release crack widths than the anticipated crack widths in these beams. As explained in the previous section, the widths of the pre-release cracks in beam MC-3C-W were larger than the pre-release crack widths in the other beams of this series. The larger pre-release crack width in beam MC-3C-W resulted in a smaller flexural cracking load than the other beams, as shown in the table.

The locations of the first visually observed flexural crack(s) for each beam are also indicated in *Table 5.15*. As shown in the table, locations of the first flexural cracks in the beams without pre-release cracks were close to the load points. On the other hand, flexural cracking in beams with pre-release cracks were localized around the pre-release crack locations.

As in the case of the single crack series beams, flexural crack initiation loads of the multiple crack series beams were determined using the strain readings from the strain gages placed at bottom surface of the beams. *Figures 5.111* through *5.116* show the plots used to determine the flexural crack initiation load of the beams. For each beam, strain readings from the gage that first indicated a constant tensile strain with increasing load, and one of the neighboring gages are plotted. The flexural crack initiation load was determined to be the load at which the strain readings from the two neighboring gages started to diverge from each other. For most of the beams this point corresponded the load where there was an abrupt slope change in one of the plots. Behavior seen in plots of bottom surface strain gages was discussed in detail in Section 5.1.2.3 for single crack series beams.

The flexural cracking loads determined from bottom surface strain readings are tabulated in *Table 5.15*. As shown, the visually observed cracking loads were larger than the crack initiation loads determined from strain gage plots for all beams except for beam MC-3C-W. The reason that the visually observed cracking load was smaller than the cracking load determined from strain gage plots for beam MC-3C-W was because of the location of the strain gages. During the flexural cracking test of this beam, at 39 kips, a flexural crack at the bottom surface of the beam close to the *north* side of the beam was detected. The strain gages at the bottom surface of beam were placed close to the *south* side of the beam. Because of this, the flexural crack that was visually observed at 39 kips was detected by the strain gage readings at 40 kips.

### 5.2.4 Flexural Crack Re-Opening Loads

The flexural crack re-opening load of the beams was determined from the LVDTs placed over and near the major flexural crack(s) after the flexural cracking tests. The plots used to determine the crack re-opening loads are shown in *Figs 5.117* through *5.122*. The behavior seen in these plots is similar to that observed in the single crack series beams, which were explained in detail in Section 5.1.2.4. Measurements from the *over-crack* LVDTs were used to determine the flexural crack re-opening load of beams MC-UC-1 and MC-UC-2. For the other beams, measurements from the *near-crack* LVDTs were used. Load versus displacement plots of the *near-crack* LVDTs in beams MC-UC-1 and MC-UC-2 did not show any sign of flexural crack re-opening. These plots are given in Appendix E.

As shown in *Figs. 5.117* through *5.122*, the crack re-opening load for each beam was determined to be the load at which the initial slope of load versus LVDT displacement plots changed. Flexural crack re-opening loads determined this way are tabulated in *Table 5.16*. As shown in the table, the crack re-opening load of beam MC-3C-W, which had the widest pre-release cracks, was smaller than the others.

Different from the single crack series beams, it was not possible to determine the crack re-opening loads of the multiple crack series beams from the bottom surface strain measurements. In the single crack series beams, re-opening of the flexural cracks caused changes in the slopes of the load versus bottom fiber strain plots. This type of change was not observed in multiple crack series beams, which was probably due to the larger spacing between the gages used in these beams.

*Predicted Flexural Cracking and Crack Re-Opening Loads*

Flexural cracking and crack re-opening loads of the beams without pre-release cracks were calculated using *Equation (5.1)*. Flexural cracking loads were determined to be *66 kips* and *70 kips* for the measured effective prestresses of 176.0 ksi and 191.0 ksi, respectively. Crack re-opening loads corresponding to these prestress values were calculated to be *35 kips* and *39 kips*.

As shown, there was a significant difference between the measured and calculated flexural crack initiation and re-opening loads of the beams with no pre-release cracks. The

possible reasons for the discrepancy were discussed in Section 5.1.2.3 for the single crack series beams. These reasons are valid for the multiple crack series beams too.

### 5.2.5 Overall Beam Stiffness

Load versus midspan response of the beams measured during flexural cracking tests are shown in *Fig. 5.123*. The figure consists of plots for four beams; one beam with no pre-release crack (beam MC-UC-2), one beam with one pre-release crack (MC-1C), one beam with three-closely spaced cracks (MC-3C-C-R), and one beam with three widely spaced cracks (MC-3C-W). A shown in the figure, none of the beams exhibit such stiffness increases as those shown in *Figs. 5.63* and *5.64* for the single crack series beams. The reason for the increase in stiffness of the single crack series beams was the increase in moment of inertia of the pre-release crack sections due to closing of the cracks. Stiffness of the multiple crack series beams was larger than those of the single crack series beams. This was probably because the bottom parts of the pre-release cracks were closed prior to load tests in multiple crack series beams. Because of this large initial stiffness, any increase in moment of inertia of the pre-release crack sections due to crack closure did not result in as significant a change in the overall stiffness of multiple crack series beams as for the single crack series beams. Moreover, widths of the pre-release cracks in the multiple crack series beams were much smaller than the pre-release crack widths in the single crack series beams, as discussed earlier. This resulted in a smaller amount of crack closure, and hence a smaller increase in the stiffness of the multiple crack series beams.

As expected, the beam without pre-release cracks (beam MC-UC-2) had the largest stiffness (*Figure 5.123)*. The stiffness of the beam with one pre-release crack (beam MC-1C) was larger than the stiffness of the beams with three pre-release cracks. The slight difference between the beams with three pre-release cracks (beams MC-3C-W and MC-3C-C-R) was probably due to a difference in the modulus of elasticity values of the concrete used in these beams.

## 5.3 Three-Point Bending Beam

A beam with two pre-release cracks placed 60 in. from midspan on both sides (beam 3P-2C) was tested under three-point bending. This beam was only subjected to a flexural cracking test to determine if flexural cracking would occur below the pre-release cracks first, even though

the maximum moment due to the applied load occurred at midspan. *Figure 5.124* shows the load versus midspan deflection plot of this beam. The two sudden load drops shown in the figure corresponded to the instants where flexural cracks formed. At 35 kips, the first flexural crack formed approximately 6 in. away from the midspan. No other cracks were detected until 40 kips. At 40 kips, another flexural crack developed below one of the pre-release cracks. The widths of both flexural cracks in this beam were much larger than the widths of flexural cracks in all other beams. Testing of the beam was stopped at 42 kips. At this load, there were no new flexural cracks other than the two mentioned above. The reason that first flexural crack occurred at midspan rather than below the pre-release cracks as was predicted by the finite element models, was because the pre-release crack widths were smaller than anticipated. *Figure 5.125* shows the amount of pre-release crack closure in beam 3P-2C. As shown in the figure, the crack closure values measured during testing were much less than the anticipated pre-release crack width of 0.0014 in. Moreover, when the crack closure values in this figure are compared with those in *Fig. 5.23*, which was for one of the single crack series beams with the same pre-release crack dimensions (beam SC-16-14), it is evident that widths of the pre-release cracks in beam 3P-2C were much smaller than widths of the cracks in single crack series beams.

# CHAPTER SIX
# SUMMARY AND CONCLUSIONS

## 6.1 Summary

As high strength concrete becomes more popular, heavily reinforced sections with longer span lengths are being used for prestressed concrete bridge girders. Pre-release cracks have been observed by researchers during the fabrication of these girders (Ahlborn, 1998; Roller, 1993; Green, 1984), and similar pre-release cracks have been observed among the producers in the industry (Zia, 1993). Despite these facts, the available literature related with the causes and effects of these cracks is limited. A two-phase research study was undertaken at the University of Minnesota to evaluate the effects of pre-release cracking on prestressed bridge girders. Phase I included an analytical investigation of the problem, and the results from this phase were documented by Wyffels (2000). Phase II, which is the study explained in this report, included the experimental validation of the previous analytical findings.

Phase II began with a finite element study to optimize the design and instrumentation of the test specimens. Two-dimensional ABAQUS models consisting of simply-supported beams having Mn/DOT Type 28M cross sections with pre-release cracks placed in the constant moment region were prepared. The effects of size (i.e. width and depth), geometry, and spacing of pre-release cracks on girder stresses and flexural cracking loads were investigated with these models.

Based on the designs optimized with the finite element models, eighteen Mn/DOT Type 28M prestressed concrete beams incorporating single and multiple pre-release cracks were fabricated. Crack-formers were used during fabrication of the beams to control the crack dimensions and locations. The specimens were divided into two series: the single crack series and the multiple crack series beams. The single crack series beams consisted of eleven 20 ft. long beams used for the investigation of the effect of a single pre-release crack. Eight of the beams in this series incorporated a single 0.008 or 0.014 in. wide pre-release crack at either 6, 16 or 22 in. depths, while three of the beams did not have pre-release cracks. The multiple crack series beams, which were 30 ft. long, were used for the investigation of multiple pre-release crack interaction. Three of the six beams in this series incorporated three 0.014 in. wide and 16 in. deep pre-release cracks that were either widely or closely spaced.

The experimental program included two testing phases: static tests, and cyclic tests. Behavior of the beams during flexural crack initiation and re-opening, near-ultimate and failure tests, as well as cyclic tests is summarized below. Effects of the existence of pre-release cracks on concrete strains, flexural crack initiation and re-opening loads, overall beam stiffness, ultimate beam capacity, strand stress range and the fatigue life of the girders are reported.

## 6.2 Conclusions from the ABAQUS Models

Existence of the pre-release cracks caused stress changes throughout the depth of the models near the crack location. The reduced moment of inertia at the crack section resulted in an increase in compressive stress near the crack tip location, and reduction in compressive stress at the bottom of the models as compared to the models of uncracked beams. The areas near the top of the section had reduced compressive stress due to the top portion of pre-release cracks remaining open during initial stages of loading.

Stress changes were dependent on the depth and width of the pre-release cracks. Deeper and wider pre-release cracks resulted in larger stress changes compared with those of the uncracked models. The effects of the pre-release cracks were localized near the crack and decayed with the distance from the crack location. Only 5% of the effect of the pre-release crack was noticeable at a horizontal distance of 20 in. from the crack in the Mn/DOT 28M beams studied.

The reduced compressive stresses at the bottom of the models caused the elements at the bottom surface to reach the tensile strength of concrete at lower loads than the models without pre-release cracks.

Models involving multiple pre-release cracks behaved similarly to the models involving a single pre-release crack. In the models where the cracks were spaced widely such that the lengths over which each crack was effective did not interact with each other the results were similar to the models involving single cracks. When the effective lengths overlapped, the total effect was the superposition of the effects from each individual crack.

## 6.3 Conclusions from the Beam Tests

The experimental results verified the results of the analytical study. The beams involving pre-release cracks experienced strain changes from the beams without pre-release cracks.

Existence of pre-release cracks caused changes in the bottom fiber strain distributions. There was a considerable increase in the superimposed bottom surface tensile strains below the pre-release cracks. The effect was localized around the pre-release cracks, and decayed almost completely at a distance equal to the depth of the beams away from the crack location.

The changes in strain distributions through beam depth included increased superimposed tensile strains below the pre-release crack, increased compressive strains near the pre-release crack tip, and reduced compressive strains at the top of the pre-release crack. A nonlinear strain distribution through the beam depth occurred during pre-release crack closure at the sections 2 in. from the pre-release cracks. The nonlinearity of the strain distribution decreased as the horizontal distance from the pre-release cracks increased.

The amount of strain change was affected by the size of the pre-release cracks. In general, deeper and wider pre-release cracks resulted in larger strain changes. In the beam with a deeper pre-release crack, the depth of the uncracked part of the section below the pre-release crack was smaller. This resulted in a smaller moment of inertia, and hence larger strain changes compared to the beam with a shallower pre-release crack. The pre-release crack width, on the other hand, determined how long the crack remained open, and hence how much load was carried by the section with the reduced moment of inertia.

The beams containing pre-release cracks underwent flexural cracking at lower loads than the beams without pre-release cracks. Flexural crack re-opening loads of the beams with pre-release cracks were also significantly lower than those of the beams without pre-release cracks. The reason for the reduced flexural crack initiation and re-opening loads of the beams with pre-release cracks was the increased superimposed bottom fiber tensile strains occurring below the pre-release cracks.

Discrepancies existed between the calculated and measured flexural crack initiation and re-opening loads of the beams without pre-release cracks. During the tests flexural crack initiation and re-opening occurred in the beams at lower loads than calculated even for the beams without pre-release cracks. The possible reason for this discrepancy was documented to be the distribution of the prestressing strands in the section through the depth and along the width directions.

Existence of the pre-release cracks also resulted in a reduction in the initial stiffness of the beams. As the loading progressed and closing of the pre-release cracks took place, stiffness of the beams incorporating pre-release cracks approached those of the beams without pre-release cracks. Smaller stiffness changes occurred in the beams with shallower pre-release cracks than the beams with deeper pre-release cracks.

No significant difference was observed between the near-ultimate behavior of the beams with and without pre-release cracks. In addition, there were marginal differences between the measured ultimate flexural capacities of the beams involving different size pre-release cracks. The measured flexural strengths of the beams involving pre-release cracks compared well with the capacities calculated using Whitney's rectangular stress block assumptions.

Results from the cyclic testing of three beams provided indication that a beam that develops pre-release cracks is more likely to experience fatigue problems than a beam with no pre-release cracks. The maximum strand stress range in the beam with pre-release cracks would occur at the pre-release crack locations, and would be higher than the stress ranges in the beam without pre-release cracks under the same load range. This would be due to the reduced moment of inertia at the pre-release crack sections. In addition, the likelihood of flexural cracking in the beam incorporating pre-release cracks would be larger, which decreases the fatigue performance of the beam and increases the probability of fatigue failure. In this particular study, the effect of early flexural cracking due to pre-release cracks did not have effect on the test results, because all three beams were subjected to flexural cracking prior to the cyclic tests.

# CHAPTER SEVEN
# RECOMMENDATIONS

## 7.1 Background

Vertical cracks, termed “pre-release cracks”, have been observed to occur in some prestressed concrete bridge girders during fabrication. The cracking is attributed to the restrained shrinkage and thermal effects prior to release of the prestressing strands. The problem tends to be more critical for long bridge girders with deep sections and large amounts of prestressing strand.

Currently, there are no guidelines available in the State of Minnesota related to the acceptance of prestressed concrete beams that develop pre-release cracks during production. Acceptance of the cracked beams without any evaluation may result in flexural cracking of these beams under an overload, or even under service loads. Such early cracking may cause fatigue problems and endanger the safety of the bridge. On the other hand, outright rejection of the beams means economical losses including delays in the construction schedule of the bridge project. Based on the results obtained in this study, the guidelines below are recommended as acceptance criteria for beams that develop pre-release cracks during production.

## 7.2 Scope

This study was limited to the investigation of the effect of vertical pre-release cracks on the flexural behavior of beams and the guidelines were prepared accordingly. The pre-release cracks are not suspected to have a significant effect on the shear performance of beams, as they have generally not been observed to occur near the ends of the beams, where shear is more critical than flexure. Pre-release cracks located near regions of higher moment are more critical than pre-release cracks at other locations with respect to the reduction in the flexural crack initiation load.

The first part of this investigation included a finite element study, where effects of different size pre-release cracks on the flexural crack initiation load of beams were evaluated by changing the crack depth and width in finite element models. An experimental study was conducted in the second part of the investigation. Full-scale Mn/DOT Type 28M prestressed concrete beams incorporating manmade pre-release cracks were subjected to static and cyclic tests under four-point bending. The effects of pre-release crack dimensions were investigated

with the single crack series beams. Multiple crack series beams were tested for the investigation of the interaction of multiple pre-release cracks.

## 7.3 General Comments Regarding Effect of Pre-Release Cracks on Flexural Cracking

### 7.3.1 Findings from Finite Element Models and Experimental Study

Results of the finite element and experimental studies are tabulated in *Table 7.1*, which includes the reduction in flexural crack initiation and re-opening loads due to the existence of different size pre-release cracks. It should be noted that the tabulated values represent the percent reduction in flexural crack initiation and re-opening loads of the models or test beams involving pre-release cracks with respect to companion models or test beams that did not have pre-release cracks, respectively. As shown in the table, larger reductions in flexural crack initiation and re-opening loads occurred for deeper and wider pre-release cracks. Moreover, in beams with wide cracks, the amount of reduction was very sensitive to pre-release crack depth.

During the experimental program, the beams that did not have pre-release cracks underwent flexural crack initiation and re-opening at lower loads than predicted by hand calculations and finite element models. The flexural cracking load of the beams with no pre-release cracks was calculated to be 70 kips.

Several different methods were used to determine the flexural cracking load of the beams during the experiments, as explained in the body of the report. For the beams with no pre-release cracks, the average of the *flexural crack initiation loads determined from the bottom fiber strain data* was 46 kips. The *visually observed flexural cracking loads* for these beams were between 57 kips and 67 kips. The *calculated flexural crack re-opening* load was 39 kips. The average *measured flexural crack re-opening load* of the three beams without pre-release cracks was 26 kips. More information about the determination of flexural crack initiation and re-opening loads can be found in the body of the report.

As mentioned in the body of the report, the discrepancy that existed between the calculated and experimentally determined flexural crack initiation loads obtained in this study for the beams with no pre-release cracks was found to exist in other studies in the literature. Results of the studies by Shanafelt and Horn (1985), Shenoy and Frantz (1991), and Halsey and Miller (1996) support the results obtained in this study.

In a test performed by Shanafelt and Horn on an AASHTO Type III prestressed concrete girder, flexural cracking was observed at a load of 55.1 kips. This load corresponded to a calculated tensile stress in the concrete of $2.7\sqrt{f'_c}$ or $4.5\sqrt{f'_c}$(in psi), which is less than the AASHTO-specified allowable tensile stress of $6\sqrt{f'_c}$.

Shenoy and Frantz tested two 27-year-old prestressed concrete box beams. The predicted flexural cracking load of the beams was 30.1 kips. Even though it was stated in their paper that visually observed flexural cracking loads were 29 and 35.5 kips, respectively for Beams 7 and 4, the strain distribution across the depth of Beam 7 showed signs of flexural crack initiation in the form of reduced tensile strains near the bottom of the beam, starting at 11.8 kips.

In the study by Halsey and Miller, two 40-year-old prestressed concrete inverted T-beams were tested. The predicted flexural cracking load was 16.2 kips for Beam 1, and 16.4 kips for Beam 2. The experimental cracking loads were reported as 18.5 and 16.5 kips for Beams 1 and 2, respectively. The strain distribution through the depth of Beam 2 became nonlinear at 10 kips. At 16.5 kips a flexural crack became visible on one side of the beam. Even though the flexural cracking load was reported as 16.5 kips for Beam 2, it is evident from the strain data that initiation of flexural cracking in this beam occurred at a lower load.

The above results obtained by different researchers suggest that prestressed concrete bridge beams might undergo flexural cracking under service loads, or more possibly under an overload, even if there are no pre-release cracks in them. The reason that most of the prestressed concrete bridge girders have remained uncracked during their service life might be attributed to as-built concrete strengths that are higher than the specified design values, which would result in higher flexural cracking loads. In addition, distribution factors used to calculate the loads on an individual beam may be conservative. It was believed that some or all of this reserve flexural cracking capacity may enable most girders to remain uncracked during their service life despite a possible reduction in the flexural crack initiation load from the calculated value.

In the experimental study, two beams were tested for each of three crack depths (6, 16, and 22 in.), one with 0.008 in. crack width and one with 0.014 in. crack width. The “crack depth-to-section depth” ratios were approximately 0.2, 0.6, and 0.8, respectively.

The investigation of the effects of full-depth pre-release cracks was out of the scope of this study, even though pre-release cracks have been observed to extend through the entire depth

of the beam in some cases (Roller et al. (1993), Green et al. (1984)). Pre-release cracks that extend through the entire depth of beams may also cause a reduction in the flexural crack initiation and re-opening loads of the beams. Closing of full-depth pre-release cracks following the release of the prestressing strands is suspected to cause a reduction in the prestressing force locally at the crack sections.

The results obtained from the beam tests are shown in *Table 7.1*. The experimentally obtained flexural crack initiation and re-opening loads of beams with pre-release cracks were normalized to the experimentally determined loads of the beams without pre-release cracks. The table also includes the pre-release crack closure values measured at the flexural cracking load.

The experimental results indicated as large as a 50% reduction in the flexural crack initiation load of a beam with a 6 in. deep pre-release crack ("crack depth/section depth" of approximately 0.2) compared to the average of the companion test beams without pre-release cracks. The reduction in flexural crack initiation load was as large as 67% and 73% for beams with 16 in. and 22 in. deep pre-release cracks, respectively ("crack depth/section depth" values of approximately 0.6 and 0.8, respectively). The corresponding reductions in flexural crack re-opening loads were as large as 63%, 78% and 85% for beams with 6 in., 16 in. and 22 in. deep pre-release cracks, respectively ("crack depth/section depth" values of approximately 0.2, 0.6 and 0.8, respectively). The reasons for the large reduction in the flexural crack initiation and re-opening of the single crack series beams is due to the fact that the pre-release cracks in these beams remained partially opened at flexural crack initiation and re-opening, as discussed in the following section.

In *Table 7.2*, the flexural crack initiation loads of the multiple crack series beams are given. Pre-release crack closure values measured at flexural crack initiation loads are also indicated in the table. As mentioned in the body of the report, pre-release crack widths in the multiple crack series beams were significantly smaller than those in the single crack series beams at the time of test, even though similar crack-formers were used for both series of beams during construction. The pre-release cracks in the multiple crack series beams were 16 in. deep. Even though the results from the single crack series beams indicated unacceptable reductions in the flexural crack initiation loads even for the 6 in. deep pre-release cracks, the 16 in. deep pre-release cracks were not observed to cause a problem in the multiple crack series beams. This is

likely due to the fact that the pre-release cracks in multiple crack series beams closed completely prior to flexural crack initiation. This result suggests that pre-release cracks in prestressed concrete beams can be acceptable if the crack widths are small prior to release of the prestressing force and the cracks close completely prior to flexural cracking.

### 7.3.2 Effect of Pre-Release Crack Opening

As seen in *Table 7.1*, there are significant reductions in the experimentally obtained flexural crack initiation and re-opening loads of the beams with pre-release cracks compared to those of the beams without pre-release cracks. The reduction in flexural crack initiation and re-opening of the beams with pre-release cracks is due to two effects. Part of the reduction in the flexural crack initiation and re-opening loads is due to closing of the pre-release cracks. Closing of the pre-release cracks occurs due to the effects of prestressing force, self weight of the beams and the externally applied loads. The crack closure results in reductions in the bottom fiber compressive stress in the vicinity of the cracks, which, in turn, reduces the flexural crack initiation and re-opening loads.

A second reason for the reduction in the flexural crack initiation and re-opening loads of the beams with pre-release cracks is the reduced sectional stiffness at the pre-release crack locations in cases where the pre-release cracks remain partially open at flexural crack initiation and re-opening loads. As mentioned earlier, the pre-release cracks in the single crack series test beams did not close completely at flexural crack initiation and re-opening loads. As the pre-release cracks remained partially open, the section at the pre-release crack location had reduced cross-sectional area and moment of inertia compared to other cross sections that were not cracked. The reduced moment of inertia at the location of pre-release cracks resulted in reductions in the flexural crack initiation and re-opening loads of the beams.

*Figures 7.1* and *7.2*, respectively, show the analytically computed change of the flexural crack initiation and re-opening loads of the test beams with respect to depth of the open part of the pre-release cracks. The crack initiation and re-opening loads in the charts were computed using the geometric properties (moment of inertia, cross-sectional area and prestressing force eccentricity) of the “uncracked” portion of the Mn/DOT Type 28M section after assuming a depth for the part of the pre-release crack that remained open. The case with zero depth for the open part of the pre-release crack indicates a beam with no pre-release crack or a beam with a

pre-release crack that closed completely. While constructing these charts, the prestressing force and the modulus of rupture of the concrete used in the beams were modified such that the computed flexural crack initiation and re-opening loads corresponded to those experimentally determined for the beams without pre-release cracks. *Figures 7.1* and *7.2* indicate that as the depth of the open part of the pre-release cracks gets larger, the flexural crack initiation and re-opening loads of the beams decrease. It should be noted that the flexural crack initiation and re-opening loads shown in these charts only include the effect of the reduction in section stiffness due to partially closed pre-release cracks, the effect of the reduction in bottom fiber compressive stress due to the portion of pre-release crack closure is not included.

As shown in *Figs. 7.1* and *7.2*, if the pre-release cracks do not close completely prior to flexural crack initiation, there will be a major reduction in the flexural crack initiation load, even if the depth of the open part of the pre-release crack is small. For example, if the top 6 in. portion of the pre-release crack remains open, the beam undergoes flexural crack initiation at 28 kips (40% reduction compared to uncracked beam), and flexural crack re-opening at 16 kips (38% reduction compared to uncracked beam). By using the charts in *Figs. 7.1* and *7.2*, the measured flexural cracking loads of the single crack series test beams, and the measured pre-release crack closure data, the reduction in flexural cracking load due the reduced bottom fiber compressive stress, which is due to pre-release crack closure, were computed. The results, presented in *Table 7.3*, indicate that for most of the beams the major part of the reduction in flexural cracking load was due to the pre-release cracks remaining partially open. However, there were also cases where the effect of the reduced bottom fiber compressive stress on the flexural cracking load was not negligible, as evident by the reduction values in the last column of *Table 7.3*.

As explained in the body of the report, closure of the pre-release cracks in the multiple crack series beams during load-testing was very small compared to those in the single crack series beams, and the pre-release cracks in the multiple crack series beams closed completely prior to flexural crack initiation. As the pre-release cracks closed completely prior to flexural crack initiation, the latter of the effects explained above (i.e., reduced $I$) was not observed for these beams, and any reduction in flexural crack initiation load of these beams was due to the reduced bottom fiber compressive stress caused by pre-release crack closure alone. The fact that the flexural crack initiation loads of the multiple crack series beams with pre-release cracks were

similar to those of the beams without pre-release cracks indicates that there was a minimal effect of the reduced bottom fiber compressive stress on flexural crack initiation load for these beams.

*Table 7.1* shows that for the cases for which both experimental and finite element results are available, the measured percent reduction in flexural crack initiation and re-opening loads are higher than the values obtained from the corresponding finite element models. A possible cause of this difference could be the fact that the pre-release cracks in the finite element models had "tapered rectangular" cross section and they started to close from the top with crack closing propagating downward, as explained in the body of the report. The reduction in the stiffness of the pre-release crack section is smaller when the pre-release cracks start to close from the top than the reduction with pre-release cracks starting to close from the bottom. When the top of the pre-release cracks is closed, which is the case in the finite element models, part of the top flange which was lost due to the existence of the cracks is regained and contributes to carry the applied loads. On the other hand, with pre-release cracks closing from the bottom, which is the case in the test beams, depending on the depth of the open part of the pre-release cracks, part of the top flange is lost. As a result, the pre-release crack section with the crack starting to close from the bottom has smaller stiffness, and hence the beam has smaller flexural crack initiation and re-opening loads, compared to the case with pre-release cracks starting to close from the top. This difference between the closing behavior of the pre-release cracks in the finite element models and the test beams is believed to be part of the reason for the predicted reductions in flexural crack initiation and re-opening loads being smaller than the measured reduction values. Another possible reason that the test beams had a larger reduction in flexural crack initiation and re-opening loads compared to the finite element models is that the pre-release crack closure values measured in the test beams were larger than the nominal crack widths used in the finite element models.

The numerical study conducted by Wyffels (2000) included finite element models of rectangular girders with "triangular-shaped" pre-release cracks such that the cracks started to close from the bottom with crack closure propagating upward, as was the case for the pre-release cracks in the test beams. In the Wyffels' study, the effect of different size pre-release cracks on the bottom fiber stress in girders with a 45 in. by 22 in. rectangular cross section with 135 ft span length was investigated. In some of the cases investigated, the pre-release cracks closed

completely under the effect of externally applied load, while in other cases the cracks remained partly open. Among the beams with pre-release cracks completely closed prior to flexural crack initiation, there were cases where closure of the pre-release cracks alone caused unacceptably large reductions in compressive stresses at the bottom fiber of the section. For example, the pre-release crack with 1/32 in. width and 33 in. depth closed completely under the effects of prestressing force and the self weight of the girder, and there was an approximately 1050 psi reduction in bottom fiber compressive stress of this beam with respect to the beam with no pre-release crack under all values of externally applied load. The pre-release crack with 1/16 in. width and 33 in. depth closed completely under 100 lb/ft externally applied load in addition to the self weight of the beam. The reduction in bottom fiber compressive stress of this beam due to pre-release crack closure was approximately 2100 psi.

These results indicate that even if a large part of the effect of pre-release cracks on flexural cracking load may be due to the reduced sectional stiffness caused by the pre-release cracks remaining open at flexural crack initiation, as observed in the single crack series girder tests, there are cases in which the effect due to the reduced bottom fiber compressive stress caused by the pre-release crack closure might be significant.

### 7.3.3 Considerations Regarding Fatigue

Re-opening of flexural cracks takes place under smaller loads than the flexural crack initiation. If the initiation of the flexural cracks was due to the reduced flexural cracking load resulting from the existence of pre-release cracks, then the re-opening loads would be smaller still compared to a beam without pre-release cracks. Repeated re-opening of the flexural cracks would cause increased strand stress ranges due to the stress concentrations in the vicinity of the flexural cracks.

The limited cyclic test results indicate that a beam that develops pre-release cracks is likely to have larger strand stress ranges than a beam without pre-release cracks at the location of a flexural crack. As explained in the literature review section, the increased stress range together with the fretting among individual wires can cause the prestressing strands to fracture at the location of the flexural cracks under repeated loading.

## 7.4 Generalization of the Results

### 7.4.1 Generalization of the Results to other Mn/DOT 28M Sections

Because the flexural cracking loads of the beams depend on the amount and eccentricity of prestressing force, the beam length, and the tensile strength of the concrete, the results presented in *Tables 7.1* and 7.*2* are applicable only to the Mn/DOT Type 28M beams with the same amount and eccentricity of prestressing force, span length, and modulus of rupture of concrete as the test beams. The information in these tables is not sufficient to determine the effect of pre-release cracks in other Mn/DOT Type 28M beams with different prestressing force, eccentricity, span length and/or concrete tensile strength. The finite element study results cannot be extended to determine the effect of pre-release cracks in different sections because of the previously explained fact that the flexural crack initiation and re-opening loads of the beams with no pre-release cracks obtained from the experiments did not match those predicted by the finite element models.

*Table 7.4* shows the effect of pre-release cracks on nominal bottom fiber cracking stresses. The bottom fiber stress values shown in this table were calculated using the measured flexural crack initiation loads and cross-sectional properties of a beam without pre-release cracks (see *Table 5.8*). The following relationship was used to calculate the nominal bottom fiber stress values.

$$\sigma_{no\min al} = -\frac{P_{eff}}{A_g} - \frac{P_{eff} e_g c_g}{I_g} + \frac{M_{self} c_g}{I_g} + \frac{M_{applied} c_{tr}}{I_{tr}} \qquad (7.1)$$

where, $\sigma_{nominal}$ is the nominal bottom fiber stress at midspan (tension is positive), $P_{eff}$ is the measured effective prestressing force (104,500 lb), $A_g$ is the cross-sectional area (285 in$^2$), $e_g$ is the eccentricity of the prestressing force (10.3 in.), $c_g$ is the depth of the neutral axis of the gross section (12.3 in.), $I_g$ is the gross moment of inertia (23,700 in$^4$), $M_{self}$ is the midspan moment due to self-weight of the beam (165 in-kips), $c_{tr}$ is neutral axis depth of the transformed section (12.1 in.), $I_{tr}$ is the transformed moment of inertia (24,100 in$^4$), and $M_{applied}$ is the midspan moment due to applied loading, which for each beam, was found by multiplying half of the flexural crack initiation load shown in *Table 7.4* by the moment arm, which was 85 in.

Shown in the last column of *Table 7.4* is the percent reduction in the measured flexural cracking loads of the specimens from the predicted flexural cracking load of 70 kips. It should be noted that these *reductions in cracking load* values are specific to the beams tested in this study, and cannot be applied to beams with different section, prestressing force, span length or concrete strength to estimate the effect of a pre-release crack. On the other hand, the *reduction in nominal bottom fiber stress* values given in the table can be used to predict the reduction in flexural crack initiation load of a beam due to a certain size pre-release crack. The procedure is explained below.

Normally, flexural crack initiation should occur when the bottom fiber stress reaches the modulus of rupture of concrete, which was measured to be *650 psi* for the concrete used in this study. As shown in *Table 7.4*, for two of the beams without pre-release cracks, the bottom fiber stresses were 163 psi and 99 psi (the corresponding reduction values with respect to the modulus of rupture of 650 psi are 75% and 85%, respectively), the average of which is 131 psi. The reduction in the bottom fiber cracking stress of the beams without pre-release cracks from 650 psi to 131 psi is consistent with the previously explained observation that the beams without pre-release cracks underwent flexural cracking at lower loads than expected. As shown in *Table 7.4*, the nominal bottom fiber cracking stresses for the beams with pre-release cracks were further reduced and become negative due to the existence of pre-release cracks. For each of the beams with a pre-release crack, the percent reduction in nominal bottom fiber cracking stress from the modulus of rupture of concrete (650 psi) is also given in *Table 7.4*. It should be noted that these *nominal bottom fiber cracking stress* values carry no physical meaning. They are numerical values obtained in an intermediate step of the procedure for estimating the effect of pre-release cracks on flexural crack initiation loads. They are important, however in the sense that their value does not change with changing amount and eccentricity of prestressing force and span length as discussed below.

It was verified with a finite element study that *nominal bottom fiber cracking stress*, and hence the *percent reduction in the nominal bottom fiber cracking stress*, does not change with changing amount and eccentricity of prestressing force and span length. However, it should be noted that neither the *bottom fiber cracking stress*, nor the *percent reduction in the nominal bottom fiber cracking stress* values remain the same for modulus of rupture values other than *650*

*psi*, which was the value for the concrete used in the test beams. On the other hand, it was determined that the flexural cracking loads of beams with pre-release cracks computed with the procedure explained below are not significantly affected by changes in modulus of rupture of concrete. Moreover, the modulus of rupture of concrete is proportional to the square-root of the compressive strength of concrete, which means that the change in the modulus of rupture of concrete will be smaller than any change in compressive strength of concrete. Therefore, for the pre-release crack dimensions tested in this study, the nominal bottom fiber cracking stress and percent reduction in nominal bottom fiber cracking stress values given in *Table 7.4* can be used to predict the flexural cracking load of a Mn/DOT Type 28M beam with any prestressing force, eccentricity and span length, and concrete strength in the practical range.

The procedure of estimating the flexural cracking load of a beam with a pre-release crack includes selection of a nominal bottom fiber cracking stress or percent reduction value from *Table 7.4* based on the dimension of the pre-release crack observed. If the pre-release crack observed in the field had a crack depth and width different than the combinations shown in *Table 7.4*, interpolation between the crack depth and width values provided in the table is possible. The pre-release crack width and depth that need to be considered during the assessment should be the values observed prior to release of the prestressing force. After deciding on the pre-release crack size, the expected nominal bottom fiber stress of the beam with pre-release cracks can be determined by using the reduction in nominal bottom fiber stress values given in *Table 7.4*. The final step is to back-calculate the expected flexural crack initiation load using the cross-sectional properties of the beam without pre-release cracks. As explained earlier, nominal bottom fiber stress and reduction in nominal bottom fiber stress values are independent of the amount of prestressing force, eccentricity and beam length, and can be used for any prestressed concrete beam with Mn/DOT Type 28M cross section.

### 7.4.2 Extension of the Procedure to other Sections

The available experimental data regarding the effect of pre-release cracks on beam strains, flexural crack initiation, and flexural crack re-opening loads of the beams was limited to Mn/DOT Type 28M sections in this investigation. The pre-release crack sizes used in this study would affect beams with sections other than Mn/DOT Type 28M differently. Therefore, the experimentally obtained reduction values cannot be used *directly* for beams with sections other

than Mn/DOT Type 28M. However, it is believed that the *ratios of pre-release crack depth to section depth* used in the test beams might be used to estimate the effect of a pre-release crack in a beam other than a Mn/DOT Type 28M section. The idea behind this statement is explained below.

Even though increase in the section depth is not proportional to the increase in the depths of all elements of the section (i.e., change in section depth is mostly accompanied by a change in the depth of web, with a small difference in flange dimensions), it is believed that using the ratio of the depth of the section covered by a pre-release crack to the total section depth to extrapolate the results to sections other than Mn/DOT Type 28M is conservative.

The Mn/DOT Type 28M girder is the shallowest section used in Minnesota. The effect of the top flange of any section other than the Mn/DOT Type 28M on the moment of inertia and the section modulus would be smaller than the effect on the Mn/DOT Type 28M. This is because of the previously mentioned fact that as the section depth increases, the depth of the web increases with a small change in flange dimensions, which in turn, reduces the contribution of the top flange to the moment of inertia of the section. Therefore, having a half-depth pre-release crack in a Mn/DOT Type 72M section, for example, would not be as detrimental as having a half-depth pre-release crack in the Mn/DOT Type 28M beam, as far as the reduction in the moment of inertia of the section is concerned. For this reason, it is believed that the ratios of pre-release crack depth to section depth in the test beams might be used to estimate the effect of a pre-release crack in a beam other than a Mn/DOT Type 28M section.

### 7.4.3 Examples with Mn/DOT 28M Section

To explain the procedure for predicting the effect of a certain size pre-release crack on the flexural cracking load, two beams with Mn/DOT Type 28M section were designed. The first beam was 50 ft long and had sixteen ½ in. diameter prestressing strands, while the second beam was 35 ft long and had ten ½ in. diameter strands. The 50 ft and 35 ft span lengths correspond to girder spacings of approximately 6 ft and 12 ft, respectively. It was assumed that the external load that the beams carried was a distributed load of magnitude $\omega$. The modulus of rupture of the concrete was assumed to be 650 psi. The bottom fiber stress at midspan of the beam under the effects of prestressing force and self-weight was calculated to be 2480 psi compressive for

the first beam and 1770 psi compressive for the second beam, and the distributed load that the beam with no pre-release crack carried before flexural crack initiation was calculated to be 1.71 kip/ft for the first beam and 2.67 kip/ft for the second beam.

The reduction in the superimposed distributed load $\omega$ carried by the beams at flexural cracking was computed for three different pre-release crack geometries. The results are shown in *Table 7.5* for the first beam and in *Table 7.6* for the second beam. The last column of the tables indicates the reduction in the externally applied distributed load due to the existence of the pre-release cracks.

As explained earlier, the flexural cracking loads of beams with pre-release cracks computed with the procedure explained above are not significantly affected by changes in modulus of rupture of concrete. To verify this, the load carried by the 50 ft beam described above with the same size pre-release crack was computed using a modulus of rupture of 500 psi (i.e. 500/650=77% reduction in modulus of rupture, which is caused by 0.77*0.77=59% reduction in compressive strength of concrete). In this case, the 30%, 37%, and 39% reduction values shown in the last column of *Table 7.5* became 24%, 30%, and 31%. This illustrates that using a modulus of rupture of 500 psi instead of 650 psi (a 59% reduction in concrete compressive strength) did not change the reduction in flexural cracking load of the beam significantly. Therefore, the nominal bottom fiber cracking stress and percent reduction in nominal bottom fiber cracking stress values given in *Table 7.4* can be used to predict the flexural cracking load of a prestressed concrete beam with any prestressing force, eccentricity and span length, and concrete strength in the practical range. The reduction in flexural cracking load determined with this procedure will be on conservative side.

## 7.5 Concluding Remarks

As indicated by the finite element and experimental study results, the existence of pre-release cracks causes a reduction in the flexural crack initiation load of beams irrespective of the crack depth. On the other hand, there are several factors, such as the as-built concrete strengths being higher than the design specified values and conservative distribution factors, which tend to increase the flexural crack initiation load above the design value. As explained earlier, irrespective of whether the girder has pre-release cracks or not, some or all of this reserve

capacity is being used by the girders so that the girders remain uncracked during their service life despite a possible reduction in the flexural crack initiation load from the design value. As a result, when making decisions about accepting or rejecting a girder that developed pre-release cracks, this reserve flexural cracking capacity due to higher concrete strength and conservative distribution factors should not be considered.

It was discussed earlier in this chapter that the reduction in section stiffness due to partly closed pre-release cracks causes unacceptable reductions in the flexural crack initiation and re-opening loads of the girders. Considering this, it is suggested that girders that develop pre-release cracks during production should be rejected if the pre-release cracks remain open following the release of the prestressing strands. This procedure might be overly conservative as in most cases a composite deck will be added on top of the girders before they are subjected to the service loads, which will reduce the detrimental effects of pre-release cracks being partially open. On the other hand, there can be cases (such as through-girder construction) where the deck is not added on top of the girders with relatively large girder lengths. In that case, the self weight of the girders constitutes the major portion of the total load, and if the pre-release cracks in these girders do not close completely after the prestress transfer they are likely to remain partially open at flexural cracking.

If the pre-release cracks are observed to close completely after the prestressing strands are released, the only effect on the flexural crack initiation and re-opening loads of the girders will be due to the reduced bottom fiber compressive stresses that occurred during pre-release crack closure. In this case, the procedure outlined earlier in this chapter can be used to predict the flexural cracking loads of the girders. It should be noted that the proposed procedure is based on the experimental data from the single crack series beam tests, which had partially open pre-release cracks at the flexural cracking load. Therefore, using this procedure to predict the flexural cracking loads of the girders with pre-release cracks completely closed after the transfer of prestressing force will be conservative.

During the evaluation of beams with pre-release cracks, it should be kept in mind that, until the release of prestressing strands, the depth of the pre-release cracks may increase with time due to shrinkage of the concrete. Increase in the depth of the cracks would probably involve corresponding increases in crack width. It should also be kept in mind that the impact of a pre-

release crack increases with increasing crack width and depth, and the effects of multiple cracks are additive when the cracks are spaced less than the depth of the beam.

## REFERENCES


Abeles, P. W., Brown, E. I., and Hu, C. H. Behavior of Under-Reinforced Prestressed Concrete Beams Subjected to Different Stress Ranges. Abeles Symposium on Fatigue of Concrete, American Concrete Institute, Detroit, 1974.

ACI Committee 215 (1997). ACI 215R-74 "Considerations for Design of Concrete Structures Subjected to Fatigue Loading." ACI Manual of Concrete Practice (2000).

ACI Committee 318 (1995). "Building Code Requirements for Structural Concrete and Commentary." ACI 318-95/ACI 318R-95. American Concrete Institute (ACI), Detroit, Michigan.

Ahlborn, T. (1998). "High Strength Prestressed Concrete Bridge Girders." Thesis, Doctor of Philosophy, Department of Civil Engineering, University of Minnesota.

American Society for Testing and Materials (ASTM). Annual Book of ASTM Standards. (1995). Philadelphia, PA.

Bentz, E. and Collins, M. RESPONSE-2000. Computer Software.
http://www.ecf.utoronto.ca/~bentz/home.shtml

Collins, M. and Mitchell, D. Prestressed Concrete Structures. Englewood Cliffs, N.J., Prentice-Hall, 1991.

Geokon, Model 4410 Vibrating Wire Strandmeter Instruction Manual.

Geokon, Models VCE-4200/4202/4210 Vibrating Wire Strain Gages Installation Manual.

Green, J. K., Cookson, P. J., and Johnson, K. A. L. (1984) "The Performance of Pretensioned Concrete Beams That Have Cracked Before Transfer of Prestress." *The Structural Engineer*, 62B(4), December, 79-85.

Halsey, J. T. and Miller, R. (1996) "Destructive Testing of Two Forty-Year-Old Prestressed Concrete Bridge Beams." *PCI Journal*, 41(5), September-October, 84-93.

Harajli, M. H. and Naaman, A. E. (1985) "Static and Fatigue Tests on Partially Prestressed Beams." *ASCE Journal of Structural Engineering*, 111(7), July, 1602-1618.

Hibbit, Karlsson & Sorensen, Inc. (1994). ABAQUS. Version 5.4, Pawtucket, Rhode Island.

Labia, Y., Saiidi, M. S., and Douglas, B. (1997) "Full-Scale Testing and Analysis of 20-Year-Old Pretensioned Concrete Box Girders." A*CI Structural Journal*, 94(5), September-October, 471-482.

Lawver, A. C. (1998). "Field Study of an Integral Abutment Bridge." Thesis, Master of Science, Department of Civil Engineering, University of Minnesota.

Lin, T. Y., and Burns, N. H. Design of Prestressed Concrete Structures. John Wiley & Sons, 1981.

Muller, J. F. and Dux, P. F. (1994) "Fatigue of Prestressed Concrete Beams With Inclined Strands." *ASCE Journal of Structural Engineering*, 120(4), April, 1122-1139.

Nordby, G. M. and Venuti, W. J. (1957) "Fatigue and Static Tests of Steel Strand Prestressed Beams of Expanded Shale Concrete and Conventional Concrete." *Journal of the American Concrete Institute*, August, 141-160.

Overman, T. R., Breen, J. E., and Frank, K. H. Fatigue Behavior of Pretensioned Concrete Girders. Research Report 300-2F, Center for Transportation Research, University of Texas at Austin, 1984.

Ozell, A. M. and Ardaman, E. (1956) "Fatigue Tests of Pretensioned Prestressed Beams." *Journal of the American Concrete Institute*, October, 413-424.

Ozell, A. M. and Diniz, J. F. (1958) "Composite Prestressed Concrete Beams Under Repetitive Loading." *PCI Journal*, June, 79-88.

Ozell, A. M. Fatigue Tests of Prestressed Concrete I-Beams with Depressed Strands. Fourth Congress, Federation Internationale de la Precontrainte, 1962.

Paulson, C. Jr., Frank, K. H., and Breen, J. E. A Fatigue Study of Prestressing Strand. Research Report 300-1, Center for Transportation Research, University of Texas at Austin, 1983.

PCI Design Handbook-Precast and Prestressed Concrete, Fifth Edition. (1999). Prestressed Concrete Institute (PCI), Chicago, IL.

Pessiki, S., Kaczinski, M., and Wescott, H. H. (1996) "Evaluation of Effective Prestress Force in 28-Year-Old Prestressed Concrete Bridge Beams." *PCI Journal*, 41(6), November-December, 78-89.

Portland Cement Association (PCA). Design and Control of Concrete Mixtures, Thirteenth Edition. (1994). Skokie, IL.

Rabbat, B. G., Karr, P. H., Russell, H. G., and Bruce, N. G. Fatigue Tests of Full Size Prestressed Girders. Research Report 113, Portland Cement Association, 1978.

Rao, C. and Frantz, G. C. (1996) "Fatigue Tests of 27-Year-Old Prestressed Concrete Bridge Box Beams." *PCI Journal*, 41(5), September-October, 74-83.

Roller, J. J., Martin, B. T., Russell, H. G., and Bruce, R. N. (1993) "Performance of Prestressed High Strength Concrete Bridge Girders." *PCI Journal*, 38(3), May-June, 34-45.

Roller, J. J., Russell, H. G., Bruce, R. N., and Martin, B. T. (1995) "Long-Term Performance of Prestressed, Pretensioned High Strength Concrete Bridge Girders." *PCI Journal*, 40(6), November-December, 48-59.

Shanafelt, G. O. and Horn, W. B. Guidelines for Evaluation and Repair of Prestressed Concrete Bridge Members. National Cooperative Highway Research Program Research Report 280, Transportation Research Board, 1985.

Shenoy, C. V. and Frantz, G. C. (1991) "Structural Tests of 27-Year-Old Prestressed Concrete Bridge Beams." *PCI Journal*, 36(5), September-October, 80-90.

Warner, R. F. and Hulsbos, C. L. (1962) "Probable Fatigue Life of Under-Reinforced Prestressed Concrete Beams. Publications." *Publications*, 22, 337-352.

Wyffels. T. Effects of Pre-Release Cracks in High-Strength Prestressed Girders. Research Report, Minnesota Department of Transportation, 2000.

Zia, P. and Caner, A. Cracking in Large-Sized Long-Span Prestressed Concrete AASHTO Girders. Research Report, Center for Transportation Engineering Studies, Department of Civil Engineering, North Carolina State University, 1993.